UNIVERSITY OF CALIFORNIA,
IRVINE

Determining the inhibitory functions of PSGL-1 and CD38 in T cells during infection and cancer

DISSERTATION

submitted in partial satisfaction of the requirements
for the degree of

DOCTOR OF PHILOSOPHY

in Biological Sciences

by

Julia DeRogatis

Dissertation Committee:
Professor Roberto Tinoco, Chair
Professor David A. Fruman
Professor Melissa B. Lodoen
Professor Craig M. Walsh

2023

DEDICATION

To my wonderful family,

Sue, Phil, and Andi

Thank you for 27 years of love and support

TABLE OF CONTENTS

LIST OF FIGURES

LIST OF TABLES

ACKNOWLEDGEMENTS

The PhD is a long and often very challenging process, and I am so thankful for the support that I have had along the way. First, I would like to thank and acknowledge Dr. Roberto Tinoco, my PI, for all his support and guidance over the last five years. He took me on as one of his first students and has worked very hard to help me grow and succeed in all my PhD endeavors. Dr. Tinoco has helped me to develop as an immunologist, as a scientific writer, and as a mentor.

The text of this dissertation is a reprint of the material as it appears in (223, 261, and 275) used with permission from Frontiers Media, American Association for Cancer Research, and American Society for Microbiology. The co-authors listed in this publication are Emily Neubert, Karla Viramontes, Monique Henriquez, Christian Guerrero-Juarez, Dequina Nicholas, and Roberto Tinoco.

I also want to thank and acknowledge my past and present committee members, Dr. David Fruman, Dr. Aimee Edinger, Dr. Craig Walsh, and Dr. Melissa Lodoen. My committee has been a constant source of insight and support, and I thank them so much for all the time they've spent helping me reach my graduate school goals. The support of my committee has meant so much to me, and they have all helped me grow as a scientist, presenter, and scientific community member. I would like to acknowledge Dr. Fruman and Dr. Edinger for giving me a place on the T32 Training Program for Interdisciplinary Cancer Research. Their support early in my graduate career helped me to feel a part of the cancer research community and to connect and learn from my peers. Dr. Fruman has been a wonderful mentor and has helped me so much over the years, I appreciate his support and guidance, as well as the time he has spent answering my questions and helping with my job search. Dr. Lodoen has also been a source of guidance and support, and I appreciate all the time she took to listen to me and help me along my grad school path.

I would like to acknowledge the Tinoco lab: Monique, Karla, Melissa, and Emily. The lab has become a second family to me, and I am so thankful that I got to spend the last five years learning and growing with all of them. I want to thank them for all the times they've stepped in to help with big experiments, all the times they've listened to my complaints and helped me problem solve, all the laughter and silly moments in lab, and all the love and support they've shown me over this whole process. I feel so lucky to be part of this team, and so grateful for everything my lab mates have done to make grad school a positive experience.

My friends, who have been my biggest support group over this process, must be acknowledged for their endless love and support. My childhood friends: Maddie, Linda, Hanna and Chandler. My college friends: Katy, Sarah, and Tina. Nick and I's friends: Rhiannon, Trevor, Jesse, Diana. My current grad school friends: Emily, Makena, Mariana, Will, and Alex. Words cannot express how much I appreciate my friends; I would not have been able to get through my PhD without them. These friends all lead busy, independent lives, and yet they are always there whenever I need them. I have received so much optimism and so much love from these friends, particularly during very challenging periods in the height of the pandemic. I am endlessly thankful they are in my life and am so appreciative of their friendship. I would like to acknowledge Emily Neubert. She has been my roommate, lab mate, co-cat parent, confidant, lab twin, and so much more during graduate school. I will forever be grateful that Emily and I got placed as roommates our first year here, it was the beginning of an epic friendship. I can honestly say that Emily made graduate school so much better, she is an amazing friend and experiment partner, and having her by my side has helped me to overcome so many challenges. Living with her has been a joy and I will cherish all the memories we made together during this crazy time. I cannot thank her enough for everything she's been to me and done for me over the last five years.

I would like to acknowledge Nick's family: Susan and Lee, Lauren and Lee, and Kerry and Michella. They have welcomed me into their family and shown so much love and support. I would like to thank my uncle Shawn and aunt Teri. They have been the best aunt and uncle in the world, they are so supportive and always encourage me to enjoy life and cherish moments with friends and family. They encourage me never to lose touch with my creative side, and to take moments to stop and take in the world and be present. I would like to acknowledge auntie E, who I love and miss dearly. She would have loved to be here for this, and I feel her love constantly, even as she is no longer with us.

My family, Sue, Phil, and Andi have been instrumental in helping me get to where I am now. I want to acknowledge the multitude of ways in which my family has been there for me. They have shown up for all the big and small moments, they check in constantly with messages of love and support, they have listened, problem-solved, and helped guide me through life. I am so lucky to have them and their unconditional love, and I appreciate so much everything they have given and done to help me get to this point. I am so fortunate to have been given so many opportunities by my parents, and so thankful for their emotional and financial support. My sister Andi has been a best friend, a confidant, and an endless well of support, and I am so lucky to have her. So, thank you to my family for everything, this defense wouldn't exist without you.

Finally, I would like to thank my partner, Nicholas Foy. Nick has been by my side since my sophomore year at Oxy, and a better partner does not exist. For so many years, he has been my number one supporter, and his unwavering love and confidence in me have helped me to feel like I can accomplish anything. He is the first person I go to with all the good and the bad, and he has supported me and helped me to grow in more ways that I can say. His support has meant everything to me, I don't know how I would have gotten through the challenges of the last few years, including the

pandemic, without him. Nick is always there with love, with hugs, with helpful advice, with ways to make me laugh, and he has also been the best Jazz dad. He is the most amazing partner, and I have loved the adventure of getting our PhDs together. So, an endless thank you to Nick, I love him so much and appreciate all the ways big and small he has been there for me. I cannot wait for the future with him, and I am endlessly grateful to have him by my side.

VITA

Julia DeRogatis

EDUCATION

Ph.D., Immunology, UC Irvine 4.0 GPA — 2023

B.A. (Magna Cum Laude), Biochemistry
Interdisciplinary Writing Minor, Occidental College 3.79 GPA — 2018

RESEARCH EXPERIENCE

Graduate Student in Immunology – University of California, Irvine — 2018-2023
In vivo study of the roles of the inhibitory receptor PSGL-1 and ectoenzyme CD38 on T cells during infection and cancer
Advisor: Professor Roberto Tinoco

Undergraduate Researcher – Occidental College, Los Angeles — 2015-2018
Study of the potential symbiosis between Elthusa isopods and their unique intestinal microbial community
Advisor: Professor Shana Goffredi

Undergraduate Researcher – City of Hope, Duarte — 2017
Selective targeting of acute myeloid leukemia with small interfering RNA
Advisor: Professor John Rossi

PUBLICATIONS

DeRogatis JM, Viramontes KM, Neubert EN, Henriquez ML, Guerrero-Juarez CF, Tinoco R. Targeting the PSGL-1 Immune Checkpoint Promotes Immunity to PD-1 Resistant Melanoma. Cancer Immunol Res. 2022; 10(5): 612–625.

DeRogatis JM, Neubert EN, Viramontes KM, Henriquez ML, Nicholas DA, Tinoco R. 2023. Cell-Intrinsic CD38 Expression Sustains Exhausted CD8(+) T Cells by Regulating Their Survival and Metabolism during Chronic Viral Infection. J Virol doi:10.1128/jvi.00225-23:e0022523.

Neubert EN, DeRogatis JM, Lewis S, Viramontes KM, Henriquez ML, Messaoudi I, Tinoco R. HMGB2 Sustains the Stemness of Exhausted $CD8^+$ T cells During Chronic Viral Infection and Cancer. 2023. In review.

Viramontes KM, Neubert EN, DeRogatis JM, Tinoco, R. PD-1 Immune Checkpoint Blockade and PSGL-1 Inhibition Synergize to Reinvigorate Exhausted T Cells. Front Immunol. 2022; 13:869768.

Kumar P*, Brazel D*, DeRogatis J* et al. The Cure From Within? A Review of the Microbiome and Diet in Melanoma. Cancer Metastasis Rev. 2022; 1–20. *Co-first authors

Han SP, Scherer L, Gethers M, Salvador AM, Salah MBH, Mancusi R, Sagar S, Hu R, DeRogatis J, Kuo YH, Marcucci G, Das S, Rossi JJ, Goddard WA 3rd. Programmable siRNA pro-drugs that activate RNAi activity in response to specific cellular RNA biomarkers. Mol Ther Nucleic Acids. 2022; 27:797–809.

DeRogatis JM, Viramontes KM, Neubert EN, Tinoco R. PSGL-1 Immune Checkpoint Inhibition for CD4+ T Cell Cancer Immunotherapy. Front Immunol. 2021; 12:636238.

AWARDS, HONORS AND GRANTS

Graduate Assistance in Areas of National Need (GAANN) Fellowship, UCI	2022-2023
NIH Cancer Biology and Therapeutics Training Grant, UCI	2020–2022
Best Poster Award, Molecular Biology and Biochemistry, UCI	2022
School of Biological Sciences Dean's Graduate Fellowship, UCI	2018

PRESENTATIONS

Talk, UCI Center for Virology Research in Progress	2022
Poster, Hallmarks of Cancer – Cell symposia in San Diego	2022
Poster, Molecular Biology and Biochemistry Retreat at UCI	2022
Poster, Campus-Wide Symposium on Basic Cancer Research	2022
Talk, T32 Cancer Biology Retreat in La Jolla	2022
Poster, UCI Center for Virology Research Retreat	2022
Poster, Asilomar Midwinter Conference for Immunologists	2022

ABSTRACT OF THE DISSERTATION

Determining the inhibitory functions of PSGL-1 and CD38 in T cells during infection and cancer

by

Julia DeRogatis

Doctor of Philosophy in Biological Science

University of California, Irvine, 2023

Professor Roberto Tinoco, Chair

T cell exhaustion occurs when T cells are engaged by persistent antigen in the context of chronic infection and cancer. The formation of the exhaustion phenotype severely limits T cell effector function and survival, leading to diminished tumor and viral control. Immune checkpoints, which are upregulated in response to chronic T cell receptor engagement, promote the dysfunctional T phenotype. P-selectin glycoprotein ligand-1 (PSGL-1) is a known immune checkpoint protein, however the biological impact and therapeutic efficacy of targeting PSGL-1 in melanoma bearing mice is unknown. In this dissertation, we utilized *in vivo* melanoma models to investigate the impact on the anti-tumor T cell response after monoclonal antibody targeting of PSGL-1. We showed that anti-PSGL-1 treatment slowed the growth of PD-1-resistant melanoma tumors and promoted increased effector functions in tumor-infiltrating T cells. Further, we show that targeting PSGL-1 significantly reduced the immunosuppressive Treg frequencies in the tumor, leading to a more pro-inflammatory tumor microenvironment. While PSGL-1 is a known immune checkpoint, the role of CD38 in shaping the T cell response to acute and chronic viral infections is currently unknown. In this dissertation, we used an adoptive co-transfer approach of WT and *Cd38*$^{-/-}$ CD8^{+} T cells into WT mice that were subsequently infected with acute or chronic strains of lymphocytic choriomeningitis virus (LCMV) to

investigate the impact of cell-intrinsic CD38 deletion on the T cell response to infection. We found that CD38 expression was important for the survival of virus-specific T cells over the course of infection. Further, while CD38 deletion did not prevent the formation of the exhaustion phenotype, we showed that T cells lacking CD38 had more proliferation and granzymeB production than WT cells, particularly the progenitor exhausted T cells (Tpex). Finally, we found that loss of CD38 caused reduced mitochondrial respiration in T cells, but only during chronic infection. Together, this dissertation provides new insight into the therapeutic efficacy of targeting PSGL-1, as well as uncovering a new role for CD38 in promoting survival of virus-specific T cells, while also limiting their effector function. This work details the impact that antibody targeting and genetic modulation of PSGL-1 and CD38 has on the exhaustion phenotype and is an important contribution to further our understanding of the proteins that shape the T cell response to infection and cancer.

INTRODUCTION

1.1 T cell exhaustion overview

During acute infection, T cells are activated through T cell receptor (TCR) signaling and co-stimulation to form effector cells. These effector cells are highly functional, capable of proliferation and cytokine release, as well as effective memory cell formation (1, 2). In the case of an acute infection, T cells successfully clear the infection and viral antigens do not persist. In contrast, during chronic infection or cancer, T cells are stimulated through their TCR and co-stimulatory pathways to become activated but are unable to clear the antigen (3, 4). This chronic TCR stimulation promotes the development of a population of dysfunctional T cells known as 'exhausted' T cells. The exhausted T cell population is unique from effector T cells genetically and phenotypically, as chronic TCR stimulation sets in motion a robust transcriptional program which drives T cell dysfunction (5, 6). The unique chromatin landscape seen in exhausted T cells begins early during chronic antigen stimulus and becomes a permanent epigenetic scar over time, resulting in severely diminished T cell effector function and failure to clear infection and tumors (7-9).

1.1.1 T cell exhaustion phenotype

Effective T cell activation requires multiple signals including TCR-pMHC, co-stimulation, and cytokines by antigen presenting cells that promote T cell proliferation and survival (10). In addition to co-stimulatory signals, T cell inhibitory pathways such as PD-1/PD-L1 and CTLA-4 are important as "brakes" that ensure effective TCR signaling required for T cell differentiation and to prevent aberrant activation (11). Both $CD4^+$ and $CD8^+$ T cells express immune checkpoints that are upregulated after activation and then downregulated after antigen clearance; however, during chronic antigen stimulation such as in tumors and chronic viral infections, the expression of immune checkpoints remains elevated to promote the generation of exhausted $CD4^+$ and $CD8^+$ T cells (12, 13). Immune

checkpoints inhibit T cells through multiple mechanisms, but their main function is to inhibit TCR signaling (12, 13). PD-1 signaling, for example, has been reported to interfere with both TCR and CD28 signaling pathways to limit T cell activation (14). Many additional immune checkpoints including TIGIT, LAG-3, TIM-3, VISTA, CD160, and BTLA have been discovered and work through diverse mechanisms to limit T cell activation and have been reviewed elsewhere (12, 15). In the exhausted state, T cells express high levels of these inhibitory receptors, have limited cytokine and granzyme production, and ultimately undergo apoptosis (16-20). However, even though exhausted cells are dysfunctional, they are still capable of some effector function and therefore provide vital viral and tumor control (21, 22). Further, although the exhaustion programming begins early, subsets of exhausted T cells can be therapeutically reinvigorated through immune checkpoint blockade (23, 24). Antibodies targeting PD-1/PD-L1, CTLA-4, and TIM-3 among others, block suppressive signals from these immune checkpoints, allowing for clinically significant improvements in T cell function and viral and tumor control (12, 25).

1.1.2: Genetic exhaustion programming/transcriptional regulation of exhaustion

The development of T cell exhaustion is set in motion by strong and persistent TCR signaling (26). Transcription factors known to respond to TCR signaling, such as nuclear factor of activated T cells, cytoplasmic component 1 (NFATC1), basic leucine zipper transcriptional factor ATF-like (BATF), and interferon regulatory factor 4 (IRF4) are vital drivers of T cell exhaustion (27-30). Many TCR-responsive transcription factors that are upregulated in exhausted T cells are also upregulated in effector T cells. However, there are a few transcription factors that have exhaustion-specific expression, with upregulation only occurring after chronic TCR engagement. One such transcription factor is thymocyte selection-associated high mobility group box protein (TOX), an essential regulator of exhausted T cells (31-33). TOX is downstream of NFAT, and its expression is significantly

upregulated by day 4 of chronic antigen engagement. While TOX is associated with hallmarks of exhaustion, such as high inhibitory receptor expression and reduced effector function, it is also essential to the maintenance of exhausted subsets, as *TOX*$^{-/-}$ T cells fail to persist during chronic infection (32). Epigenetic analysis revealed that TOX supports expression of the transcription factors TCF-1 and Eomes, as well as downregulates genes involved in effector function such as *Klrg1*, *Gzmb*, *Cx3cr1*, and *Prf1* (31, 32). TOX expression during chronic TCR engagement reshapes the genetic landscape of T cells, pushing them toward the unique exhaustion identity, which results in limited effector function but allows for long term persistence of T cells in environments with chronic antigen.

As the field of T cell exhaustion expanded, so has our understanding of the subsets that make up the exhausted population. While TOX expression is necessary to sustain the exhausted T population, it is particularly linked to the formation of a more terminal subset known as the terminally dysfunctional, or Tex, subset (34). Numerous reviews cover the full characterization of Tex cells; however, they are largely defined by high expression of inhibitory receptors, retention of limited cytokine and granzyme production, and high rates of apoptosis (34-36). In contrast to the Tex population, there is a more stem-like, progenitor population of exhausted T cells, known as Tpex (30). Tpex cells share some similarities to memory cells, in that they are long-lived and able to self-renew as well as seed Tex populations (37, 38). While Tex cells are phenotypically characterized by high PD-1, CD101, CCR5, and TIM-3, Tpex are defined by expression of Slamf6, CXCR3, CXCR5, and low PD-1 (**Fig. 1.1**) (34). Like Tex, Tpex cells are a unique population, generated by chronic TCR stimulation. However, the transcriptional landscape of Tpex cells differs from that of Tex cells, as Tpex are shaped by the expression of the transcription factor T cell factor 1 (TCF1) (21). As with TOX, the upregulation of TCF1 is linked with TCR signaling and activation of transcription factors NFAT, AP-1, and IRF (27, 28, 30). TCF1 expression drives the Tpex phenotype, resulting in expression of genes linked with memory and stemness (*Cxcr5*, *Il7r*, *Myb*, *Cd28*, *Icos*, *Id3*) and

suppression of genes associated with the terminal exhaustion and effector function (*Lag3*, *Cd160*, *Gzmb*, *Tbx21*, *Fasl*, *Id2*, *Runx3*, *Cd38*) (39). The Tpex population is key to the anti-viral and anti-tumor immune response, as it seeds the Tex population and can respond to immune checkpoint blockade (21, 37, 40).

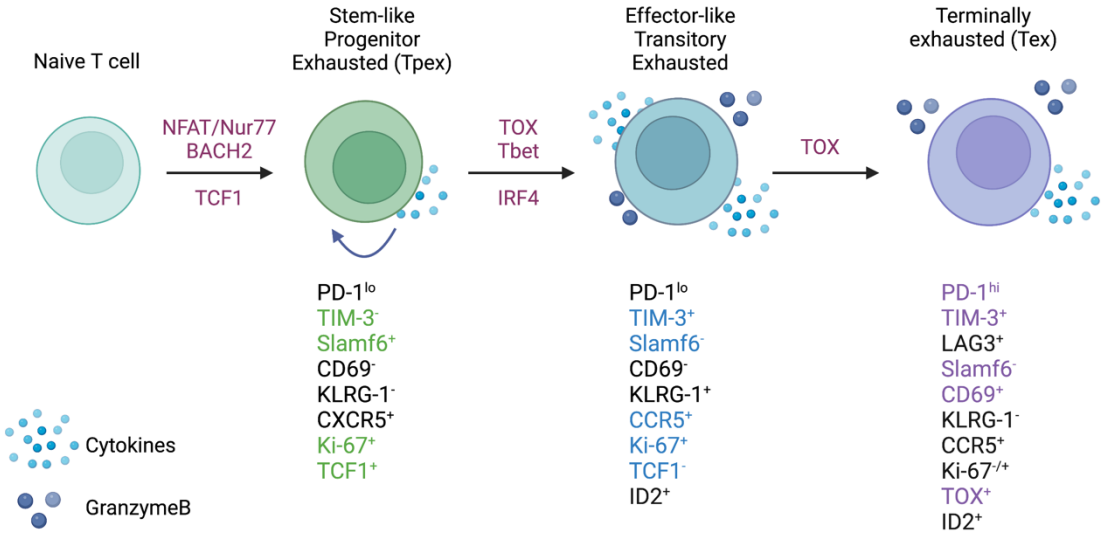

Figure 1.1 Subsets of exhausted T cells. Transcription factors and surface markers of stem-like progenitor exhausted (Tpex), transitory effector-like exhausted, and terminally exhausted (Tex) T cell subsets. Markers used to define subsets by flow cytometry are highlighted.

1.2 PSGL-1 overview

The initial studies of PSGL-1 focused primarily on its expression and role in neutrophils, but PSGL-1 has since been identified on all myeloid and lymphoid lineages. Despite the ubiquitous expression of PSGL-1 on all hematopoietic lineages, its expression level and functionality differ among these cell types. On myeloid cells, PSGL-1 is constitutively expressed in its functional form, which has the posttranslational modifications required for selectin binding (41). Within the lymphocyte lineage, all T cell subsets express PSGL-1, whereas very low to undetectable expression is present in B cells (42). Like myeloid cells, T cell binding and endothelial migration is regulated by PSGL-1. Unlike myeloid cells, however, T cells do not constitutively express functional PSGL-1 and must express the enzymatic machinery required to modify PSGL-1 during T cell activation (41). Although PSGL-1 is expressed on all T cell subsets, including both Th1 and Th2 $CD4^+$ T cells, Th2 cells do not express the functional form and thus have decreased binding capacity to P- and E-selectins when compared to Th1 cells (43). In follicular T helper cells (Tfh), PSGL-1 downregulation by the transcription factors Bcl6 and Ascl2 facilitate migration in follicles (44). Tregs also express highly functional PSGL-1 and in a model of experimental autoimmune encephalomyelitis (EAE), PSGL-1 expression was linked to the suppressive capacity of Tregs (45). PSGL-1 is also expressed by Th17 and $CD8^+$ T cells (46, 47). The widespread expression of PSGL-1 on immune cells, as well as its roles in adhesion and immunosuppression make PSGL-1 an interesting area of study and potential target for immunotherapeutic treatments.

1.2.1 Human and mouse PSGL-1

While humans and mice both express PSGL-1, it is important to consider the similarities and differences between these two proteins (**Fig. 1.2**). Murine PSGL-1 is encoded as a 397 amino acid (a.a.) protein (48). The mature form of murine PSGL-1 has a 290 aa extracellular domain (ECD),

which contains 10 decameric repeats. In contrast, human PSGL-1 is encoded as a 412 aa protein and has a 279 aa ECD that contains 16 decameric repeats (49). The sequence of the decameric repeats also differs between human and murine PSGL-1. Studies comparing the amino acid sequence of human and murine PSGL-1 have found the two proteins only share 43% sequence similarity in the ECD, although the transmembrane and cytoplasmic domain are more similar (48). While the sequences may be different, murine and human PSGL-1 share important similarities in the regions of the protein that are involved in ligand binding and signaling. In order to interact with selectins, the N-terminus of PSGL-1 must undergo Core-2 O-glycosylation of a threonine and sulfation at tyrosine residues (50). In murine PSGL-1, O-glycosylation occurs at Thr17 and only one tyrosine is sulfated, Tyr13 (51). In human PSGL-1, the O-glycosylation occurs at Thr16 and there are three sites of tyrosine sulfation (Tyr5, 7, and 10) instead of one (**Fig. 1.2**). In both human and mice, PSGL-1 has a cysteine residue that precedes the transmembrane domain and facilitates dimerization, as well as conservation of serine, lysine, and arginine residues in the cytoplasmic moesin-binding sequence (52). Additionally, an aspartic acid, a lysine, and a valine are conserved between species in the versican-binding region of the protein (52, 53). While more research is needed into the signaling differences between human and murine PSGL-1, the selectin-binding function of the protein is conserved, as well as the types of post-translational modifications that occur at the N-terminus (**Fig. 1.2**).

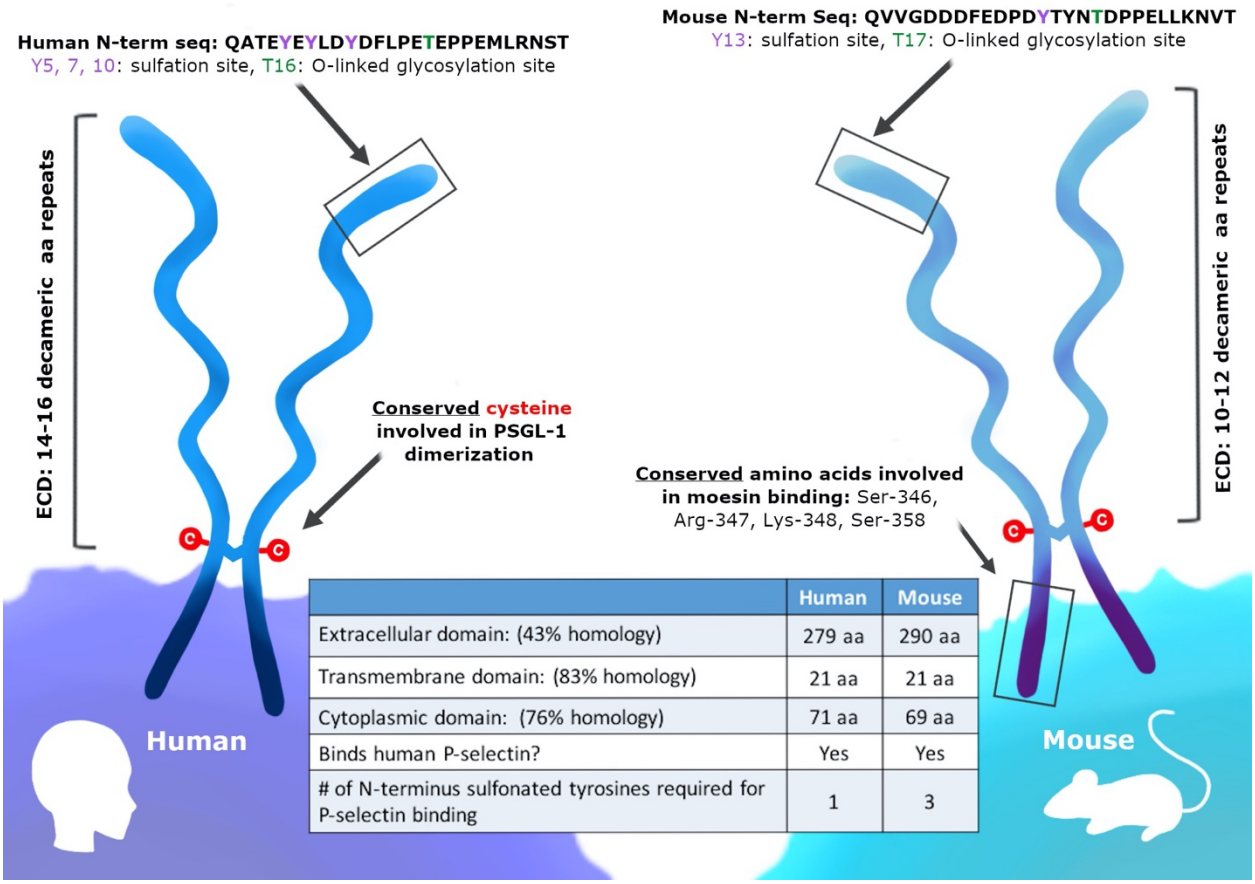

	Human	Mouse
Extracellular domain: (43% homology)	279 aa	290 aa
Transmembrane domain: (83% homology)	21 aa	21 aa
Cytoplasmic domain: (76% homology)	71 aa	69 aa
Binds human P-selectin?	Yes	Yes
# of N-terminus sulfonated tyrosines required for P-selectin binding	1	3

Figure 1.2 PSGL-1 is expressed in mice and humans. PSGL-1 is expressed as a homodimer on the surface of most hematopoietic cells. Similarities and differences between mouse and human PSGL-1 are shown.

When considering the translatability of mouse PSGL-1 studies, the differences between mouse and human PSGL-1 biology must be understood. While the selectin-binding function of the N-terminus of murine and human of PSGL-1 is conserved, the differential requirements for P-selectin binding are important to note. As mentioned above, human PSGL-1 requires a core-2 O-glycan plus three sulfated tyrosine residues to bind P-selectin, of which two sulfated residues form direct bonds to the lectin domain (54-56). In contrast, the binding of murine PSGL-1 to P-selectin is facilitated largely by a core-2 O-glycan and a single sulfated tyrosine (51). When the canonically-glycosylated threonine residues were mutated in human and murine PSGL-1, only human PSGL-1 binding to P-selectin was abolished, indicating that murine PSGL-1 does not depend on these glycosylated residues for binding. These studies highlight the differential contributions of post-translational modifications surrounding protein structure to the selectin binding ability of human and murine PSGL-1. These differences are important to understand, as targeting N-terminal residues or post-translational modifications on PSGL-1 may have different outcomes in human and mouse. The differences in the ligands that bind PSGL-1 should also be noted. While human PSGL-1 can bind Siglec-5, this ligand is not present in mice, and therefore may contribute to a phenotype in human studies not seen in mice (57). The possible ligand-receptor pairs can also differ from mice to humans, and these interactions may change depending on the immune cells and the microenvironments in which are they located. In a murine AML cell line, only PSGL-1 was capable of binding E-selectin (58). However, in human AML cells lines, both CD44 and PSGL-1 could bind E-selectin. The differences in PSGL-1 between species are important to consider, especially when these findings are applied for translational purposes for immune modulation.

1.2.2 PSGL-1 ligands

Selectins

PSGL-1 protein engages a diverse array of ligands at steady state and at different stages of the immune response. While multiple PSGL-1 ligands have been identified, the selectins were the first to be characterized and are the most studied (48). All three selectins, platelet (P), endothelial (E), and leukocyte (L) have been well characterized to bind PSGL-1 through the N-terminus extracellular domain (59-61) (**Fig. 1.3, Table 1.1**). However, PSGL-1 binding affinities differ between the three, with P-selectin having the highest affinity, followed by E- and L-selectins, respectively (62-65). Importantly, while all leukocytes can bind selectins due to PSGL-1 post-translational modifications (64, 66, 67), naïve $CD4^+$ and $CD8^+$ T cells engage selectins only after T cell activation (41). Naïve T cells express PSGL-1, however lack of sialylation and fucosylation on PSGL-1 prevent selectin binding (41). Various enzymes are involved in modifying PSGL-1 to allow P-selectin binding, including fucosyltransferase IV and VII, core 2 b1,6-glucosaminyltrasferase-I, b1,4-galactosyltransferase-I, sialyl 3-transferase IV, and tyrosylprotein sulfotransferase 1 or 2 (68). $CD4^+$ and $CD8^+$ T cell activation induces enzymatic activity which facilitate P-selectin binding (69-71). Furthermore, IL-12 signaling in Th1 cells was shown to induce PSGL-1 functionality, while IL-15 in $CD8^+$ T cells induced core 2 O-glycan expression *in vitro* and *in vivo* (69, 72). PSGL-1 binding of these selectins plays a major role in leukocyte migration and recruitment. PSGL-1 expressing leukocytes circulating in the blood attach to activated endothelium expressing P- and E-selectins. This PSGL-1-mediated attachment allows leukocytes traveling at high velocities to attach, roll and tether to the endothelium and transmigrate to sites of inflammation, infection, and in tumors (73-76).

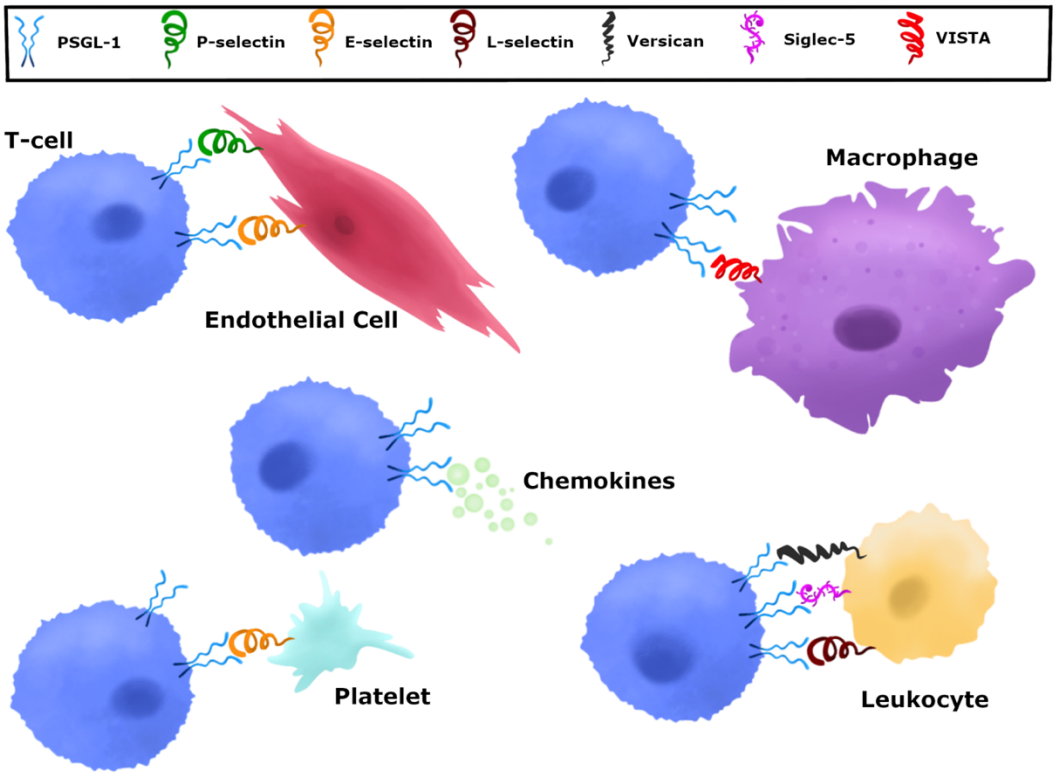

Figure 1.3 Various ligands can engage PSGL-1. PSGL-1 can bind P-, E-, and L-selectin. P-selectins are present in a variety of cells including platelets and endothelial cells. E-selectins are expressed by endothelial cells and L-selectin by leukocytes. CCL19 and CCL21 chemokines are present in secondary lymphoid organs and can be produced by endothelial cells, stromal cells, and mature dendritic cells. Versican is produced by epithelial, endothelial, stromal cells, and leukocytes. Siglec-5, which is only present in humans, is expressed in neutrophils, mast cells, monocytes, DCs, NK cells, and stimulated T cells. VISTA is expressed on myeloid cells and granulocytes.

TABLE 1.1 PSGL-1 and its binding partners.

Molecule	Gene Name	Cells expressed
P-selectin glycoprotein ligand-1 (PSGL-1)	*Selplg*	$CD4^+$ T cells, $CD8^+$ T cells, Tregs, HSCs, DCs, neutrophils, monocytes, macrophages, most lymphocytes and granulocytes
V-domain Ig suppressor of T cell activation (VISTA)	*Vsir*	Myeloid cells, granulocytes, T cells
Platelet selectin (P-selectin)	*Selp*	Platelets, endothelial cells
Endothelial selectin (E-selectin)	*Sele*	Endothelial cells
Leukocyte selectin (L-selectin)	*Sell*	Granulocytes, monocytes and most lymphocytes
Versican	*Vcan*	Epithelial, endothelial, stroma and leukocytes
Sialic Acid Binding Ig Like Lectin 5 (Siglec-5)	*SIGLEC5 (Human)*	Neutrophils, mast cells, monocytes, DCs, NK, T cells
C-C motif chemokine ligand 19 (CCL19)	*Ccl19*	Stromal cells and mature DCs
C-C motif chemokine ligand 21 (CCL21)	*Ccl21a, Ccl21b, Ccl21c*	Lymphatic endothelial and stromal cells

Limiting PSGL-1 and selectin interactions may promote improved T cell responses. Recent work has shown that cDC1 cells are required to effectively activate both $CD4^+$ and $CD8^+$ T cell responses to tumors (77). Whether PSGL-1 on T cells and/or cDC1 dendritic cells contributes to T cell activation is unknown, but studies show that P-selectin engagement on DCs can induce a tolerogenic phenotype that can suppress T cells (78). When T cells exit the lymph node and enter circulation, they can activate additional signaling pathways through PSGL-1/selectin interactions on endothelial cells, inducing cellular migration through cytoskeleton rearrangement (79). It is unknown whether migration signaling pathways alter the function of anti-tumor T cells as they enter tumors. Whether anti-tumor $CD4^+$ and $CD8^+$ T cells engage selectins in tumors and if these interactions contribute to T cell exhaustion is unknown. However, a chronic viral infection model showed that blocking P, E, and L selectins did not reverse anti-viral $CD8^+$ T cell exhaustion (80), indicating that other PSGL-1 binding partners outside of selectins may promote T cell exhaustion.

Chemokines

While the selectins have been well studied as receptors for PSGL-1 and their involvement in immune cell trafficking during inflammation, the chemokines CCL19 and CCL21 have also been shown to bind PSGL-1 under steady state conditions (81-83) (**Fig. 1.3, Table 1.1**). The interactions between PSGL-1 and these chemokines are important for homing of resting lymphocytes into secondary lymphoid tissues. Mature dendritic cells can produce and secrete CCL19, whereas CCL21 is secreted by endothelial cells in lymphatic vessels. Both CCL19 and CCL21 are produced and secreted by stromal cells in the spleen, lymph nodes, and the lumen of high endothelial venules (84). Naïve and memory T cells can all bind these chemokines through CCR7 interactions, which provide lymphocytes multiple opportunities to circulate through secondary lymphoid tissues and detect antigens presented by antigen presenting cells (85, 86). Importantly, as $CCR7^+$ effector T cells progress

to an exhausted state during viral infection, they downregulate CCR7 expression (85). This CCR7 downregulation is also observed in virus specific $CD8^+$ T cells during lymphocytic choriomeningitis virus (LCMV) infection (87). It is at these key stages when $CD4^+$ and $CD8^+$ T cells downregulate CCR7 that they may have PSGL-1 accessible to interact with CCL19 and CCL21 chemokines (**Fig. 1.3, Table 1.1**). These chemokines could impact anti-tumor T cell responses through PSGL-1 engagement in the tumor draining lymph nodes. Indeed, CCL19 and CCL21 have been shown to induce activation induced cell death (AICD) of responding $CD4^+$ T cells (88). PSGL-1 engagement by these chemokines in tumor draining lymph nodes may induce cell death of anti-tumor T cells, resulting in decreased effector T cells exiting lymph nodes and thereby reducing infiltration in tumors. $CD4^+$ and $CD8^+$ T cells interactions with dendritic cells during priming and later stages of T cell activation could be meditated by PSGL-1 and CCL19/CCL21 interactions since inflammatory dendritic cells also express PSGL-1 (89). Furthermore, whether cDC1 cells utilize PSGL-1 during tumor antigen presentation to both $CD4^+$ and $CD8^+$ T cells is unknown. More work is needed to provide insight into how PSGL-1/chemokine interactions and signals may be playing a role in the T cells response to virus infection and tumors.

Versican

Versican, a chondroitin sulfate proteoglycan that is found in the extracellular matrix of a wide range of cell types including epithelial, endothelial, stromal cells and leukocytes has also been shown to bind PSGL-1 (90-92) (**Fig. 1.3, Table 1.1**). Some of its functions include mediating cellular adhesion, migration, proliferation, and differentiation (93-96). The specific binding between PSGL-1 and versican has been reported to mediate leukocyte aggregation (92). In addition to binding PSGL-1, versican can also bind TLR2, and P- or L-selectin (92, 97-101) and is reported to be both pro- and anti-inflammatory. Mice treated with LPS and siRNA to inhibit versican showed increased leukocyte

infiltration into the lungs and inflammatory TNF-a, NFkB and TLR2 levels, illustrating that versican can limit inflammation (102). Macrophages stimulated with LPS showed an increase in versican expression as these cells became more inflammatory (103, 104). Versican is a relevant PSGL-1 ligand to consider during therapeutic design, as versican has been found to be increased in several cancers (105-107). In the tumor microenvironment (TME), both cancer cells and stromal cells can be a source of versican (108-110). Myeloid cells also produce versican, high levels of which can promote tumor metastasis reduce $CD8^+$ T cell infiltration (91, 111, 112). Tumor cell-derived versican can also induce the upregulation of PD-L1 on monocytes and macrophages (113), an important molecular driver of T cell exhaustion. As it is known that PSGL-1 binds versican, and that versican seems to be playing a pro-tumoral role in the TME, it is possible that versican-PSGL-1 interactions in the tumor microenvironment may inhibit T cell infiltration and prevent tumor killing (**Fig. 1.3, Table 1.1**). Versican is an important PSGL-1 ligand that should be investigated further and considered as a target for cancer immunotherapy.

Siglec-5

Sialic acid-binding immunoglobulin-type lectins (Siglecs), are expressed on the cell surface of both innate and adaptive immune cells (114). These surface receptors recognize and bind glycans and are involved in various diseases including sepsis and cancer (115-118). While multiple Siglecs have been identified in humans and mice, Siglec-5 (only expressed in humans), has been shown to bind PSGL-1 (119) (**Fig. 1.3, Table 1.1**). Siglec-5 is expressed in neutrophils, mast cells, monocytes, pDCs, *in vitro* generated DCs, NK cells and in T cells after stimulation (120-125). PSGL-1 is highly sialylated and was found to bind soluble Siglec-5 in a calcium- and dose-dependent manner (119). Furthermore, sialidase treatment of PSGL-1 reduced Siglec-5 binding. Studies also showed that on human PBMCs, both Siglec-5 and PSGL-1 are closely associated, and *in vitro* perfusion assays demonstrated that

soluble Siglec-5 inhibited leukocyte rolling on E- and P-selectin, indicating that Siglec-5 may have an anti-adhesive role. This was also observed in a model of TNF-α induced inflammation, wherein injection of soluble Siglec-5 in mice prevented inflammatory leukocyte recruitment (119). While it appears that Siglec-5 may inhibit leukocyte migration, the role of PSGL-1 and Siglec-5 binding in the T cell response is unknown.

VISTA

Recently, V-domain immunoglobulin suppressor of T cell activation (VISTA), a known negative regulator of T cells, was shown to be another ligand for PSGL-1 (126). Myeloid and granulocytes are the primary VISTA-expressing cells, however, T cells express low levels and tumor cells can also express VISTA (126-128). VISTA was reported to bind PSGL-1 and suppress T cell activity in acidic conditions *in vitro*, like those found in tumor microenvironments (129) (**Fig. 1.3, Table 1.1**). P-selectin binding to PSGL-1 is dependent on sulfotyrosine and sialyl-Lewis X tetrasaccharide modifications (130), while VISTA- binding depends on tyrosine sulfation but not sialyl-Lewis X modifications on PSGL-1 (129). Moreover, blocking PSGL-1/VISTA binding reversed VISTA-mediated immune suppression (129). The suppressive binding of VISTA to PSGL-1 in acidic conditions may be a potential tumor evasion strategy, highlighting both a new role for PSGL-1 in tumors and the possibility of targeting PSGL-1 and/or VISTA for future immunotherapies.

1.2.3 PSGL-1 signaling

Numerous studies have focused on understanding the signaling pathways that are activated upon PSGL-1 engagement. Some of the earliest studies looking into PSGL-1 signaling have demonstrated that engagement of PSGL-1 promotes tyrosine phosphorylation, as well as activation of MAPKs (131). As research progressed, it has become clear there are multiple, complex PSGL-1 signaling pathways in different cell types. In neutrophils, signaling through PSGL-1 is induced through

PSGL-1-selectin interactions. PSGL-1 engagement with P- and E-selectin results in the phosphorylation of the src family kinases (SFKs), Fgr, Lyn, and Hck, as well as Akt, spleen tyrosine kinase (Syk), and phospholipase C (PLC) γ2 (132-134). This signaling cascade results in lymphocyte function-associated antigen 1 (LFA-1) activation and engagement with intercellular adhesion molecule 1 (ICAM-1), leading to slow rolling in neutrophils. Interestingly, it has been found that L-selectin is vital to this signaling pathway, as *Sell*$^{-/-}$ neutrophils failed to phosphorylate SFKs and downstream proteins *in vitro*, and showed increased rolling velocities and diminished adhesion *in vivo* (132).

Specifically, in the context of E-selectin engagement of PSGL-1 on neutrophils, the cytoplasmic domain of PSGL-1 signals through the src-family kinase Fgr and the ITAM adapters DAP12 and FcRγ (133). While initial results showed that mice lacking Fgr fail to transmit adhesion signals, a follow up study showed that a combined deletion of both Hck and Lyn had a similar result, indicating that while Fgr may be the dominant SFK involved in the PSGL-1-selectin signal transduction, Hck and Lyn together play an important role in this pathway (135). The importance of the ITAM adaptor proteins to PSGL-1 signaling has also been demonstrated. In DAP12 and FCRγ-deficient neutrophils, engagement with E-selectin failed to phosphorylate Syk, and slow rolling was not achieved, indicating the necessity of these two adapter proteins in PSGL-1 driven adhesion signaling. The final steps after Syk recruitment in the E-selectin/PSGL-1-mediated signaling cascade involve the activation of SH2 domain–containing leukocyte phosphoprotein of 76 kD (SLP-76), which in turn activates the Tec kinase Bruton tyrosine kinase (Btk) (135-137). Btk facilitates the phosphorylation of Akt, PLCγ2, and p38 mitogen-activated protein kinase (p38 MAPK), which cumulate in LFA-1-dependent slow rolling of neutrophils on ICAM-1 (134, 138).

PSGL-1 has also been shown to associate with ezrin and moesin. While the interactions of PSGL-1 with SFKs and ITAM adaptor proteins signal to promote slow rolling, it appears that the

interactions of PSGL-1 with ezrin and moesin promote leukocyte transcriptional changes and transient MAPK activation. It has been shown that PSGL-1 interacts directly with the amino-terminal domain of both moesin and ezrin, and that these interactions take place in the uropods of activated neutrophils (139, 140). Moesin and ezrin, like DAP12 and FcRγ, are ITAM-adapters that are able to recruit Syk (141). While moesin and ezrin are capable of Syk activation, the signaling outcomes seem to differ from the previously detailed PSGL-1 signaling pathway involving SFKs, DAP12 and FcRγ. *In vitro* experimentation using a leukocyte cell line found that PSGL-1 signaling through ezrin and moesin resulted in an increase in serum response element (SRE) transcription and expression of the early-activation *C-fos* gene. Further *in vitro* experiments showed that the ezrin-radixin-moesin-binding Sequence (EBS) on the cytoplasmic tail of PSGL-1 was not necessary for Syk activation (139). While the EBS sequence was shown to support leukocyte tethering to selectins, integrin activation and slow rolling on ICAM-1 is not dependent on ezrin and moesin binding to PSGL-1. Instead, ezrin and moesin engagement with PSGL-1 promotes transient phosphorylation of ERK. From these studies, it is clear that PSGL-1 signaling is multi-faceted and that its engagement with selectins can result in numerous outcomes, ranging from increased activation signals to increased adherence and slow rolling.

There has been less research evaluating PSGL-1 signaling in T cells, however it has been found that PSGL-1 on T cells can have a similar role in signaling integrin-driven adhesion. The use of a PSGL-1 cross-linking antibody resulted in increased LFA-1 clustering (142). This upregulation of LFA-1 promoted adhesion of Th1 cells to ICAM-1 and was driven at least in part by PSGL-1 signaling through PKCα or PKCβII. In addition to promoting adhesion and migration of T cells, PSGL-1 ligation can promote inflammatory responses. Although, many experiments that investigate PSGL-1 inflammatory signaling involve a ligating antibody, these approaches may result in signaling outcomes that differ from PSGL-1 ligand binding. *In vitro* experiments using leukemic Jurkat cells found that

antibody ligation of PSGL-1 upregulated transcription of the inflammatory cytokine IL-18 through a pathway involving phosphatidylinositol 3-kinase (PI3K) (79). Antibody ligation of PSGL-1 on Jurkat cells was also found to increase transcription of colony-stimulating factor 1 (CSF-1) in a Syk-dependent manner (143). While these studies show that PSGL-1 can promote inflammatory transcriptional responses, the transcriptional responses peaked at 30 or 60 minutes, indicating that PSGL-1 inflammatory signals may be transient and require further study.

The question then is raised as to the timing of PSGL-1 signaling, and whether signaling output changes depending on the duration of PSGL-1 engagement and the length of time that a T cell has been activated. While direct mAb engagement of PSGL-1 *in vitro* promoted an increase in inflammatory signals, the timing of PSGL-1 engagement does result in differential signaling outputs. On late stage activated T cells, PSGL-1 signaling has been shown to promote T cell death (144). Both the binding of activated T cells to P- and E-selectin under flow, as well as antibody crosslinking of PSGL-1, can trigger apoptosis in late-stage activated T cells. This PSGL-1-driven apoptosis involves Apoptosis Inducing Factor (AIF) translocation to the nucleus and the subsequent release of cytochrome C, although the full pathway through which PSGL-1 signals induce apoptosis remains to be identified. Further, PSGL-1 signaling has been shown to transduce suppressive signals in periods of prolonged T cell activation. During chronic viral infection, PSGL-1 engagement promotes effector T cell exhaustion (80). While the intracellular signals that direct this PSGL-1 driven enhancement of T cell exhaustion are not known, it has been shown that ligation of PSGL-1 on exhausted $CD8^+$ T cells resulted in diminished ERK and AKT signaling (80).

How PSGL-1 signaling in anti-tumor T cells supports their functional exhaustion and inhibitory signaling is not fully known. Since T cells will be in an immunosuppressive environment with chronic antigen stimulation inside tumors, PSGL-1 signals may be transient or prolonged

depending on ligand binding. In steady-state conditions, PSGL-1 engagement promotes a tolerogenic DC phenotype *in vivo*, increasing the formation of $CD4^+FOXP3^+$ T regulatory cells in the thymus (78). When considering that PSGL-1 signaling prompts immunosuppression both through an increase in the tolerogenic DC phenotype and Treg formation, as well through a decrease in T cell receptor (TCR) signaling, targeting PSGL-1 presents a viable path to increase the inflammatory phenotype of $CD4^+$ and $CD8^+$ T cells. Although PSGL-1 plays a role in signaling for slow rolling and adhesive behavior, this pathway shows redundancy, as PSGL-1 genetic deletion did not decrease migration/infiltration of T cells to the tumor site (80). PSGL-1 signaling is complex and much remains to be discovered, but its suppressive signaling in T cells makes it an attractive target for reinvigorating the immune response.

1.2.4 PSGL-1 in disease

When considering PSGL-1 as a therapeutic target, it is necessary to understand the differing roles that PSGL-1 plays depending on the cancer context. As PSGL-1 is known to facilitate attachment and migration, a large body of research has been centered around the role of PSGL-1 in cancer metastasis. In a murine model of multiple myeloma (MM), PSGL-1 on MM cells was shown to interact with P-selectin to promote adhesion signaling and homing of MM cells to the bone marrow (145). In this model, the deletion of PSGL-1 on MM cells led to a significant decrease in tumor initiation and proliferation, illustrating the importance of PSGL-1 in promoting tumorigenesis.

Interestingly, PSGL-1 has also been found on bone-metastatic prostate cancer and lung carcinomas (146, 147). PSGL-1 was linked with metastasis, as it was expressed on a bone-metastatic prostate cancer cell line and in metastatic prostate tumor tissue, indicating that certain cancer types may gain PSGL-1 expression as a part of a metastatic phenotype. The mechanism through which PSGL-1 may facilitate prostate cancer metastasis is unknown, however, in a non-small cell lung cancer

(NSCLC) cell line, PSGL-1 was found to facilitate interactions between lung cancer cells and activated platelets (147). This interaction between P-selectin on activated platelets and PSGL-1 on tumor cells is hypothesized to drive metastasis, as activated platelets are known to facilitate metastatic movement of cancer cells (148). In the context of small cell lung cancer (SCLC), cancer cell interactions with P- and E-selectin have been shown to promote robust metastasis. As PSGL-1 is a ligand for both selectins, it is likely that PSGL-1 is involved in the selectin-mediated metastatic behavior of SCLC cells as well (149). Additionally, P-selectin blockade in mice with gastric cancer decreases metastasis and allows for sustained immune function, a phenotype showing that PSGL-1 likely plays a role in as the main P-selectin ligand (150). While these experiments show that PSGL-1 plays a pro-metastatic role, the contributions of PSGL-1 on immune cells to this phenotype are still being uncovered. One study showed that PSGL-1 promoted colon cancer metastasis through the recruitment of monocytes to metastatic sites, illustrating how PSGL-1 on immune cells may modulate cancer cell behavior and the TME (151). Although the impact that targeting PSGL-1 on T cells or cancer cells will have on cancer metastasis is unknown, these studies illustrate that PSGL-1 presents an exciting target for potentially reducing metastatic behavior of tumors.

In addition to promoting cancer metastasis, PSGL-1 is involved in the development of drug resistance, particularly in blood cancers. It has been shown that PSGL-1-mediated interactions between multiple myeloma (MM) cells and macrophages increased ERK1/2 activation, myc upregulation, proliferation, and drug resistance in MM cells (152). The use of a PSGL-1 neutralizing antibody abrogated this MM drug resistance *in vivo*, signifying PSGL-1 as an important driver of MM therapeutic escape. In a separate model of MM, it was found that combination antibody blockade of PSGL-1 and P-selectin lessened bortezomib resistance in MM cells, and led to increased mouse survival (153). Additionally, PSGL-1 was shown to promote chemoresistance in a human acute myeloid leukemia (AML) cell line through interactions with E-selectin (58). Through *in vivo* mouse

models of AML, it was seen that *Selplg*$^{-/-}$ AML blasts showed increased cell cycling, decreased homing to the bone marrow, and increased chemosensitivity. This study showed that PSGL-1 is involved in the formation of bone marrow reservoirs of quiescent, chemoresistant AML cells and is correlated with worse disease outcomes in mice with WT AML blasts.

Taken together, the current body of research has found PSGL-1 to be expressed on numerous human SCLC cells lines (149, 154), on a human alveolar cell carcinoma cell line (147), on human MM cell lines (152), and on a metastatic prostate cancer cell line (146). In the clinic, PSGL-1 expression has been detected in primary acute leukemia cells as well as in some acute lymphoblastic leukemia cells from large patient cohorts (58, 155). Further, a link between disease progression and PSGL-1 expression was shown in a group of MM patients, PSGL-1 was significantly increased in active MM disease when compared to both monoclonal gammopathy of undetermined significance (MGUS) and healthy donors (145). PSGL-1 is expressed in many cancers and is involved in disease progression, metastasis, and drug resistance. Importantly, few studies have examined how PSGL-1 expression is regulated in cancers that are not hematopoietic cell-derived. The potential impact of targeting PSGL-1 on tumor control is evident from mouse studies, however the question remains as to whether PSGL-1 blockade affects $CD4^+$ and $CD8^+$ T cells and other immune cells within the TME of human cancers.

1.2.5 PSGL-1 as an immune checkpoint protein

When investigating the role of PSGL-1 on immune cells in numerous diseases, there is a growing body of literature supporting the notion that PSGL-1 functions as a negative regulator of the immune system. In a murine DSS-induced colitis model, PSGL-1 was shown to decrease the inflammatory immune response, resulting in reduced disease severity (156). There is evidence that in diseases of chronic inflammation, such as systemic lupus erythematosus (SLE), PSGL-1 signaling works to suppress inflammation, as *Selplg*$^{-/-}$ mice with SLE suffer more inflammation and early death

(157). In this murine SLE model, *Selplg*$^{-/-}$ mice had increased amounts of the inflammatory chemokine CCL2 present in the kidneys. CCL2 is known to promote cytokine production in CD4^{+} T helper cells, and chemotaxis of T cells and monocytes (158-161). The reduction in CCL2 production driven by PSGL-1 demonstrates a possible mechanism through which PSGL-1 controls inflammation and limits the induction of T cells responses. Immunotherapeutic blockade of PSGL-1 may increase inflammatory chemokines present *in vivo* and promote a more inflammatory CD4^{+} T cell phenotype.

Mice with genetically deleted PSGL-1 have been valuable in showing the role that PSGL-1 plays in inflammatory immune responses. *Selplg*$^{-/-}$ mice have shown to develop a systemic sclerosis (SSc)-like syndrome. In these mice, the absence of PSGL-1 led to a notable decrease in Tregs in the lungs and an increase in IFN-γ-producing T cells and macrophages, highlighting the role of PSGL-1 in suppressing autoimmunity (162). Another autoimmunity study of SSc-like disease in *Selplg*$^{-/-}$ mice found increased serum levels of autoantigens, activated DC and CD4^{+} T effector cells in the skin, vascular damage, and increased mortality rates in mice due to loss of PSGL-1 (163). In the absence of PSGL-1, T cells become more inflammatory and can cause chronic inflammation and autoimmunity. The inflammatory T cell phenotype seen in *Selplg*$^{-/-}$ mice provides support for the therapeutic targeting of PSGL-1 on T cells in cancer, as it may provide a way to lessen immune suppression and increase the activation of T cells. However, these studies showed that deletion of PSGL-1 led to increased autoimmune occurrences, so patients treated with PSGL-1-targeting treatments would need to be monitored closely for treatment side effects.

Understanding the differential roles of PSGL-1 on effector T cells and Tregs is particularly important when considering PSGL-1 as an immunotherapeutic target. Sustaining a more effector-like T cell response is vital for the immune system to control cancer, and PSGL-1 can affect the balance of inflammatory and suppressive cells. As mentioned previously, *Selplg*$^{-/-}$ mice with DSS-induced colitis

show an increased effector T cell to Treg ratio in the colon, a trend that was also observed in the lungs of *Selplg*$^{-/-}$ mice (156, 162). In an experimental autoimmune encephalomyelitis (EAE) model, PSGL-1 on Tregs was found to be necessary for suppression of the late stage T cell response (45). Tregs lacking PSGL-1 were unable to limit T cell proliferation and interactions with DCs in the late stages of T cell activation, leading to worsening of the EAE disease phenotype. In addition to limiting the immune response in autoimmune diseases, PSGL-1 on Tregs can affect immune control of cancer (164). Mice lacking P-selectin showed a largely diminished tumor size and a markedly small presence of Tregs in tumors (164). The absence of P-selectin leads to an increase in tumor-infiltrating effector $CD8^+$ T cells, an increase in pro-inflammatory cytokines, and a decrease in tumoral TGF-β (164). Although this study did not directly address the role of PSGL-1, as the primary ligand for P-selectin, it is likely supporting P-selectin driven phenotypes. Taken together, PSGL-1 promotes development and Treg function and may lead to a reduction in immunosuppression when targeted as an immunotherapy.

Effector T cells are also affected by PSGL-1 signaling. In an *in vitro* setting, stimulated T cell proliferation was negatively regulated by PSGL-1 (165). *In vivo*, PSGL-1-mediated suppression of effector T cell functions has been seen in multiple disease models. In mice with T cell driven inflammatory bowel disease, deletion of PSGL-1 on T cells caused a significant worsening of the disease. The absence of PSGL-1 in mice with a chronic infection led to much more functional, effector-like T cells (80). Although the mechanism is still being studied, it has been shown that PSGL-1 can dampen TCR signals and effector functions. Further, mice lacking PSGL-1 showed increased melanoma tumor control and reduced T cell exhaustion within the tumor environment (80). In models of chronic infection and cancer, antigen-specific *Selplg*$^{-/-}$ T cells had increased tumor infiltration and increased response to PD-L1 blockade (166). Interestingly, PSGL-1 deletion resulted in decreased Tpex frequencies, although the full impact of PSGL-1 on Tpex and Tex formation and phenotype are still under investigation. The work done to understand the roles of PSGL-1 in disease has shown that

PSGL-1 can function as a potent suppressor of immune responses. Targeting PSGL-1 on $CD4^+$ T cells may be new opportunity to not only increase effector T cells, but also to reduce the detrimental presence of Tregs in the TME.

1.3 CD38 overview

CD38 is an ectoenzyme expressed on the surface of most innate and adaptive immune cells (167-169). CD38 plays an important role in energy metabolism, as its enzymatic activity drives the consumption of nicotinamide adenine dinucleotide (NAD^+) and supports adenosine generation (170-172). More specifically, CD38 catalyzes the conversion of NAD^+ to ADP-ribose (ADPR), cyclic-ADPR (cADPR), and $NAADP^+$ (167, 168, 170, 171). Additionally, CD38 in combination with CD203a and CD73, form an enzymatic axis capable of converting NAD^+ to adenosine (172). CD38 enzymatic activity has numerous physiological impacts, as ADPR, cADPR, and $NAADP^+$ all regulate cytoplasmic Ca^{2+} levels while NAD^+, which is consumed by CD38, is a modulator of cellular metabolism, stress response, and circadian rhythms (167, 168). Increased CD38 expression depletes NAD^+ levels and increases intracellular Ca^{2+}, illustrating how CD38 expression functions as an important immune modulator (173-175). CD38 expression is directly linked with activation signals: CD38 is induced by CD3 stimulation and reduced when CD3 is diminished, and agonistic engagement of CD38 *in vitro* resulted in increased expression of IL-2, IL-1, and IL-6 mRNA (169). *In vitro* activation of T cells caused CD38 upregulation and co-expression with activation markers such as CD25 and CD44, further demonstrating a link between activation and CD38 expression(176). Additionally, CD38 acts as a receptor on the surface of T cells, the ligation of which can further increase T cell activation through Lck-mediated activation of MAP kinase and CD3**ζ** signaling pathways (177).

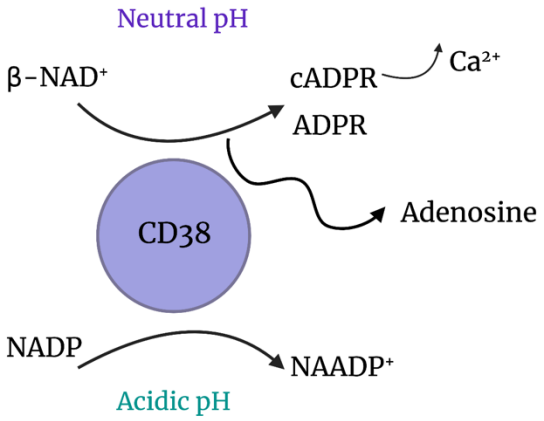

Figure 1.4 CD38 enzymatic activity at neutral and acidic pH.

1.3.1 CD38 in disease

Given the prevalence of CD38 on most immune cells, it is notable that CD38 has been implicated in numerous infections and disease. In a mouse model of *Listeria monocytogenes*, DCs, neutrophils, monocytes, and macrophages upregulated CD38 in response to infection, and $Cd38^{-/-}$ mice had increased susceptibility to infection (178). A similar result was seen in a mouse model of *Streptococcus pneumoniae*, in which mice lacking CD38 were more susceptible to infection (179). Further, mice lacking CD38 had diminished cADPR in myeloid and lymphoid tissues, an important metabolic mediator of inflammation (179, 180). The upregulation of CD38 in response to infection is in part due to regulation of the Cd38 gene locus by interferon signaling and transcription factors NF-κB and AP-1(181-183). Further, the endothelial adhesion molecule CD31 is a known ligand for CD38 and is involved in recruitment of immune cells to sites of infection and inflammation (184, 185). In addition to bacterial infections, numerous autoimmune diseases display CD38 upregulation. Murine models of experimental autoimmune encephalomyelitis (EAE) and multiple sclerosis (MS) revealed an

upregulation of CD38 in cells from lymph nodes of diseased mice (186). CD38 was also found to be highly expressed on B cells, macrophages, and monocytes from patients with active systemic lupus erythematosus (SLE) (187, 188). CD38 expression correlated with higher scoring on the SLE disease activity index, indicative of worse disease pathology (188). The prevalence of CD38-expressing cells in inflammatory conditions has resulted in a clinical push to target CD38 for the treatment of autoimmune disorders such as rheumatoid arthritis and SLE (189, 190).

CD38 is also upregulated in response to viral infection. CD38 is a key indicator of T cell activation during viral infection, and $CD38^{hi}CD8^{+}$ T cells have been detected in patients infected with HCV, HIV, Dengue, H1N1 IAV, H7N9, Ebola, and SARS-CoV-2 (191-199). In the case of chronic viral infections, such as HIV, CD38 expression is correlated with disease severity (200). During HIV infection, CD38 is upregulated on T cells and can serve as a marker of disease progression (201-203). As patients develop acquired immune deficiency syndrome (AIDS), the frequency of CD38 expressing $CD8^{+}$ T cells increases, and then declines with antiretroviral treatment (201, 204, 205). In cases of H7N9 avian influenza, a larger population of $CD38^{+}$HLA-$DR^{+}CD8^{+}$ T cells are found in patients who succumb to flu (196). In both Dengue and Ebola-infected patients, $CD8^{+}CD38^{+}$ T cells are upregulated in febrile patients (194, 196, 206).

The disease area with the largest body of literature and clinical trials with respect to CD38 is cancer. CD38 is highly expressed on multiple myeloma (MM) cells and has been effectively utilized as a target for MM treatment (207). Chronic lymphocytic leukemia also highly expresses CD38, and expression levels have been linked to poor prognostic outcomes in patients (208). Numerous other blood cancers upregulate CD38, and there are multiple FDA-approved therapies targeting CD38 including the 2018 approval of Janssen's human anti-CD38 IgG1 daratumumab (209). In addition to CD38 as a marker for cancer, its expression has numerous impacts on tumor growth and

immunogenicity. Murine lung adenocarcinoma cells express CD38 and use the product of its enzymatic activity, cADPR, to promote Ca^{2+} and tumor progression (210). Further investigation showed that CD38 is upregulated in lung cancer by all-trans retinoic acid (ATRA) and IFNβ, and that CD38 expression in murine lung and melanoma models, as well as in patient samples, promotes resistance to PD-L1 and PD-1 treatment (211). A key component of tumor growth and resistance to immune-checkpoint blockade is adenosine, which is enriched in $CD38^{+}$ tumors and suppresses the anti-tumor immune response. The impact of CD38 activity on tumor-infiltrating immune cells is two-fold: CD38 depletes NAD^{+}, an important molecule for T cell metabolism and effector function, and adenosine is created, which suppresses effector T cells (211-213). CD38 is also upregulated on Tregs from patients with multiple myeloma, and these $CD38^{hi}$ Tregs were highly immunosuppressive and tumor-promoting (214). Macrophages in the tumor environment are also high expressors of CD38 and can promote tumor growth through adenosine production as well (215). Our current knowledge highlights the importance of CD38 as a marker of infection and disease, as a target for cancer and autoimmunity treatment, and as modulator of inflammation and immunotherapy response. However, the precise roles of CD38 on activated and exhausted T cells in response to cancer and chronic infection remain to be investigated.

1.3.2 CD38 on T cells and possible role in exhaustion

A strong link between T cell activation and CD38 has been established, as CD38 is upregulated on activated T cells, localizes to the immunological synapse upon interaction between antigen presenting cells (APC) and T cells, and has a role in MAPK and Ca^{2+} signaling (167, 177, 216). Further, the enzymatic activity of CD38 alters T cell functioning through the depletion of NAD^{+} and the formation of ADPR, cADPR, $NAADP^{+}$, and downstream adenosine (167, 168, 170, 171). Although CD38 is highly upregulated on T cells in multiple infection types as well as on tumor-infiltrating T

cells, the impact of CD38 expression on T cell biology is still being investigated. In the case of chronic infection and cancer, several pieces of evidence have emerged linking CD38 to T cell exhaustion. A study by Philip *et al* analyzed the transcriptional landscape and chromatin accessibility of tumor-specific exhausted T cells and found that *Cd38* mRNA and CD38 surface expression were markers of terminal exhaustion state (217). Tumor-specific T cells that expressed CD101 and CD38 had a fixed chromatin state associated with dysfunction and were unable to produce cytokines in response to *in vitro* stimulation. The expression of CD38 as a marker for terminal exhaustion was corroborated in two separate chronic infection studies, showing that *Cd38* mRNA is significantly upregulated in terminal exhausted cells (39, 218). Further, when improperly primed, PD-$1^{+}$$CD38^{+}$ cells from tumor-bearing mice showed increased death and decreased expression of CD40L and IFN-γ production (219). When data from patients with melanoma tumors was investigated, high frequencies of PD-$1^{+}$$CD38^{+}$ T cells correlated with immunotherapy non-responders. CD38 has also been found to reduce mitochondrial fitness and cytotoxic responses in SLE and LCMV models, and CD38-expressing $CD4^{+}$ T cells from patients with inflammatory bowel disease showed elevated expression of exhaustion markers TIGIT, CTLA4, PD-1, TIM-3, and CX3CR1 (220, 221). Recently, a study investigating the impact of CD38 deletion on the formation of antigen-specific exhausted T cells in tumors found that *Cd38*$^{-/-}$ cells still became functionally exhausted (222). This study opens more questions about the role that CD38 may play in shaping the T cell response to infection and cancer, as it is uniquely upregulated in response to strong TCR signaling but may be dispensable for the formation of the exhaustion phenotype.

CHAPTER 2

Targeting the PSGL-1 Immune Checkpoint Promotes Immunity to PD-1 Resistant Melanoma

Julia M. DeRogatis[1], Karla M. Viramontes[1,7], Emily N. Neubert[1,7], Monique L. Henriquez[1], Christian F. Guerrero-Juarez[2,3,4,5,6], and Roberto Tinoco[1]

[1]Department of Molecular Biology and Biochemistry, School of Biological Sciences, University of California, Irvine, CA 92697, USA
[2]Department of Developmental and Cell Biology, University of California, Irvine, CA 92697, USA
[3]Sue and Bill Gross Stem Cell Research Center, University of California, Irvine, CA 92697, USA
[4]Department of Mathematics, University of California, Irvine, CA, 92697, USA
[5]Center for Complex Biological Systems, University of California, Irvine, CA 92697, USA
[6]NSF-Simons Center for Multiscale Cell Fate Research, University of California, Irvine, CA, 92697, USA
[7]Contributed equally

Published in *Cancer Immunology Research*. DeRogatis JM, Viramontes KM, Neubert EN, Henriquez ML, Guerrero-Juarez CF, Tinoco R. 2022. Targeting the PSGL-1 Immune Checkpoint Promotes Immunity to PD-1-Resistant Melanoma. Cancer Immunol Res 10:612-625 (223)

ABSTRACT

Immune checkpoint inhibitors have had impressive efficacy in some cancer patients, reinvigorating long-term durable immune responses against tumors. Despite the clinical success of these therapies, most cancer patients continue to be unresponsive to these treatments, highlighting the need for novel therapeutic options. While PSGL-1 has been shown to inhibit immune responses in a variety of disease models, previous work has yet to address whether PSGL-1 can be targeted therapeutically to promote antitumor immunity. Using an aggressive melanoma tumor model, we targeted PSGL-1 in tumor-bearing mice and found increased effector $CD4^+$ and $CD8^+$ T cell responses, and decreased Tregs in tumors. T cells exhibited increased effector functions, activation, and proliferation, which delayed tumor growth in mice after anti-PSGL-1 treatment. Targeting PD-1 in PSGL-1-deficient tumor-bearing mice led to an increased frequency of mice with complete tumor eradication. Targeting both PSGL-1 and PD-1 in WT tumor-bearing mice also showed enhanced anti-tumor immunity and slowed melanoma tumor growth. Our findings show that therapeutically targeting the PSGL-1 immune checkpoint can reinvigorate anti-tumor immunity and suggest that targeting PSGL-1 may represent a new therapeutic strategy for cancer treatment.

INTRODUCTION

Immune checkpoint inhibitors have revolutionized the treatment of many cancer types, including melanoma, and are now standard of care (224, 225). Blocking the PD-1/PD-L1 and CTLA-4 pathway in melanoma has shown efficacy in patients through the reinvigoration of anti-tumor T cells (226, 227). While these immune checkpoint inhibitors show significant clinical success in multiple cancer types, most patients with melanoma remain unresponsive, and many develop immune-related adverse events (irAEs) (225, 228-231). Immune checkpoints in melanoma actively suppress T cells to induce an exhausted dysfunctional state, which promotes tumor growth and metastasis (232). The high expression of these immune checkpoints on exhausted T cells diminishes their effector functions and cytotoxicity (233). While PD-1 and CTLA-4 have been well studied, additional immune checkpoints have been identified that also promote T cell exhaustion, including P-selectin glycoprotein ligand-1 (PSGL-1) (234).

Most tumor-infiltrating leukocytes involved in the immune response express PSGL-1 (81, 235, 236). While T cells utilize PSGL-1 for migration through selectin interactions, PSGL-1 binds additional molecules such as Siglecs, chemokines, and the recently identified ligand, VISTA (82, 83, 119, 129). PSGL-1 and selectin-mediated migration has been extensively studied, however, less is known regarding PSGL-1 engagement in the tumor microenvironment, and whether these interactions promote T cell exhaustion (68). Much of what is known regarding PSGL-1 immune inhibitory function has relied on the use of PSGL-1-deficient mice (*Selplg*$^{-/-}$) (74). Studies have shown that *Selplg*$^{-/-}$ mice develop autoimmunity involving the skin, lungs, and kidneys (237). In addition, *Selplg*$^{-/-}$ mice were shown to develop glomerulonephritis in lupus-prone mice, scleroderma, ulcerative colitis and experimental autoimmune encephalomyelitis (73, 238-240). *Selplg*$^{-/-}$ dendritic cells (DCs) are more immunogenic, and PSGL-1 signaling in human monocyte-derived DCs leads to a tolerogenic phenotype that promotes Treg differentiation (241). Furthermore, *Selplg*$^{-/-}$ mice were found to generate

less Tregs in the thymus (241-243). PSGL-1 inhibitory function in T cells was also found during immune responses to viral infections and tumors (234, 244). *Selplg*$^{-/-}$ mice were shown to control chronic viral infection and melanoma tumors through increased effector T cell responses (234), and PSGL-1 was also shown to restrain proliferation of memory T cells during acute viral infection (245). These studies also showed that despite lacking PSGL-1 expression, *Selplg*$^{-/-}$ effector T cells efficiently migrated to infected tissues and tumors (234). Together, these studies identify PSGL-1 as an important negative immune regulator that not only facilitates T cell migration, but also functions as an immune checkpoint in T cells (234, 245, 246). While studies using *Selplg*$^{-/-}$ have been important for our understanding of PSGL-1 biology, it has not been explored whether PSGL-1 can be therapeutically targeted in WT mice with established aggressive melanoma tumors. Here we report therapeutic efficacy targeting the PSGL-1 immune checkpoint *in vivo* in melanoma tumor-bearing mice which resulted in delayed tumor growth attributed to enhanced effector T cell responses. Our findings highlight that targeting the PSGL-1 inhibitory pathway therapeutically is an effective strategy to enhance anti-tumor immunity in melanoma.

MATERIALS AND METHODS

Mice and Experimental Model

All experimental animal procedures were approved by the Institutional Animal Care and Use Committee of University of California, Irvine (AUP-18-148) and complied with all relevant ethical regulations for animal testing and research. C57BL/6J and *Selplg*$^{-/-}$ mice were purchased from the Jackson Laboratory, then bred in SPF facilities. Male mice ≥6 weeks of age were used in experiments. Mouse selection for experiments was not formally randomized or blinded. For tumor growth experiments, mice were injected subcutaneously (s.c.) with 1x10^6 B16-GP_{33} or D4M-3A tumor cells and designated into treatment groups on 8dpi. For survival experiments, mice were injected with 1x10^6 B16-GP_{33} s.c. and tumors of <2000mm^3 were designated as surviving at 18dpi. Mice in each treatment group had an average tumor size of 60-100mm^3 on 8dpi, mice exceeding 100mm^3 at 8dpi were euthanized. For YUMMER1.7 study, mice were s.c. injected with 2x10^6 YUMMER1.7 tumor cells. Tumor size was measured using calipers at the indicated time points. Tumors were weighed at the time of excision.

Cell Lines

Braf$^{V600E/+}$; *Pten*$^{-/-}$; and *Cdkn2a*$^{-/-}$ mouse melanoma cells (YUMMER1.7) were kindly provided by Marcus Bosenberg (Yale). B16GP_{33} melanoma cells were kindly provided by Dr. Ananda Goldrath (UCSD). Dartmouth murine mutant malignant melanoma-3A (D4M-3A) were kindly provided by Dr. Francesco Marangoni (UC Irvine). Cell lines were maintained in Dulbecco's modified eagle's medium (D4M-3A) or Iscove's Modified Dulbecco's medium (YUMMER1.7 and B16-GP_{33}) supplemented with 10% fetal bovine serum and antibiotics. All cell lines were free of mycoplasma.

Tumor digestion

Tumors were excised, minced, and digested for 40 min at 37°C using the gentleMACS tumor kit and gentleMACS™ dissociator (Miltenyi Biotec). Digests were then passed through a 70-μm cell strainer to generate a single-cell suspension. The cells were then stained for flow cytometry.

Flow Cytometry

Tumor-derived single-cell suspensions were washed twice with FACS staining buffer, fixed for 15 min with 1% formaldehyde in PBS, washed twice, and resuspended in FACS staining buffer. For intracellular cytokine staining, cells were resuspended in complete RPMI-1640 (containing 10 mM HEPES, 1% nonessential amino acids and L-glutamine, 1 mM sodium pyruvate, 10% heat inactivated fetal bovine serum (FBS), and antibiotics) supplemented with 50 U/mL IL-2 (NCI) and 1 mg/mL brefeldin A (BFA, Sigma), and then incubated with phorbol myristate acetate (10 ng/ml) and ionomycin (0.5 μg/ml) at 37°C for 16h overnight. Cells were then fixed and permeabilized using a Cytofix/Cytoperm Kit (BD Biosciences) before staining. For intranuclear transcription factor staining, cells were fixed and permeabilized using a Foxp3/transcription factor fixation/permeabilization kit (Invitrogen). Antibodies are listed in Supp. Table 1. Surface stains were performed at a 1:200 dilution, while intracellular and intranuclear stains were performed at a 1:100 dilution. All data were collected on a Novocyte 3000 (Agilent) and analyzed using FlowJo Software (Tree Star).

Tetramer Staining

Tumor-derived single-cell suspensions were stained with tetramer antibodies for an hour and 15 minutes at room temperature in complete RPMI-1640 (containing 10 mM HEPES, 1% nonessential amino acids and L-glutamine, 1 mM sodium pyruvate, 10% heat inactivated fetal bovine serum (FBS), and antibiotics), washed twice, fixed for 15 min with 1% formaldehyde in PBS, washed twice, and resuspended in FACS staining buffer.

In vivo antibody treatments

For antibody treatments, mice were injected i.p. with 200 μg anti-PD-1 (clone RMP1-14), anti-PSGL-1 (clone 4RA10), or rat IgG (Sigma) isotype control on day 8, 10, and 12 after tumor inoculation ($B16GP_{33}$ and D4M-3A) or day 11, 13, and 15 after tumor inoculation (YUMMER1.7). All mAbs for in vivo use were from BioXcell (New Hampshire, USA). $CD8^+$ T cells were depleted by intraperitoneal (i.p.) injection of 400 μg of anti-mouse Thy1.2 (CD90.2) (clone 30H12 from BioXCell), 400ug of anti-mouse Thy1.1 (CD90.1) (clone 19E12 from BioXCell), or rat IgG isotype control. Antibodies were injected at day -1, 0, and 3 ($B16\text{-}GP_{33}$) or day -1, 0, 3, and 14 (YUMMer1.7) in respect to tumor inoculation occurring at day 0. The efficacy of depletion was assessed by FACS analysis of blood samples collected on day 8 ($B16\text{-}GP_{33}$) or day 8, 14, and 21 (YUMMER1.7).

3'-single cell RNA-seq data analyses

WT mice were injected s.c. with (1×10^6) $B16\text{-}GP_{33}$ melanoma cells and treated with IgG, anti-PD-1, anti-PSGL-1, or anti-PSGL-1/anti-PD-1 at 8, 10, and 12dpi. Tumors were excised and processed at 18dpi and immune cells sorted ($PI^-CD45.2^+$) and processed for 3'-single cell RNA sequencing. Sorted cells were subjected to 10X Genomics Chromium Single-Cell Platform manipulation, followed by sequencing using an NovaSeq 6000. Raw reads were subjected to quality control analysis with FASTQC software and aligned to the reference transcriptome mm10 using a short-read aligner STAR68 via 10X pipeline cellRanger (v.3.1.0) software. The following represent the number of cells obtained per sample processed: IgG (9726 cells), anti-PD-1 (5614 cells), anti-PSGL-1 (7292 cells), Combo (4596 cells). All cells had an average read depth of approximately 18,763 reads per cell with 2,500 to 3,000 median unique molecular identifiers across approximately 15,000 genes each.

Doublets observed predominantly in larger analyses, particularly the IgG analysis, were identified and removed using Scrublet (247). Expression matrices underwent filtering (nFeature_RNA

> 200 and < 5,500 - 6000, percent.mt < 5), normalization, scaling, PCA and subsequent UMAP analysis using Seurat packages (248). Resultant Seurat objects were integrated using a CCA (canonical correlation analysis)–based integration method (249). Unique functional cell types were identified by gene expression profiling and query against Immgen gene expression databases (www.immgen.org) using the interactive tool "MyGeneSet". Results were visualized using Seurat FeaturePlot, DotPlot and HeatMap functions. Feature plots and dot plots were generated using Seurat pipeline functions and log-normalized raw counts (data slot). Heatmaps were created using the Seurat DoHeatMap function with log-normalized and scaled raw counts (scale.data slot). All functions were run in the RNA assay.

Data and code availability

The authors declare that all supporting data are available within the Article and its Supplementary Information files. 3'-scRNA-seq data sets will be deposited in the Gene Expression Omnibus (GEO) database under the accession code: GSE196112.

Quantification and statistical analysis

Data were analyzed using Prism GraphPad software. Analysis was performed using two-tailed *t*-test or Mann–Whitney *U* test. Tumor volume growth curves were analyzed by 2nd way ANOVA with Sidak's multiple comparisons test (two groups) or 2nd way ANOVA with Tukey's multiple comparisons test (four groups). Survival was analyzed by log-rank (Mantel-Cox) test. Unless otherwise noted, all data are shown as the mean ± s.e.m.

RESULTS

Selplg is expressed by melanoma tumor-infiltrating immune cells

To determine how PSGL-1 is regulated in tumor-infiltrating immune cells, we implanted wild type (WT) mice with B16-GP_{33}-expressing melanoma cells (250) and evaluated *Selplg* gene expression at 18 days post injection (dpi). We analyzed *Selplg* levels in $CD45.2^+$ sorted cells using 3'-single-cell RNA sequencing (scRNA-seq) (**Fig. 2.1A,B**). We characterized the tumor-infiltrating $CD45.2^+$ cells as both myeloid and non-myeloid immune cells including macrophages, dendritic cells, neutrophils, T cells, NK cells and B cells (**Fig. 2.1A, S2.1 and S2.2A-F**). *Selplg* was expressed by subsets of macrophages, dendritic cells, and neutrophils, with very low expression in B cells (**Fig. 2.1B**). The highest *Selplg* expression levels were observed in $CD4^+$ and $CD8^+$ T cells and NK cells (**Fig. 2.1B**). We analyzed expression levels of the PSGL-1 ligands P-selectin (*Selp*) and VISTA (*Vsir*), and detected uniformly low *Selp* levels, while high *Vsir* expression was observed in macrophages, neutrophils and T cells (**Fig. 2.1C,D and S2.2G,H**). These findings showed that while *Selplg* was expressed in most immune cells, the highest expression was observed in T cells and NK cells that infiltrated melanoma tumors.

PSGL-1 is upregulated and co-expressed with immune checkpoints on tumor-infiltrating T cells

Since we found high *Selplg* expression in tumor-infiltrating T cells, we next characterized how PSGL-1 protein expression was regulated during the anti-tumor response. We detected high PSGL-1 expression in effector $CD4^+$ T cells ($CD4^+CD44^+FoxP3^-$), $CD8^+$ T cells ($CD8^+CD44^+$), and Tregs ($CD4^+CD44^+FoxP3^+$) in tumor draining lymph nodes (TdLN), and significant upregulation in tumors (**Fig. 2.1E,F and S2.3A**). We next determined whether PSGL-1 was co-expressed with additional immune checkpoints and found the majority of tumor-infiltrating $CD8^+$ T cells expressed both PSGL-1 and PD-1, TIM-3, and LAG3 (**Fig. 2.1G and S2.3B,C**). The majority of effector $CD4^+$ T cells and

Tregs also had this phenotype, with most tumor infiltrates being PSGL-1^{+}PD-1^{+}, PSGL-1^{+}TIM-3^{+}, and PSGL-1^{+}LAG3^{+} (**Fig. 2.1G and S2.3B,C**). While T cells in TdLN expressed PSGL-1, the frequencies of co-inhibitory expression (PD-1, TIM-3, LAG3) were lower when compared to the high co-expression found in tumors (**Fig. 2.1G and S2.3D,E**). These findings showed that PSGL-1 was highly expressed in T cells in the tumor-draining lymph nodes (TdLN) and was further upregulated along with other immune checkpoints on tumor-infiltrating T cells.

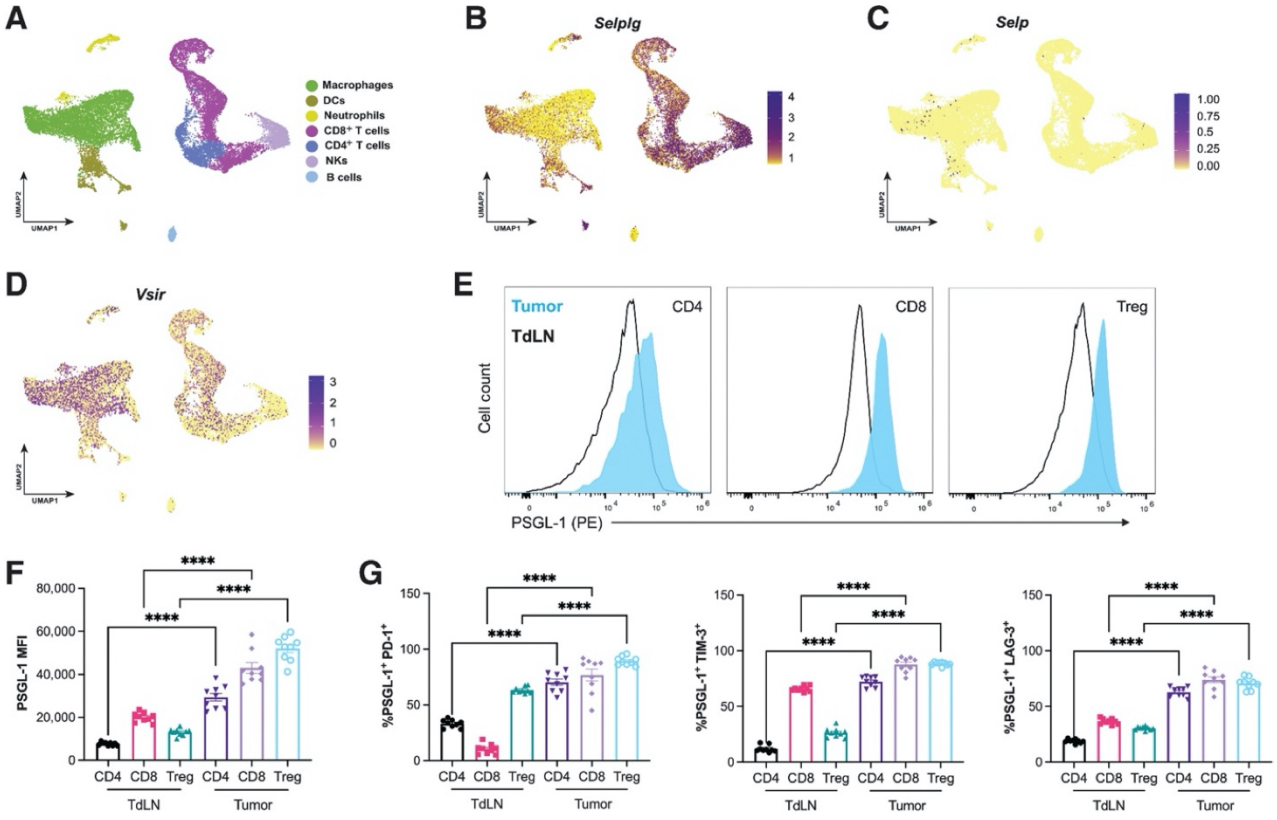

Figure 2.1 PSGL-1 expression in tumor-infiltrating T cells. WT mice were injected s.c. with B16-GP$_{33}$ (1×10^{6}) melanoma cells, and tumors and TdLNs were isolated at 18 dpi and tumors assessed via scRNA-seq. **A,** Integration of Seurat clustering analysis of sorted CD45.2^{+} immune cells isolated from B16-GP$_{33}$ melanoma tumors projected in UMAP with color-coded cluster identities. Integrated Seurat immune cell clusters with relative (**B**) *Selplg*, (**C**) *Selp*, and (**D**) *Vsir* expression are shown. Yellow indicates low and purple indicates high expression. **E** and **F,** The mean fluorescence intensity (MFI) of PSGL-1 on CD4^{+}, CD8^{+}, and Tregs in the tumor and TdLNs is shown and quantified. **G,** PSGL-1 coexpression with PD-1, TIM-3, and LAG3 is shown for CD4^{+}, CD8^{+}, and Tregs in TdLNs and tumors. Data are representative of three independent experiments ($n \geq 8$ mice/group) and show the mean ± SEM. *, $P < 0.05$; **, $P < 0.005$; ***, $P < 0.001$; ****, $P < 0.0001$ by ordinary one-way ANOVA with the Tukey multiple comparisons test.

PSGL-1 immune checkpoint targeting changed the melanoma tumor immune landscape

Since we observed *Selplg* expression in various immune cells and PSGL-1 upregulation on all T cell subsets in melanoma tumors, we next determined whether targeting PSGL-1 and PD-1 in tumor-bearing mice alone or in combination could alter tumor growth. We observed large B16-GP_{33} tumors in the IgG and anti-PD-1 treated mice, and significantly smaller tumors in the anti-PSGL-1 and anti-PD-1/anti-PSGL-1 (combination) treated mice (**Fig. 2.2A**). We next evaluated the immune cell landscape in these mice by scRNA-seq and identified 18 cell clusters using Immgen (**Fig. 2.2B and S2.2A-F**). We determined changes in cell type frequencies between all four treatment groups. Compared to the IgG and anti-PD-1 groups, the anti-PSGL-1 and combination groups had an increase in neutrophils and T cells, while DCs and NK cells were decreased (**Fig. 2.2B,C**). Compared to the anti-PD-1 group, the anti-PSGL-1 and combination groups had increased DCs, neutrophils, B cells, and T cells and decreased macrophages and NK cells (**Fig. 2.2B,C**).

Since we observed an increase in T cells after anti-PSGL-1 and combination treatments, we further evaluated these clusters independently. We observed six *Cd4*$^+$ clusters that mapped to Tregs, $CD4^+$ cells and $CD4^{lo}$ NK T cells (**Fig. 2.2D,E and S2.4A,B**). Compared to IgG and anti-PD-1 treated tumors, the anti-PSGL-1 and combination had decreased Tregs and increased $CD4^+$ T cells (**Fig. 2.2F**). Further gene expression profiling revealed that compared to IgG, the anti-PSGL-1 group had decreased expression of inhibitory receptor genes (*Havcr2*, *Lag3*, *Entpd1*, *Cd38*, *Cd101*, *Tigit*, *Ctla4*, *Btla*), increased activation (*Cd69*, *Cd44*, *Cd28*, *Klrg1*) and effector function genes (*Ifng*, *Tnf*, *Il2*, *Cd40lg*, *Bhlhe40*), increased survival (*Il2ra*, *Il2*, *Il7r*) and decreased inhibitory genes (*Il10*, *Tgfb1*, *Foxp3*) (**Fig. 2.2G**). Interestingly, many of the inhibitory genes downregulated in the anti-PSGL-1 tumors were increased in the anti-PD-1 group, while effector genes (*Ifng*, *Tnf*, *Il2*, *Cd40lg*, *Bhlhe40*) were decreased with anti-PD-1 treatment (**Fig. 2.2G**).

We next evaluated *Cd8*$^+$ cells and identified four subclusters (**Fig. 2.2H and S2.4C,D**). Slingshot trajectory analysis showed a developmental trajectory which originated with C2, progressed through C0 and C1, and ended at C3 (**Fig. 2.2H**). Most clusters had similar frequencies between treatment groups, except for C2, which was lowest in the anti-PD-1 treated group (**Fig. 2.2I**). Based on the trajectory analysis we next evaluated whether there were changes in progenitor (Tpex) and terminal (Tex) exhausted T cell gene signatures in these clusters (**Fig. 2.2J**) (38, 251). We found that C2 represented the Tpex population while C0, C1, and C3 were terminally exhausted clusters (**Fig. 2.2J**). C2 had the highest expression of *Tcf7*, *Slamf6*, *Cd69*, and *Bcl2*, while the other clusters had the lowest expression of these genes (**Fig. 2.2J**). Following the terminal exhausted trajectory, C0 and C1 had higher *Cd200*, *Havcr2*, *Cd244*, *Cd160*, and *Gzmb* (**Fig. 2.2J**). Additional global changes in activation and inhibitory markers and transcription factors were observed within the treatment groups (**Fig. S2.4E,F**). These findings showed that targeting PSGL-1 alone or in combination with PD-1 in melanoma tumor-bearing mice changed the immune landscape, resulting in decreased Tregs and increased effector CD4$^+$ and CD8$^+$ T cell gene signatures.

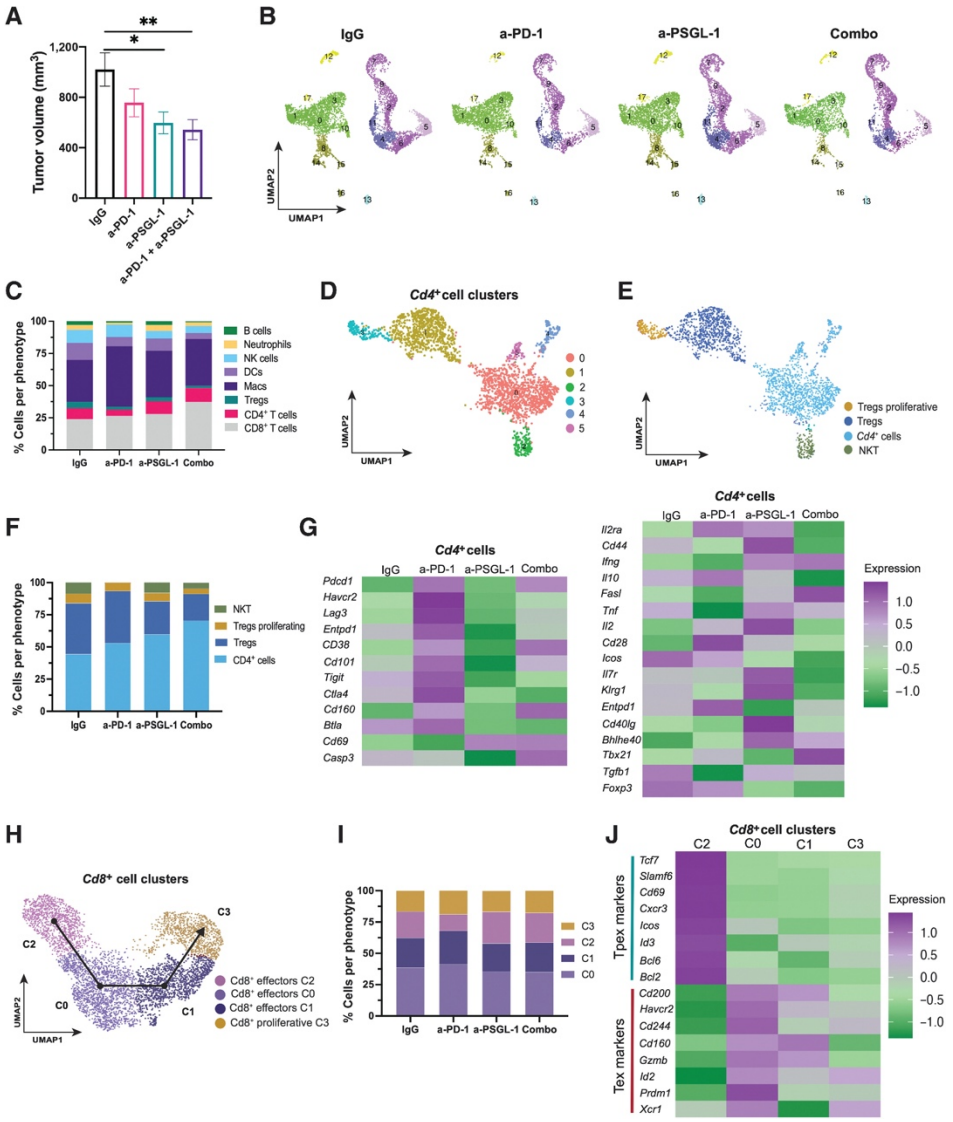

Figure 2.2 Immune cell changes in tumors after immune-checkpoint blockade. WT mice were injected s.c. with (1×10^6) B16-GP$_{33}$ melanoma cells and treated with IgG or anti–PSGL-1 at 8, 10, and 12 dpi. **A,** B16-GP$_{33}$ tumor volume at 18 dpi is shown for IgG, anti–PD-1, anti–PSGL-1, and combination anti–PD-1/anti–PSGL-1–treated mice. Tumors were harvested and assess via scRNA-seq at 18 dpi. **B,** Seurat clustering analysis of sorted CD45.2$^+$ immune cells projected in two-dimensional UMAP with color-coded cluster identities. **C,** Stacked bar graphs of immune cell frequencies derived from Seurat cluster analysis are shown for each treatment group. Seurat subset clustering analysis of (**D**) *Cd4*$^+$ immune cells with (**E**) color-coded identities. **F,** Stacked bar graph showing Tregs, proliferating Treg, NKT, and CD4$^+$ T-cell frequencies in each treatment group. **G,** Heatmaps displaying relative expression of the indicated inhibitory and effector genes in *Cd4*$^+$ subset clusters from all four treatment groups. **H,** Seurat subset clustering of *Cd8*$^+$ cells with slingshot cluster trajectory (black arrow) and (**I**) corresponding stacked bar graphs of *Cd8*$^+$ cluster frequencies for all four treatment groups. **J,** Heatmaps displaying relative expression of T-cell precursor exhausted (Tpex) or terminally exhausted (Tex) genes in *Cd8*$^+$ subset clusters from all four treatment groups.

Anti-PSGL-1 and combination treatments increased effector gene signatures in *Cd4*$^+$ and *Cd8*$^+$ T cells

We further evaluated the gene expression patterns in *Cd4*$^+$ clusters within treatment groups (**Fig. S2.5A**). We observed that compared to IgG, all treatment groups increased *Il10*, *Tgfb1*, *Il2ra*, *Itk*, *Cd28* in Treg clusters (C1 and C3) (**Fig. S2.5A**). Interestingly, non-proliferative Tregs (C1) had higher *Klrg1* in anti-PSGL-1 and combination, while *Klrg1* expression in proliferative Tregs (C3) was highest in anti-PSGL-1 and anti-PD-1 groups (**Fig. S2.5A**). *Pdcd1* expression in non-proliferative Tregs was highest in anti-PD-1 and combination, yet proliferative Tregs showed the lowest *Pdcd1* in the anti-PD-1 group (**Fig. S2.5A**). Analysis of the effector *Cd4*$^+$ cell clusters (C0,C2,C4,C5) showed that compared to IgG and anti-PD-1, higher *Il2*, *Tnf*, *Ifng*, *Fasl*, *Itk*, and *Cd28* (except for C5) expression was observed with anti-PSGL-1 and combination treatment (**Fig. S2.5A**). There were unique changes in gene expression with anti-PSGL-1 treatment, which included higher *Il2*, *Tnf*, *Cd40lg*, and *Cd69* expression in many clusters (**Fig. S2.5A**). Combination treatment often led to the highest expression of effector genes, even showing synergy in some effector genes (*Il2*, *Tnf*, *Fasl)* (**Fig. S2.5A**).

We next evaluated the gene expression in *Cd8*$^+$ clusters and observed that compared to IgG, clusters from all three treatments groups had higher *Ifng*, *Prf1*, *Lamp1*, *Fasl*, *Cd28*, *Itk*, *Entpd1*, *Cd44*, *Cd69*, *Havcr2* (**Fig. S2.5B**). Anti-PD-1 treatment caused an upregulation of *Il2* and *Il2ra*, as well as *Cd200* (**Fig. S2.5B**). Anti-PSGL-1 treatment led to an increase in *Klrg1* and Slamf6 expression, as well as the survival genes *Il7r* and *Bcl2* (**Fig. S2.5B**). The combination treatment group had the highest expression of the effector genes *Tnf, Gzma*, and *Gzmb,* and many clusters showed synergistic expression of *Tnf, Gzma, Gzmb, Itk,* and *Icos*. *Tox2* was also upregulated in combination treatment clusters (**Fig. S2.5B**). These findings showed that anti-PSGL-1 monotherapy increased expression of

activation and pro-survival genes, while the combination treatment resulted in enhanced effector T cell gene signatures.

PSGL-1 antibody treatment in tumor-bearing mice delays B16-GP$_{33}$ melanoma tumor growth

We next sought to verify our findings from the scRNA-seq analysis by evaluating T cell changes between WT and anti-PSGL-1 treated mice. WT mice were injected subcutaneously with B16-GP$_{33}$ melanoma tumor cells and at 8dpi, when tumors were palpable, mice received either IgG or anti-PSGL-1 antibodies (**Fig. 2.3A**). We found that melanoma tumors grew in IgG treated mice, but tumor growth rate was significantly decreased in anti-PSGL-1 treated mice (**Fig. 2.3B,C**). Furthermore, tumors from the anti-PSGL-1 treated mice had lower masses compared to control IgG groups (**Fig. 2.3D**). We next examined how anti-PSGL-1 treatment changed the infiltration and activation of T cells within melanoma tumors. We found that anti-PSGL-1 treated mice had a higher frequency of activated CD8$^+$ T cells in tumors, although nearly all the tumor-infiltrating CD8$^+$ T cells were activated in both treatments (**Fig. 2.3E**). In contrast, activated CD4$^+$ T cell frequencies were increased, while Treg frequencies were decreased in the tumors of mice that received anti-PSGL-1 treatment (**Fig. 2.3E,F**). Since we observed a difference in Tregs, we compared the ratio of effector T cells to Tregs in tumors and found a significant increase in effector T cells compared to Tregs in mice that received PSGL-1 antibody **(Fig. 2.3G,H**). Therefore, anti-PSGL-1 therapy in melanoma tumor-bearing mice resulted in tumor control and changed the landscape of T cells that infiltrated these tumors, favoring an increase in effector CD4$^+$ and CD8$^+$ T cells while decreasing the frequency of Tregs.

PSGL-1 targeting increased effector T cell responses in melanoma tumors

We next determined the extent that anti-PSGL-1 treatment changed the functionality of the tumor-infiltrating CD4$^+$ and CD8$^+$ T cells. The frequency of GranzymeB$^+$ CD8$^+$ T cells was increased in anti-PSGL-1 treated mice when compared to CD8$^+$ T cells from IgG treated mice (**Fig. 2.3I,J**). We

also detected low IFN-γ and TNF-α production in T cells from IgG treated mice after PMA/Ionomycin re-stimulation, while $CD4^+$ and $CD8^+$ T cells in the anti-PSGL-1 treated group had a significantly higher frequency of IFN-γ and TNF-α production (**Fig. 2.3K-M**). Our findings showed that anti-PSGL-1 therapy in tumor-bearing mice increased effector functions in tumor-infiltrating $CD4^+$ and $CD8^+$ T cells.

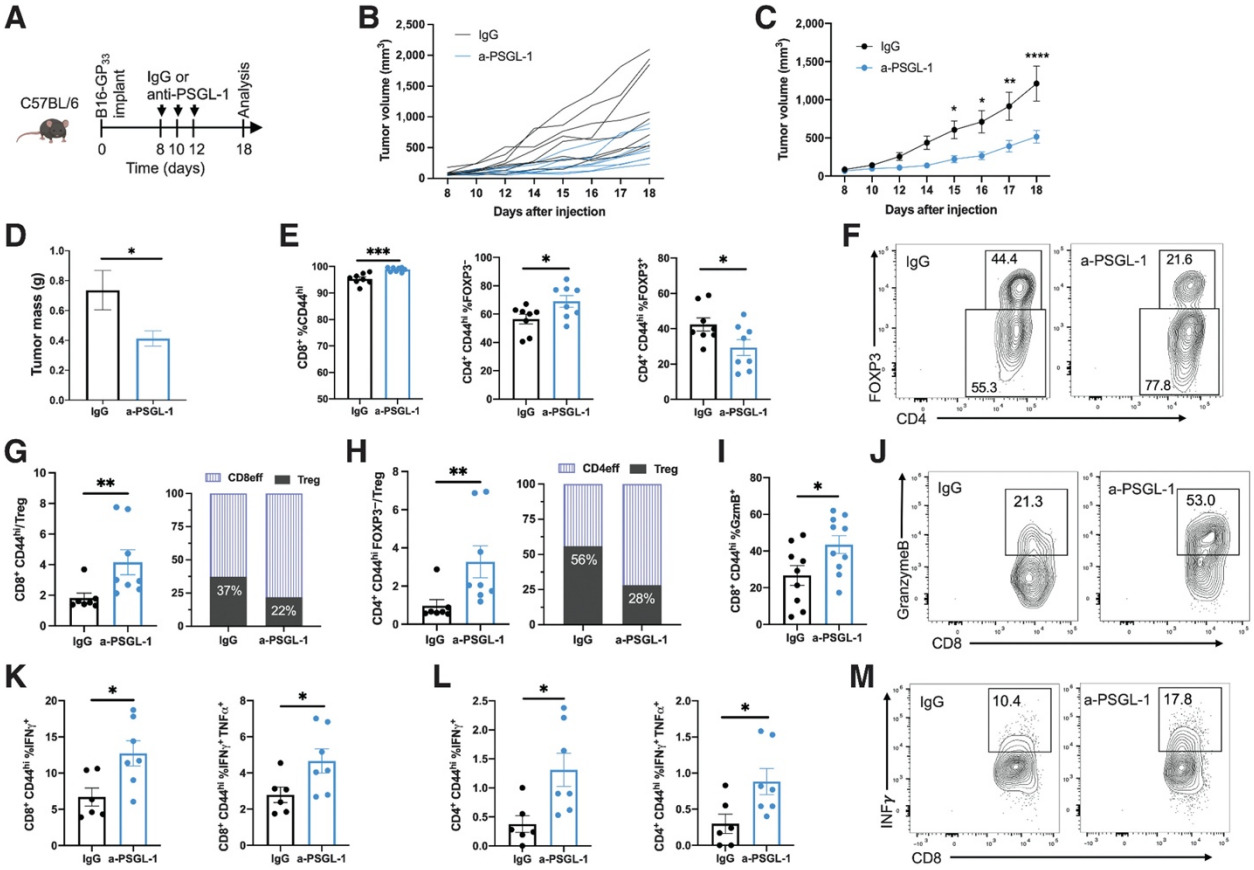

Figure 2.3 WT mice treated with anti–PSGL-1 have improved tumor immunity. A, WT mice were injected s.c. with (1×10^6) B16-GP_{33} melanoma cells and treated with IgG or anti–PSGL-1 at 8, 10, and 12 dpi. **B** and **C,** Tumor volume and (**D**) tumor mass at 18 dpi. Tumors were harvested and analyzed by flow cytometry at 18 dpi. **E,** Frequencies of tumor-infiltrating T cells and (**F**) representative FACS plots of Tregs. **G** and **H,** Ratio of T-cell subsets to Tregs in tumors. **I,** Frequency of granzyme B^+ $CD8^+$ T cells in the tumor and (**J**) representative FACS plots. **K** and **L,** Frequency of cytokine producing $CD8^+$ and $CD4^+$ T cells and (**M**) representative FACS plots. Data are representative of four independent experiments ($n \geq 8$ mice/group). Graphs show the mean ± SEM. *, $P < 0.05$; **, $P < 0.005$; ***, $P < 0.001$; ****, $P < 0.0001$ by two-way ANOVA with the Sidak multiple comparisons test (tumor growth curve) or two-tailed *t* test or Mann–Whitney *U* test.

PSGL-1 targeting differentially modulates immune checkpoints on T cells

Since anti-PSGL-1 treatment increased effector functions in anti-tumor T cells, we next evaluated how targeting PSGL-1 modulated immune checkpoint expression in these cells. We observed high PD-1, LAG3, and TIM-3 levels in $CD8^+$ T cells from IgG treated mice with melanoma tumors (**Fig. 2.4A**). Surprisingly, $CD8^+$ T cells from tumors of anti-PSGL-1 treated mice had even higher surface levels of these immune checkpoints than IgG treated mice (**Fig. 2.4A and S2.6A**). In contrast to $CD8^+$ T cells, $CD4^+$ T cells from tumors of anti-PSGL-1 treated mice had no difference in PD-1 expression but had decreased TIM-3 and LAG3 expression (**Fig. 2.4B and S2.6B**). Like effector $CD4^+$ T cells, Tregs also expressed similarly high PD-1 levels in IgG and anti-PSGL-1 treated mice (**Fig. 2.4C and S2.6C**). In contrast to $CD4^+$ and $CD8^+$ T cells, Tregs had no difference in expression levels of TIM-3 and LAG3 between IgG and anti-PSGL-1 treated mice (**Fig. 2.4C and S2.6C**). These data showed that while all T cells in tumors expressed high PSGL-1 levels, PSGL-1 targeting differentially changed expression of inhibitory receptors in $CD4^+$ and $CD8^+$ T cells, but not in Tregs.

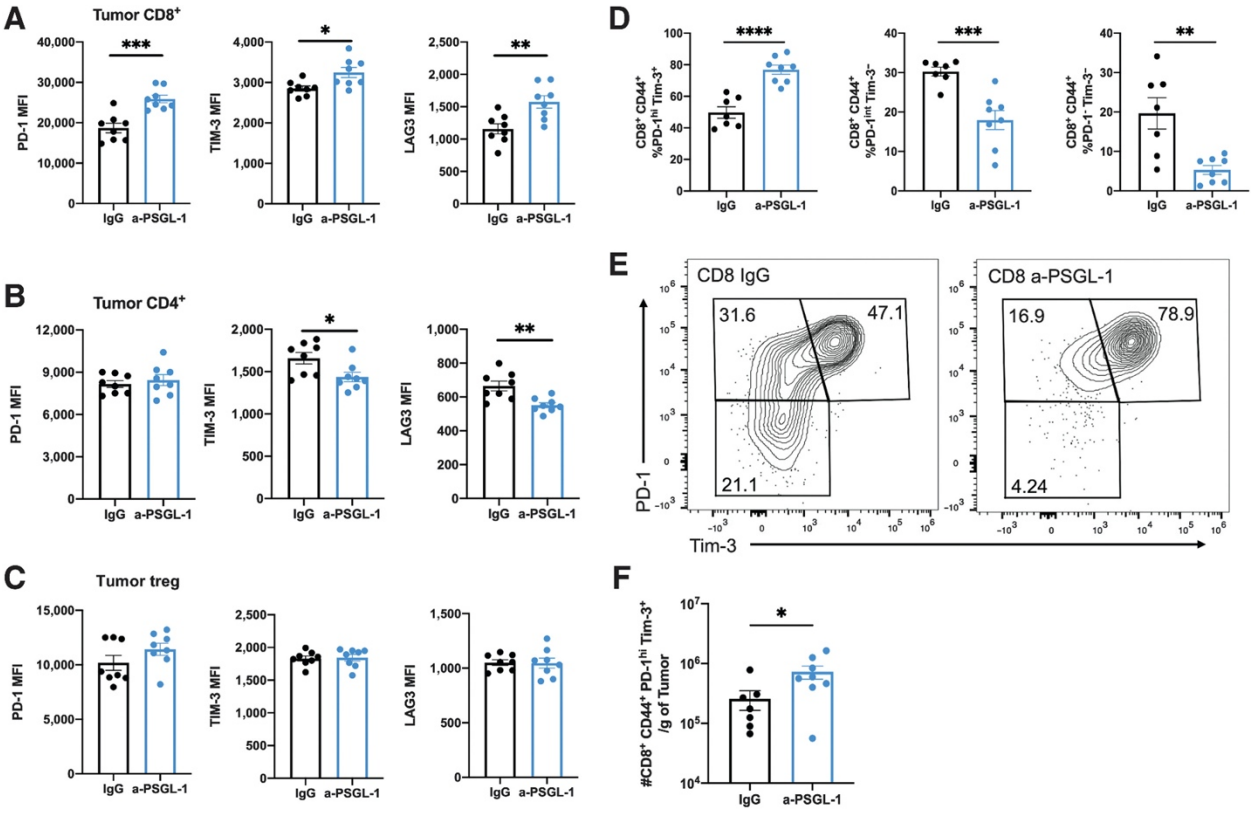

Figure 2.4 Activated CD8⁺ T cells are increased in tumors after anti–PSGL-1 therapy. WT mice were injected s.c. with (1×10^6) B16-GP_{33} melanoma cells and treated with IgG or anti–PSGL-1 at 8, 10, and 12 dpi, and tumors were isolated at 18 dpi and analyzed via flow cytometry. **A,** PD-1, TIM-3, and LAG3 MFI on $CD8^+$ T cells, (**B**) $CD4^+$ T cells, and (**C**) Tregs in tumors. **D,** $CD8^+$ T-cell populations in tumors were phenotyped as terminally exhausted ($PD\text{-}1^{hi}TIM\text{-}3^+$), progenitor exhausted ($PD\text{-}1^{int}TIM\text{-}3^-$), and $PD\text{-}1^-$ $TIM\text{-}3^-$ and (**E**) representative FACS plots are shown. Quadrants were set using isotype controls. **F,** The number of $CD8^+$ $PD\text{-}1^{hi}TIM\text{-}3^+$ T cells per gram of tumor. Data are representative of four independent experiments ($n \geq 8$ mice/group). Graphs show the mean ± SEM. *, $P < 0.05$; **, $P < 0.005$; ***, $P < 0.001$; ****, $P < 0.0001$ by two-tailed *t* test or Mann–Whitney *U* test.

Terminal exhausted CD8$^+$ T cells are increased after anti-PSGL-1 treatment

Since we observed increased expression of immune checkpoints in CD8$^+$ T cells from anti-PSGL-1 treated mice, we next evaluated whether terminal vs progenitor exhausted T cell subsets were different between treatment groups. We observed an increased frequency of terminal exhausted (PD-1^{hi}TIM-3$^+$) CD8$^+$ T cells and decreased frequency of progenitor exhausted (PD-1^{int}TIM-3$^-$) CD8$^+$ T cells in tumors after anti-PSGL-1 treatment (**Fig. 2.4D,E**). We also detected a population of PD-1$^-$ TIM-3$^-$ CD8$^+$ T cells that was decreased in anti-PSGL-1 treated mice (**Fig. 2.4D,E**). Terminal exhausted T cells, which retain cytotoxic function, are increased after anti-PD-1 immune checkpoint therapy (252-254). We observed that terminal exhausted T cells proliferated more than progenitor exhausted T cells in both treatment groups as shown by their higher Ki67$^+$ cells (**Fig. S2.6D**). We observed increased proliferation in the anti-PSGL-1 treated PD-1$^-$TIM-3$^-$ population (**Fig. S2.6D**) despite their lower frequencies in the anti-PSGL-1 treated mice (**Fig. 2.4D**). Ki67 may last longer in cells than the period of proliferation, therefore, the increased Ki67 in the PD-1$^-$TIM-3$^-$ population could indicate more rapid differentiation into the terminal state. Since the proliferative burst after anti-PD-1 treatment results in the accumulation of the PD-1^{hi}TIM-3$^+$ population, we examined whether anti-PSGL-1 treatment changed the absolute number of these T cells within tumors. We detected an increase in the accumulation of these terminal exhausted CD8$^+$ T cells in melanoma tumors after anti-PSGL-1 treatment (**Fig. 2.4F**). Since our earlier findings showed a decrease in Tregs after anti-PSGL-1 treatment, we evaluated whether the PSGL-1 antibody (clone 4RA10 IgG_1) depleted cells *in vivo*. We found no depletion of Tregs, CD4$^+$, or CD8$^+$ T cells in spleen or lymph nodes in anti-PSGL-1 treated mice (**Fig. S2.6E**). These findings indicate that after anti-PSGL-1 treatment, there is an increase in the presence of terminal exhausted (PD-1^{hi}TIM-3$^+$) T cells in tumors.

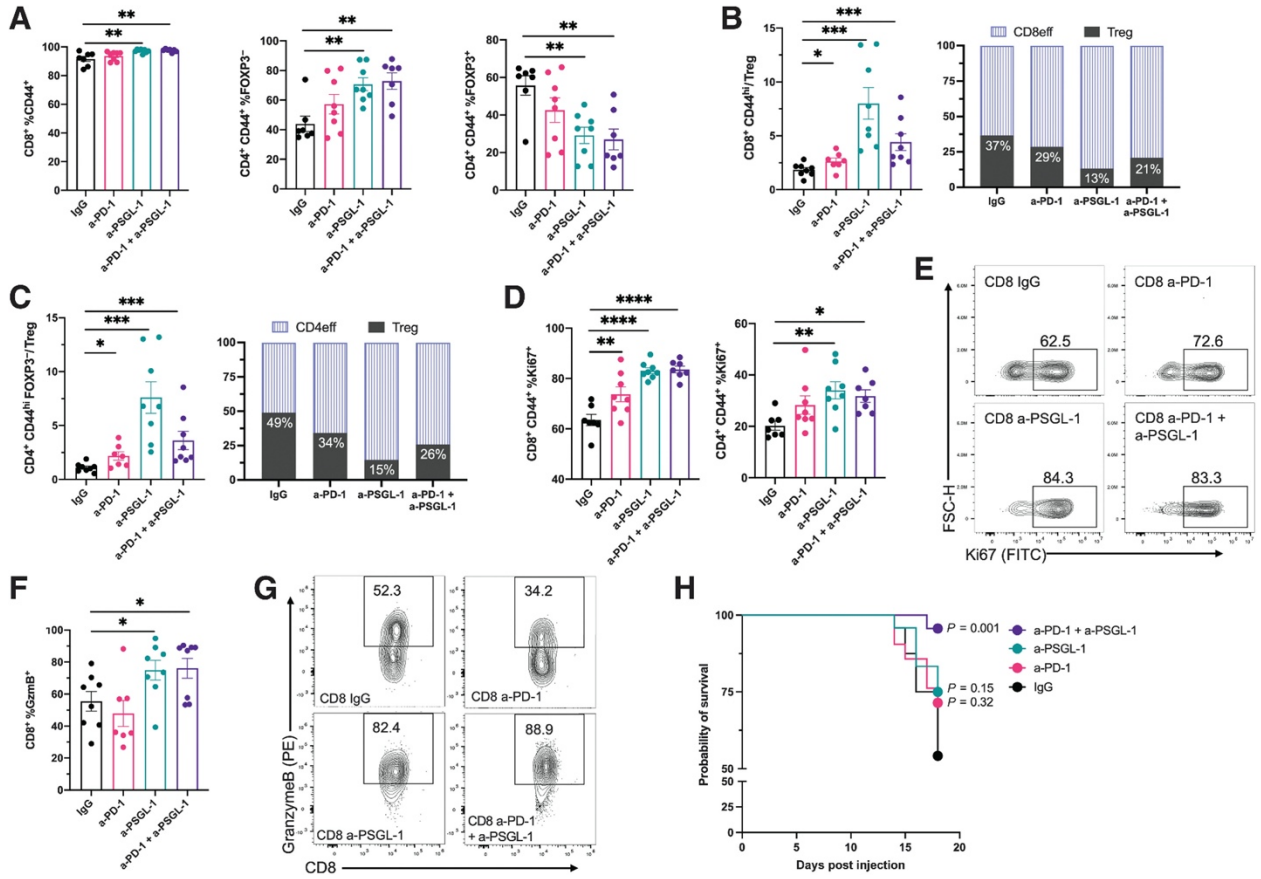

Figure 2.5 Tumor immune responses after anti–PSGL-1 and anti–PD-1 combination therapy. WT mice were injected s.c. with (1×10^6) B16-GP_{33} melanoma cells and treated with IgG, anti–PD-1, anti–PSGL-1, or both anti–PD-1 and anti-PSGL-1 at 8, 10, and 12 dpi. Tumors were isolated at 18 dpi, and (**A**) frequencies of activated ($CD44^+$) $CD8^+$ and $CD4^+$, T cells, Tregs, and (**B–C**) the ratio of $CD4^+$ and $CD8^+$ effector to Tregs are shown. **D** and **E,** Frequencies of $Ki67^+$ T cells and representative FACS plots for $CD8^+$ T cells. **F,** Frequencies of granzyme B^+ $CD8^+$ T cells and (**G**) representative FACS plots. **H,** Survival curve of IgG, anti–PD-1, anti–PSGL-1, or both anti–PD-1 and anti–PSGL-1–treated mice up to 18 dpi. Data are representative of four independent experiments ($n \geq 7$ mice/group). Graphs show the mean ± SEM. *, $P < 0.05$; **, $P < 0.005$; ***, $P < 0.001$; ****, $P < 0.0001$ by two-tailed t test or Mann–Whitney U test (tumor mass) or log-rank (Mantel–Cox) test (survival).

Targeting PSGL-1 with PD-1 blockade promotes anti-tumor immunity to melanoma

We next assessed the efficacy of combination therapy with antibodies targeting PSGL-1 and PD-1 in B16-GP_{33} tumor-bearing mice (**Fig. S2.7A**). We evaluated the frequencies of activated T cells in tumors and found that the majority of $CD8^+$ T cells in tumors were $CD44^+$, with a small increase in activated $CD8^+$ T cells in mice treated with anti-PSGL-1 and combination therapy (**Fig. 2.5A**). We observed increased frequencies of $CD4^+$ T cells in mice that received anti-PSGL-1 monotherapy and combination therapy compared to IgG or anti-PD-1 treated mice (**Fig. 2.5A**). While we observed a large Treg infiltrate in tumors from IgG and anti-PD-1 treated mice, anti-PSGL-1 monotherapy and combination therapy both caused a significant decrease in frequencies of Tregs (**Fig. 2.5A**). Furthermore, we found an increased ratio of effector $CD4^+$ and $CD8^+$ T cells to Tregs in mice treated with anti-PSGL-1 and combination therapy compared to IgG treated mice (**Fig. 2.5B,C**). We next determined if antibody therapy affected T cell proliferation in tumors and found that compared to IgG, anti-PD-1 treatment increased $CD8^+$ but not $CD4^+$ T cell proliferation as measured by Ki67 levels (**Fig. 2.5D,E**). We did detect, however, a significant increase in $Ki67^+$ $CD8^+$ and $CD4^+$ T cells after both anti-PSGL-1 monotherapy and combination therapy (**Fig. 2.5D,E**). While we detected increased proliferation in T cells from anti-PSGL-1 treated mice, the combination therapy had similar results, showing no synergistic increase from the addition of anti-PD-1 (**Fig. 2.5D,E**). To determine how combination therapy changed T cell function, we evaluated GranzymeB levels in $CD8^+$ T cells (**Fig. 2.5F,G**). We found similar frequencies of $GranzymeB^+$ $CD8^+$ T cells in tumors from IgG and anti-PD-1 treated mice, and increased frequencies after anti-PSGL-1 monotherapy and combination therapy (**Fig. 2.5F,G**). We again did not detect synergy in terms of GranzymeB production when anti-PD-1 was combined with anti-PSGL-1 treatment. Although we saw increased anti-tumor immunity with anti-PSGL-1 treatment in experiments performed with B16-GP_{33} melanoma cells, tumors eventually grew in all treatment groups and mice had to be euthanized. However, we observed the

highest median survival at 18dpi in mice treated with combination therapy (**Fig. 2.5H**). These findings showed that anti-PSGL-1 therapy improved anti-tumor immunity in melanoma tumors that were largely unresponsive to PD-1 therapy.

Antigen-specific $CD8^+$ T cells are increased relative to Tregs in tumors after antibody targeting of PSGL-1

We next quantified the number of T cells infiltrating tumors and found increased infiltration of $CD8^+$ and $CD4^+$ T cells in anti-PSGL-1 treated mice compared to IgG control (**Fig. 2.6A**). We observed similar numbers of Tregs in IgG and anti-PD-1 treated mice, but found a significant decrease in anti-PSGL-1 and combination treated mice (**Fig. 2.6B**). No differences in Treg numbers in tumors were observed between mice receiving anti-PSGL-1 monotherapy or combination therapy (**Fig. 2.6B**). We next examined the frequencies of antigen-specific $CD8^+$ T cells by staining with MHC class I tetramers specific for the GP_{33} peptide expressed by B16-GP_{33} melanoma. We found similar frequencies of $GP_{33}^+CD8^+$ T cells in IgG and anti-PD-1 treated mice, a significant increase in the frequency of GP_{33}^+ $CD8^+$ T cells in anti-PSGL-1 treated mice, and a trend towards increased frequencies in combination treated mice compared to IgG (**Fig. 2.6C,D**). We observed no differences in the numbers of $GP_{33}^+CD8^+$ T cells per gram of tumor between treatment groups (**Fig. 2.6C**). We quantified the ratio of $GP_{33}^+CD8^+$ T cells to Tregs in tumors and found a significant increase in $GP_{33}^+CD8^+$ T cells compared to Tregs in anti-PSGL-1 and combination treated mice compared to IgG and anti-PD-1 treated mice (**Fig. 2.6E**). To assess the role of T cells in this model, we next depleted T cells in tumor-bearing mice that received immune checkpoint antibody therapy (**Fig. S2.7B**). We found no differences in tumor volume or mass in any of the antibody-treated groups (**Fig. S2.7C,D**). We next evaluated the efficacy of anti-PSGL-1 treatment in a different melanoma tumor model. We treated WT mice harboring D4M-3A tumors with anti-PSGL-1 and found a significant

decrease in tumor volume and mass when compared to IgG treated mice (**Fig. 2.6F,G**). These findings showed increased ratio of tumor-infiltrating antigen-specific $CD8^+$ T cells to Tregs after anti-PSGL-1 and combination treatment. Importantly, anti-PSGL-1 treatment also slowed D4M-3A melanoma tumor growth, which like B16-GP_{33}, is also an aggressive tumor resistant to anti-PD-1 treatment (255).

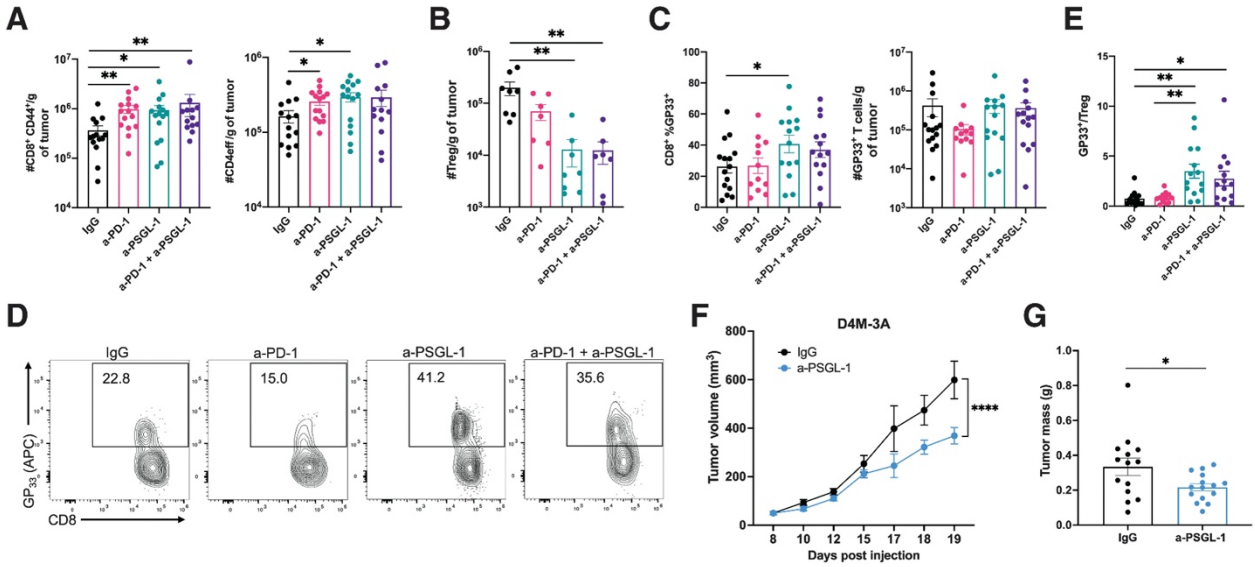

Figure 2.6 Tumor-specific $CD8^+$ T cells and Tregs after anti–PD-1/anti–PSGL-1 combination therapy. WT mice were injected with (1×10^6) B16-GP_{33} melanoma cells s.c. and injected with IgG, anti–PD-1, anti–PSGL-1, or anti–PD-1/anti–PSGL-1 at 8, 10, and 12 dpi. Tumors were harvested and assessed via flow cytometry at 18 dpi. **A,** The number of $CD8^+$, $CD4^+$ T cells, and (**B**) Tregs per gram of tumor at 18 dpi. **C,** The frequencies and numbers of $GP_{33}^+CD8^+$ T cells per gram of tumor. **D,** Representative FACs plots showing the frequency of $tetramer^+(GP_{33}^+)$ $CD8^+$ T cells in tumors. **E,** The ratio of $GP_{33}^+CD8^+$ T cells to Tregs in tumors. **F** and **G,** WT mice were injected with (1×10^6) D4M-3A melanoma cells s.c. and injected with IgG or anti–PSGL-1 antibodies at 8, 10, and 12 dpi. **F,** Tumor volume and (**G**) tumor mass are shown at 19 dpi. Data are representative of four (**A–B**) or two (**C–G**) independent experiments ($n \geq 5$ mice/group). Graphs show the mean ± SEM. *, $P < 0.05$; **, $P < 0.005$; ***, $P < 0.001$ by two-tailed *t* test or Mann–Whitney *U* test or by two-way ANOVA with the Sidak multiple comparisons test (tumor growth curve).

PSGL-1 deficiency with anti-PD-1 treatment promotes melanoma tumor control

We next determined whether immune checkpoint therapy could be combined with PSGL-1 deficiency to promote melanoma tumor control. We injected WT and *Selplg*$^{-/-}$ mice subcutaneously with YUMMER1.7 melanoma cells, a highly immunogenic, anti-PD-1 sensitive cell line (**Fig. 2.7A**) (256), and treated these mice with either IgG or anti-PD-1 antibodies when tumors were measurable. We found that WT IgG treated mice developed tumors which continued to increase in size (**Fig. 2.7B,C**). WT anti-PD-1 treated mice also developed tumors and their average tumor volume was similar to IgG treated mice (**Fig. 2.7B,C**). In contrast, *Selplg*$^{-/-}$ mice treated with IgG had significantly smaller tumors compared to WT IgG or anti-PD-1 treated mice (**Fig. 2.7B,C**). Furthermore, when *Selplg*$^{-/-}$ mice were injected with anti-PD-1 antibodies, they demonstrated the most robust tumor control of all four groups examined, eliminating their tumors by 24 dpi (**Fig. 2.7B,C**). Despite some small tumors present in some WT IgG treated mice, none of these (0/6) controlled their tumors, while WT anti-PD-1 treated mice (2/6) showed some tumor control (**Fig. 2.7D**). In contrast, *Selplg*$^{-/-}$ IgG-treated mice (3/6) eliminated tumors, whereas all *Selplg*$^{-/-}$ anti-PD-1 treated mice (6/6) eradicated their tumors (**Fig. 2.7D**). To demonstrate the robustness of this phenotype, we combined tumor control data from three independent experiments. We determined complete responses (CR) leading to tumor clearance in 0/18 (0%) WT IgG, 4/18 (22%) WT anti-PD-1, 4/19 (21%) *Selplg*$^{-/-}$ IgG, and 13/20 (65%) in *Selplg*$^{-/-}$ anti-PD-1 treated mice (**Fig. 2.7E**). Even though some *Selplg*$^{-/-}$ anti-PD-1 treated mice had tumors, the tumors never reached the larger volumes observed in the IgG or anti-PD-1 treatment groups (**Fig. 2.7E**). To confirm the role of T cells in the observed phenotypes, we depleted T cells in WT and *Selplg*$^{-/-}$ mice before anti-PD-1 therapy and observed tumor growth and no tumor clearance in all mouse groups by 28dpi (**Fig. 2.7F,G**). These findings showed that while *Selplg*$^{-/-}$ mice had better tumor control than WT mice, combining PSGL-1 deficiency with PD-1 blockade resulted in the highest frequency of tumor-free mice.

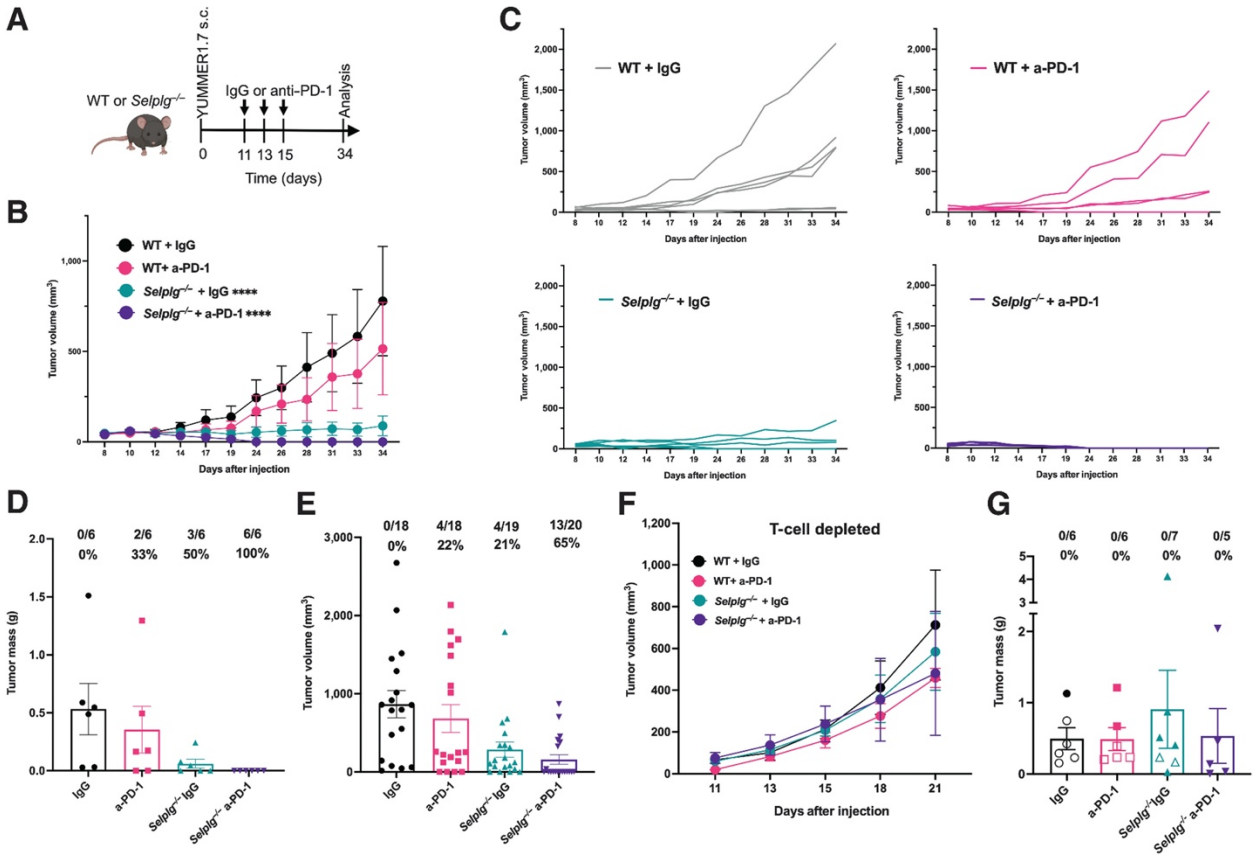

Figure 2.7 PD-1 blockade in *Selplg*$^{-/-}$ mice promotes complete responses to melanoma. A, WT and *Selplg*$^{-/-}$ mice were injected s.c. with (2×10^6) YUMMER1.7 melanoma cells and then treated with IgG or anti–PD-1, or with T-cell–depleting antibodies and IgG or anti–PD-1 at the indicated times. **B** and **C,** Tumor volume over time. **D,** Quantification of tumor mass at 34 dpi and (**E**) tumor volumes. Tumor volumes are representative of three combined experiments. **F** and **G,** Quantification of tumor volume over time, and tumor mass in T cell–depleted mice. **G,** Mice euthanized at 21 dpi (open symbols) or 28 dpi (filled symbols). Data are representative of three combined independent experiments in **A–E** ($n \geq 6$ mice/group, endpoints 34 and 38 dpi) or one experiment in **F–G** ($n \geq 6$ mice/group, endpoint 28 dpi). Fraction of mice without tumors at the end of each experiment is shown at (**D–E**) 34 dpi and (**G**) 21 dpi (open symbols) or 28 dpi (filled symbols). Graphs show the mean ± SEM. *, $P < 0.05$; **, $P < 0.005$; ***, $P < 0.001$; ****, $P < 0.0001$ as determined by two-way ANOVA with the Tukey multiple comparisons test (tumor volume growth curve).

DISCUSSION

In this study, we targeted PSGL-1 in tumor-bearing mice and uncovered an increased anti-tumor T cell response in the tumor microenvironment, which slowed melanoma tumor growth. Targeting PSGL-1 increased the activation phenotype of effector $CD4^+$ and $CD8^+$ T cells in tumors. T cells from anti-PSGL-1 treated mice had increased effector functions, proliferation, and were essential in delaying tumor growth after antibody treatment. We found that targeting PSGL-1 decreased the frequencies of Tregs in tumors, resulting in an increased presence of effector T cells. We assessed whether combination treatment further improved anti-tumor responses in WT mice and found that while targeting PSGL-1 and PD-1 resulted in smaller tumors compared to IgG controls, combination therapy had a similar efficacy to anti-PSGL-1 monotherapy. Even though combination therapy did not eliminate the poorly immunogenic B16-GP_{33} cell line, we did find complete responses when *Selplg*$^{-/-}$ tumor-bearing mice were given anti-PD-1 therapy using the more immunogenic YUMMER1.7 cell line.

It is well established that immune checkpoints are upregulated on exhausted T cells in tumors, which inhibits T cell effector functions (257). While most immune checkpoints are induced upon T cell activation, PSGL-1 is constitutively expressed on T cells. However, PSGL-1 expression does increase significantly as T cells move from the TdLN into the tumor microenvironment. Even though PSGL-1 was expressed on all tumor-infiltrating T cells, expression levels differed in $CD4^+$ and $CD8^+$ T cells, and Tregs, with Tregs expressing the highest levels. Furthermore, most T cells in melanoma tumors co-expressed PSGL-1 and additional immune checkpoints (PD-1, TIM-3, LAG3). This suggests potential co-regulation of these inhibitory receptors and possible cooperation in promoting the T cell exhaustion state. Indeed, *Selplg*$^{-/-}$ T cells in melanoma tumors were shown to have decreased PD-1, TIM-3, and LAG3 levels (234). Our findings suggest that these varying PSGL-1 levels in tumor-infiltrating T cells may result in different phenotypic and functional changes as these cells respond to

tumor antigens. This concept is supported by our observations of increased PD-1, TIM-3, and LAG3 levels on $CD8^+$ T cells, decreased TIM-3 and LAG3 on $CD4^+$ T cells, and unchanged immune checkpoint levels in Tregs from anti-PSGL-1 treated mice. While $CD8^+$ T cells expressed higher immune checkpoint levels after PSGL-1 targeting, these levels are proposed by others to indicate T cell activation (258). Furthermore, it was recently shown that exhausted $CD8^+$ T cells increase their PD-1 expression levels and TCR signaling after anti-PD-L1 blockade *in vivo* (259). Anti-tumor $CD8^+$ T cells responding to PD-1 checkpoint blockade have increased frequencies of the exhausted terminal $PD\text{-}1^{hi}TIM\text{-}3^+$ population, seeded by proliferation of progenitor exhausted T cells (38). Although this is a terminally exhausted population, these T cells retain effector functions that promote tumor killing (38). Like PD-1 blockade, we found that after anti-PSGL-1 treatment, $PD\text{-}1^{hi}TIM\text{-}3^+$ $CD8^+$ T cells were enriched in tumors, indicating that this population may be key in promoting tumor killing. This conclusion was supported by the increased IFN-γ^+, TNF-α^+, and GranzymeB production, increased proliferation, and the increased T cell activation gene signatures we observed in $CD8^+$ T cells in tumors from anti-PSGL-1 treated mice. $CD4^+$ T cells had decreased TIM-3 and LAG3 immune checkpoint expression and were more functional in anti-PSGL-1 treated mice, suggesting improved help to $CD8^+$ T cells during therapy, as $CD4^+$ T cell help is critical in melanoma tumor control (260, 261). Indeed, our scRNA-seq analyses showed improved $CD4^+$ T cell helper functions after anti-PSGL-1 treatment.

The cellular mechanisms that promote melanoma tumor control during anti-PSGL-1 treatment require T cells, as shown by our studies in which T cell-depleted mice treated with anti-PSGL-1 antibodies had no observable tumor control. While we found that T cells were critical in mediating melanoma tumor control, it is possible that additional immune cells may also be modulated after anti-PSGL-1 therapy. Others have shown that *Selplg*$^{-/-}$ DCs are more stimulatory and that PSGL-1 signaling can induce tolerogenic DCs that support Tregs (241). Future studies will address how anti-

PSGL-1 therapy alters the differentiation and function of additional immune cells in the melanoma tumor microenvironment to support an improved anti-tumor T cell response.

Our finding that Treg frequencies were decreased in melanoma tumors after anti-PSGL-1 therapy further highlights the inhibitory role of Tregs in limiting effector T cell responses. Studies have shown that depleting Tregs in melanoma tumors can promote tumor rejection (262), and the ratio of Tregs to effector T cells increases in growing tumors (263). Decreasing Tregs in murine and human cancers has been suggested to predict immunotherapy efficacy (264-266). We found decreased Tregs and increased effector T cells after anti-PSGL-1 treatment. These findings suggest that a more pro-inflammatory environment was present in tumors from anti-PSGL-1 treated mice. Our findings that anti-PSGL-1 treatment reinvigorated $CD4^+$ and $CD8^+$ T cell proliferation in tumors supports the concept that targeting PSGL-1 can relieve Treg-mediated inhibition. This was further supported by our scRNA-seq analysis showing upregulated activation and effector genes in *Cd4*$^+$ and *Cd8*$^+$ cells after anti-PSGL-1 treatment. Important for therapeutic purposes, these immune changes occurred after melanoma tumors were already palpable in mice, indicating that reducing Tregs in established tumors is attainable when PSGL-1 is targeted.

Melanoma is a very aggressive cancer and until recently, patients with metastatic disease had few treatment options and most died within months of diagnosis (267). Immune checkpoint blockade therapies, such as anti-PD-1 and anti-CTLA-4 treatment, have saved the lives of patients worldwide, but many continue to be unresponsive to these therapies (268). While the human disease differs from melanoma in animal models, preclinical studies have been key in testing the efficacy of new approaches to reinvigorate T cells in tumors. We injected highly immunogenic YUMMER1.7 melanoma cells into mice and discovered that *Selplg*$^{-/-}$ mice had better tumor control than WT IgG or WT anti-PD-1 treated mice. When tumor-bearing *Selplg*$^{-/-}$ mice were additionally injected with anti-PD-1 antibodies, these

mice showed complete responses with many mice eliminating their tumors. These findings mirror clinical findings showing that immune checkpoint blockade therapies are more effective in patients with highly mutated melanomas (269). Our findings in *Selplg*$^{-/-}$ mice underscore the relevance of combining PSGL-1 inhibition with PD-1 blockade as a new strategy to promote tumor control.

Our studies using the highly aggressive B16 melanoma model revealed that anti-PSGL-1 antibody therapy was effective in slowing melanoma growth through mechanisms leading to increased T cell activation, proliferation, and effector functions. While B16 melanomas have been reported to be resistant to anti-PD-1 and anti-PD-L1 therapy (270, 271), we found that anti-PSGL-1 treatment in tumor-bearing mice could delay B16 tumor growth. We also observed delayed D4M-3A melanoma tumor growth in anti-PSGL-1 treated mice, an additional melanoma cell line resistant to anti-PD-1 therapy (255). When we combined therapies in B16-tumor bearing mice by injecting them with anti-PSGL-1 and anti-PD-1 antibodies, we observed no synergy in T cell effector phenotypes. However, the combination treatment increased the medial overall survival of these mice. While our work focused on targeting PSGL-1 to promote anti-tumor immunity, others have shown tumor control through blockade of known PSGL-1 ligands, such as the recently identified VISTA ligand (126, 272, 273). Our scRNA-seq showed that most immune cells in melanoma had low to undetectable P-selectin (*Selp*) expression, but they did express high VISTA (*Vsir*) levels. The anti-PSGL-1 antibody (4RA10 clone) has been shown to block P-selectin binding (274), but since more *Vsir* than *Selp* is present in the cells in the tumor microenvironment, our data suggest that VISTA-PSGL-1 binding may be a dominant interaction. It is also possible that additional PSGL-1 binding partners may contribute to PSGL-1-dependent inhibition in the tumor draining lymph node and/or the tumor microenvironment. Our findings showing that anti-PSGL-1 treatment was effective against anti-PD-1/anti-PD-L1 resistant B16-GP_{33} and D4M-3A melanomas indicate that targeting PSGL-1 may represent a new therapeutic approach to control tumors that are unresponsive to standard therapies.

We showed that PSGL-1 is highly expressed and upregulated on T cells in the melanoma tumor microenvironment and is co-expressed with multiple immune checkpoints on exhausted T cells and Tregs. Given the importance of immune checkpoint blockade therapies that reinvigorate T cells in tumors, it is significant that anti-PSGL-1 therapy in mice harboring aggressive B16-GP_{33} and D4M-3A melanomas delayed tumor growth. Furthermore, combining anti-PD-1 therapy in PSGL-1-deficient mice showed complete responses in mice harboring highly mutated YUMMER1.7 melanomas. Our findings identify PSGL-1 as an immune checkpoint target and suggest that inhibiting this pathway may provide new treatment options with the possibility of eliciting anti-tumor immunity in patients with cancer.

ACKNOWLEDGEMENTS

We would like to thank all the current and former members in the Tinoco Laboratory (Twitter: @Tinoco_Lab) for all their constructive comments and advice during this project. We would like to thank Dr. David Fruman and Dr. Francesco Marangoni for critical review of our manuscript (UC Irvine). We would like to thank Melinda Gormley (UC Irvine) for editing our manuscript. This work was supported by the National Institutes of Health (R01 AI13723 to R.T.), Department of Defense (W81XWH-18-1-0738 to R.T.), The Melanoma Research Alliance (571135 to R.T.), and in part by (American Cancer Society Institutional Research Grant IRG-16-187-13 to R.T.) from the American Cancer Society, T32 Training Program for Interdisciplinary Cancer Research IDCR (T32CA009054 to J.M.D.), NIH IMDS training grant (GM055246 to K.M.V.), T32 Microbiology and Infectious Diseases training grant (T32AI141346 to K.M.V.), and T32 virus-host interactions: a multi-scale training program (T32AI007319 to E.N.N.). C.F.G-J. is supported by UC Irvine Chancellor's ADVANCE Postdoctoral Fellowship Program, NSF-Simons Postdoctoral Fellowship, and NSF Grant DMS1763272 (to Qing Nie), and a kind gift from the Howard Hughes Medical Institute Hanna H. Gray Postdoctoral Fellowship Program. The authors would like to thank Dr. Denise Gay (DLG Biologics) for assistance processing scRNA-seq data and Dr. Jie Wu and Dr. Melanie Oakes (UCI Genomics High Throughput Facility) for setup and analysis of scRNA-seq.

SUPPLEMENTARY FIGURES

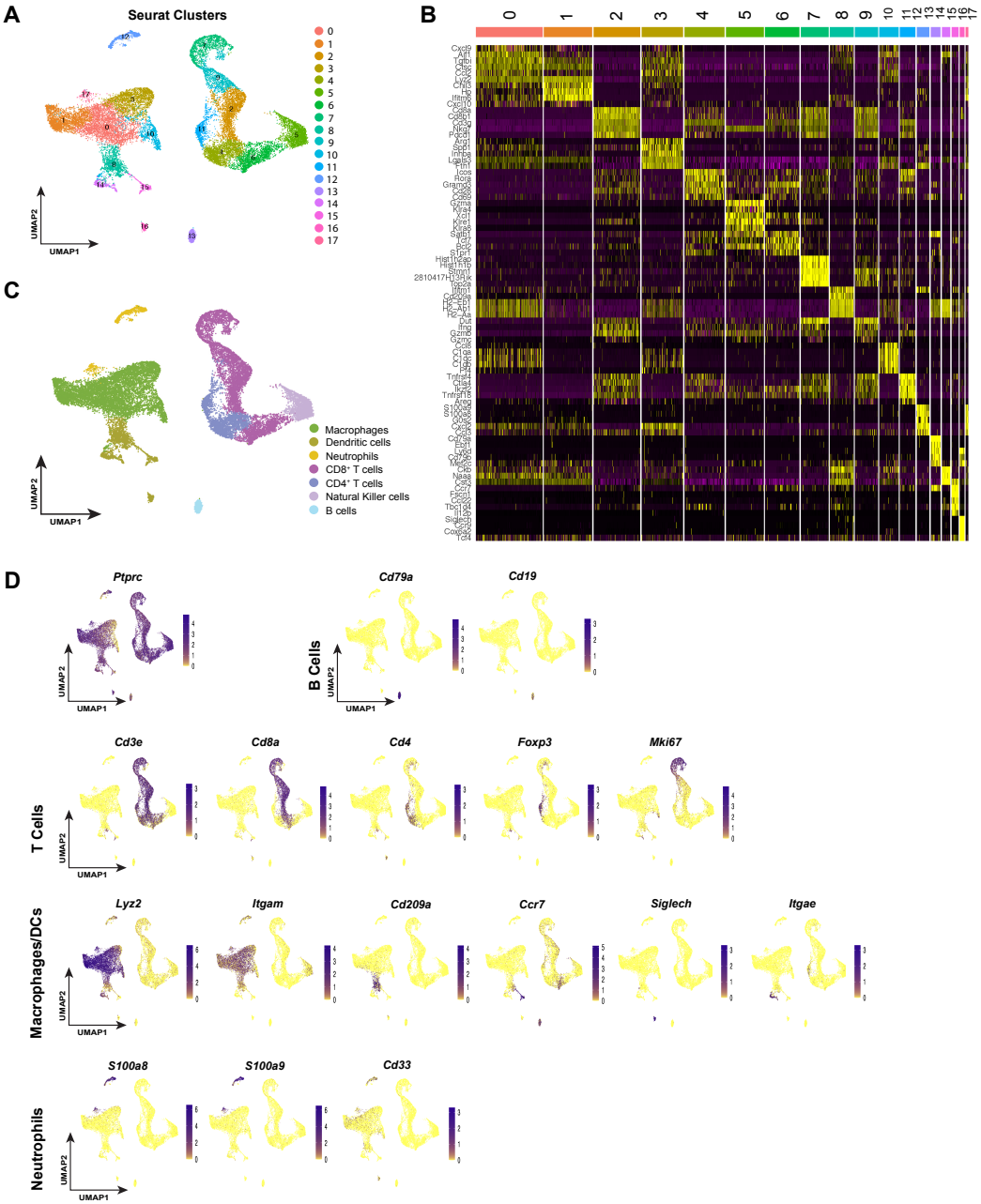

Figure S2.1 Immune cell clusters and cell types in melanoma tumors after antibody treatment. Two-dimensional Uniform Manifold Approximation and Projection (UMAP) plot of single-cell transcriptomic profiles of 23,858 CD45.2+ immune cells from IgG, a-PD-1, a-PSGL-1, and anti-PD-1/anti-PSGL-1 treated B16GP33 melanoma tumors (**A**). Heatmap displaying expression levels of top marker genes for cluster identification (**B**). Seurat clustering analysis projected in two-dimensional UMAP of combined treatment groups with color coded cell identities derived from expression of hallmark genes (**C**). Feature plots of established markers of T cells, macrophages/DCs, neutrophils, and B cells. Yellow is high expression and purple is low expression (**D**).

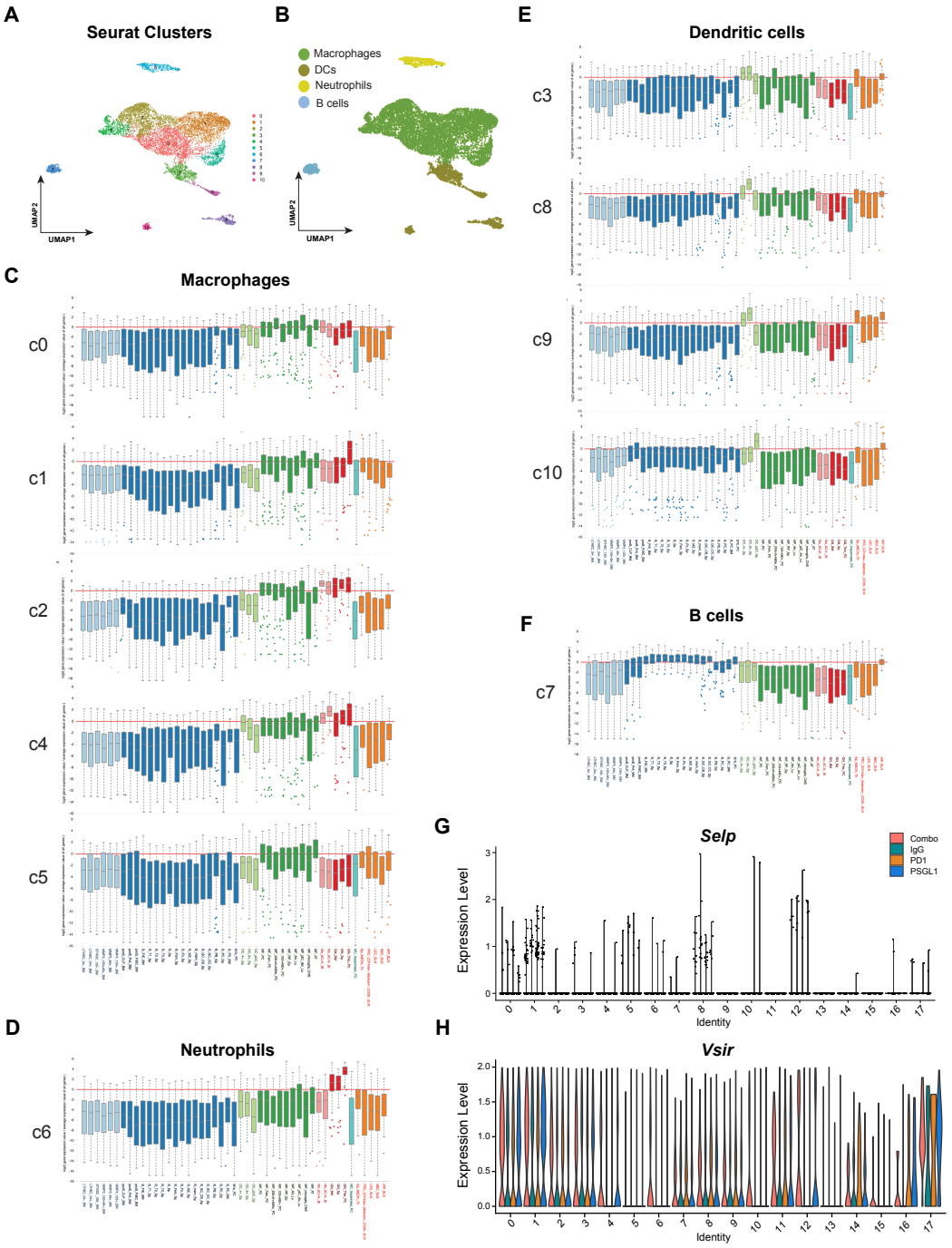

Figure S2.2 Seurat clustering analysis of myeloid and B cells and expression of PSGL-1 ligands. IgG, a-PD-1, a-PSGL-1, and anti-PD-1/anti-PSGL-1 treated B16GP33 melanoma tumor populations projected in two-dimensional UMAP (**A**). Unbiased Seurat clustering analysis projected in two-dimensional UMAP of combined treatment groups with color coded cell identities (macrophages, DCs, neutrophils, B cells) derived from expression of hallmark genes (**B**). Immgen plots of macrophage clusters c0, c1, c2, c4, and c5 (**C**). Immgen plot of neutrophil cluster c6 (**D**). Immgen plots of dendritic cell clusters c3, c8, c9, and c10 (**E**). Immgen plot of B cell cluster c7 (**F**). Violin plots of *Selp* (**G**) and *Vsir* (H) expression in Seurat-generated immune clusters.

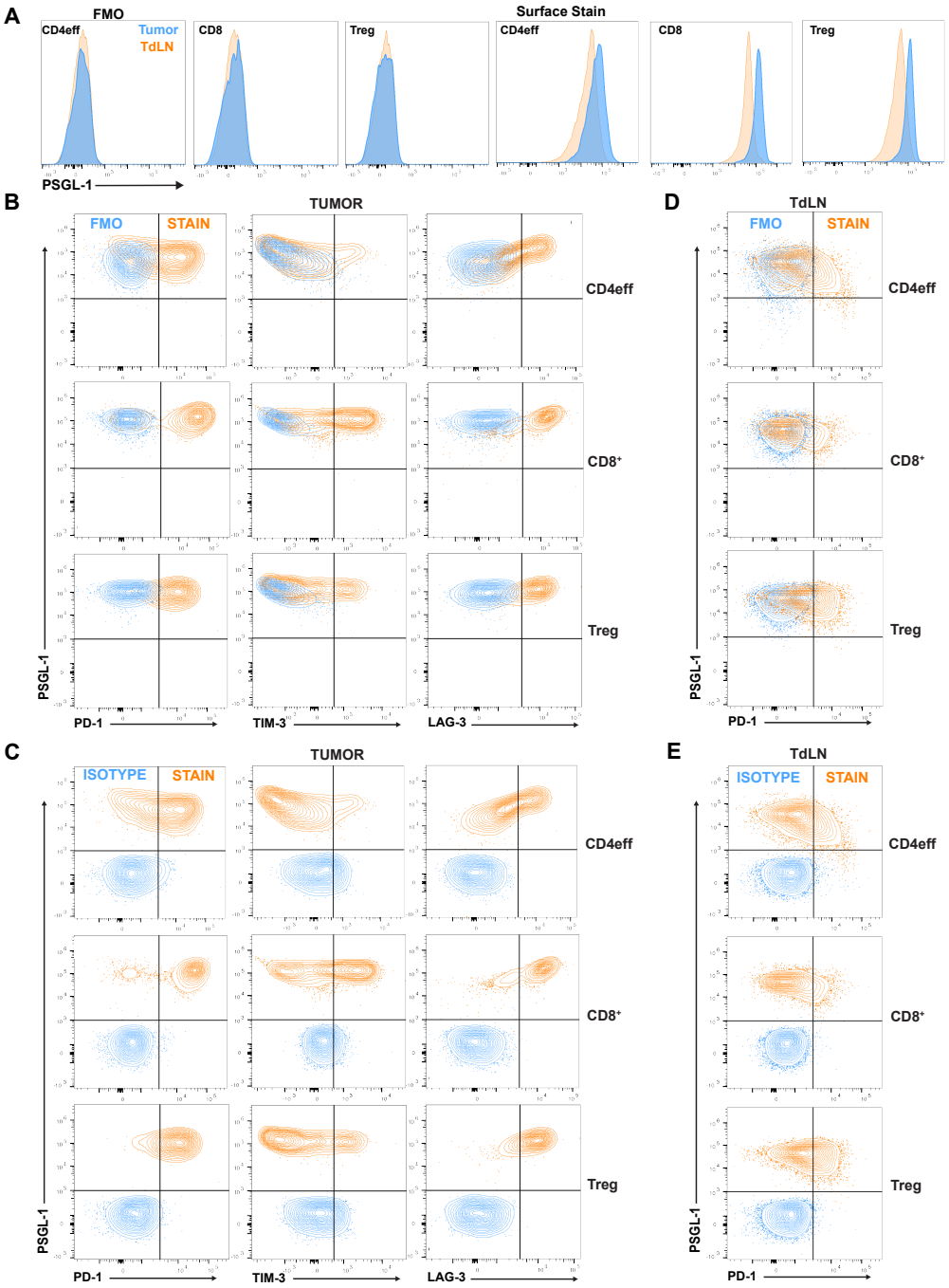

Figure S2.3 PSGL-1 expression and co-expression with inhibitory receptors in melanoma tumors and TdLNs. WT mice were injected s.c. with ($1x10^6$) B16-GP33 melanoma cells. Representative FACS plots of PSGL-1 fluorescence in $CD8^+$, $CD4^+$, and Tregs in the tumor and TdLN at 18dpi (**A**). Control FMOs are shown. Representative FACS plots of PSGL-1 co-expression with PD-1, TIM-3, and LAG3 in tumors (**B,C**). Control FMO and isotype staining are shown. Representative FACS plots of PSGL-1 co-expression with PD-1, TIM-3, and LAG3 in the TdLN (**D,E**). Representative PD-1 FMO and isotype control stains are shown.

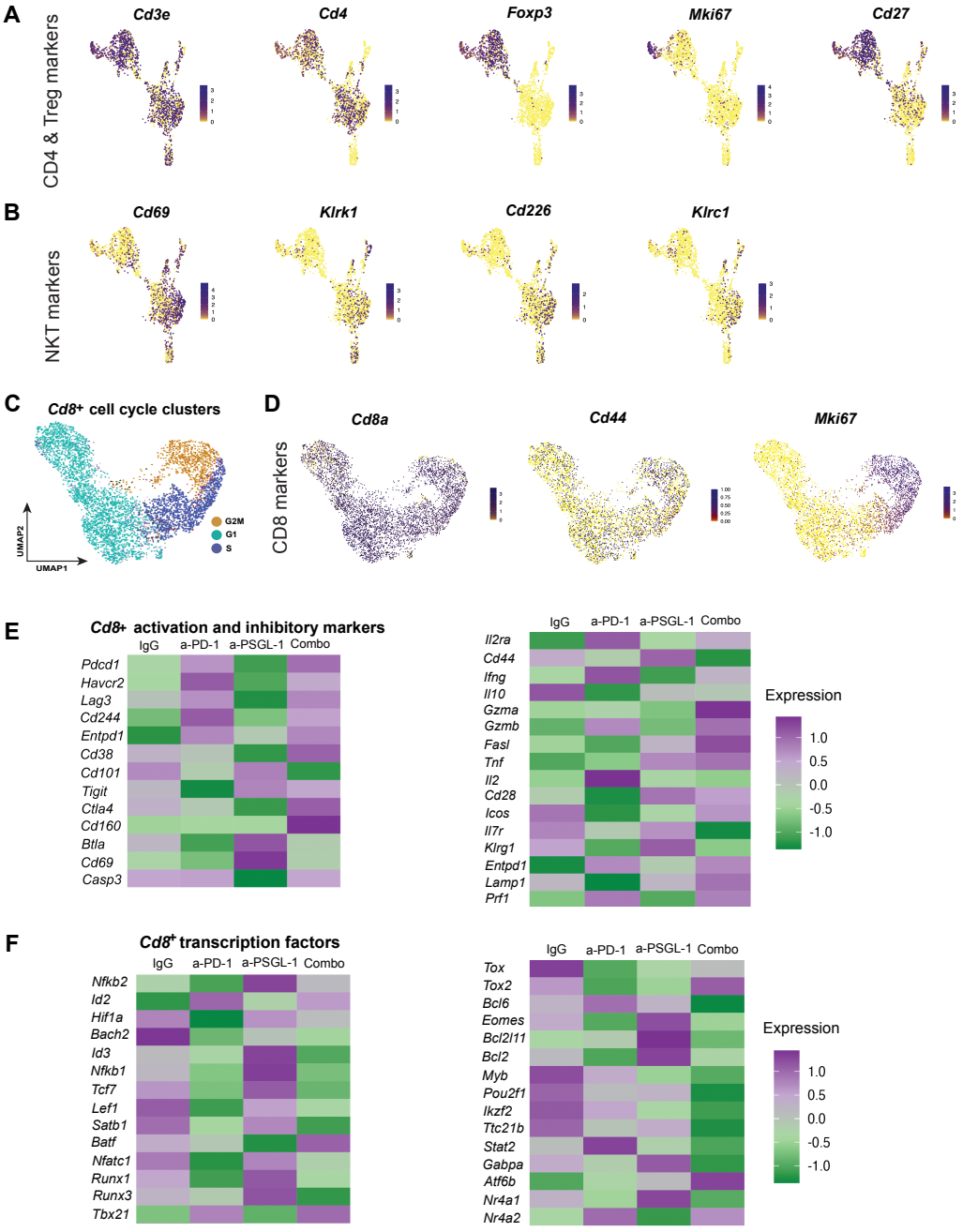

Figure S2.4 Seurat subset T cell clustering and heatmaps. Feature plots of established markers of CD4+ T and NKT cells are shown for the *Cd4*$^{+}$ and *Cd4*^{lo} subset clusters, yellow is high expression and purple is low expression (**A,B**).Seurat clustering analysis of *Cd8*$^{+}$ immune cells projected in two-dimensional UMAP with color coded cell cycle designations (**C**). Feature plots of established markers of CD8+ T cells are shown for the *Cd8*$^{+}$ subset clusters, yellow is high expression and purple is low expression (**D**). Heatmap displaying expression levels of activation and inhibitory marker (**E**) and transcription factor (**F**) genes for Cd8+ clusters from IgG, a-PD-1, anti-PSGL-1, and combo anti-PD-1/anti-PSGL-1 treatments. Purple is high and green is low expression.

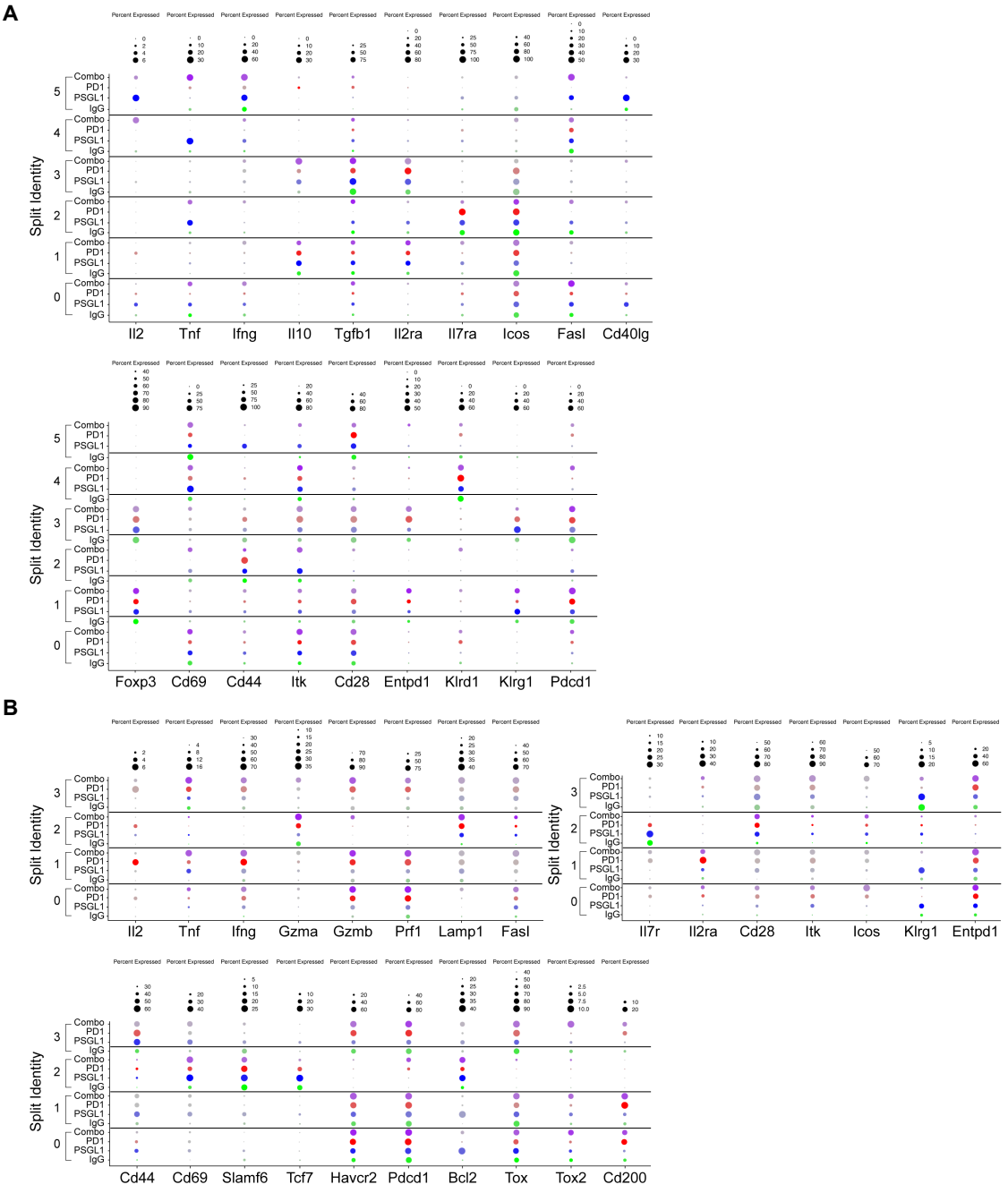

Figure S2.5 Regulation of activation and effector genes within *Cd4*⁺ and *Cd8*⁺ subclusters. Dot plots show percent expression and relative intensity of expression of activation and effector genes in *Cd4*⁺ subclusters (**A**). Dot plots show percent expression and relative intensity of expression of activation, effector, precursor, and terminal exhaustion genes in Cd8+ subclusters (**B**).

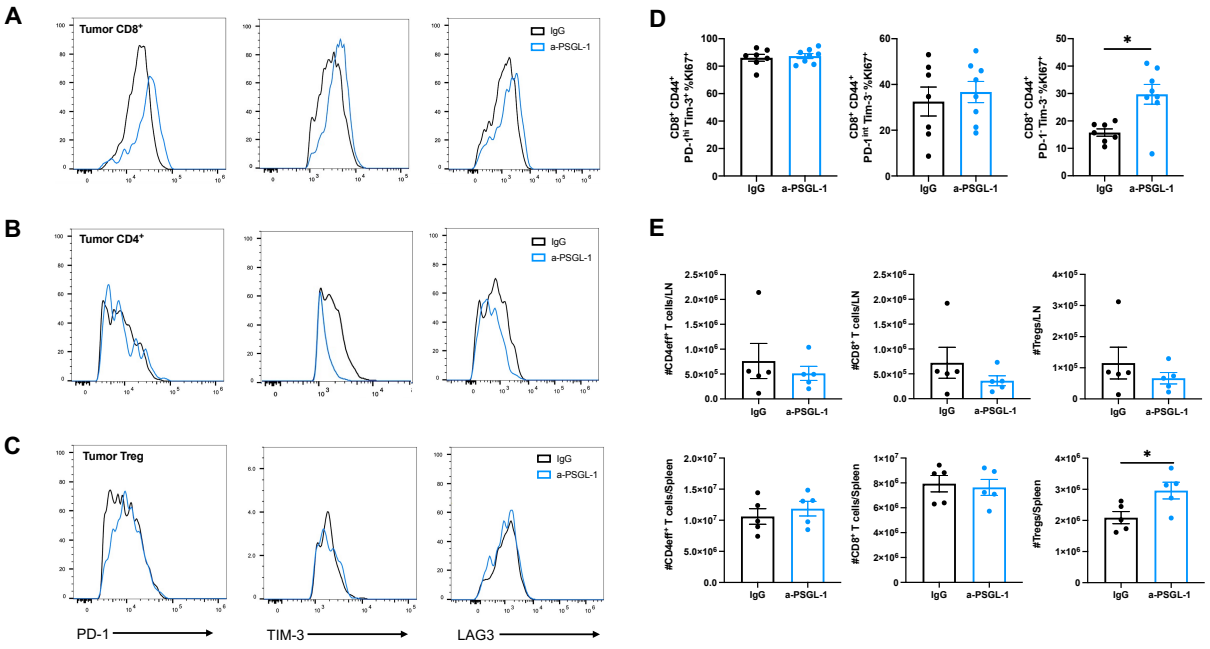

Figure S2.6 Immune checkpoint expression and proliferation in antitumor T cells. WT mice were injected s.c. with ($1x10^6$) B16-GP_{33} melanoma cells and treated with IgG or anti-PSGL-1 at 8, 10, and 12dpi. Representative FACS plots showing PD-1, TIM-3 and LAG3 expression in $CD8^+$ (**A**), $CD4^+$ (**B**), and Treg cells (**C**) in tumors. The frequencies of $Ki67^+$ $CD8^+$ T cell subsets ($PD\text{-}1^{hi}TIM\text{-}3^+$, $PD\text{-}1^{int}TIM\text{-}3^-$, $PD\text{-}1^-$ $TIM\text{-}3^-$) are shown in (**D**). WT mice were injected i.p. with IgG or anti-PSGL-1 at 0, 2 and 4dpi and LNs and spleen were dissected at 10dpi to check for T cell depletion with treatment. The number of $CD8^+$, $CD4^+$, and Tregs in LN and spleen are shown (**E**). Data are representative of four independent experiments (n ≥7 mice/group) (**A-D**) or one experiment (n ≥5 mice/group) (**E**). Graphs show the mean ± s.e.m. *P< 0.05 by two-tailed t-test.

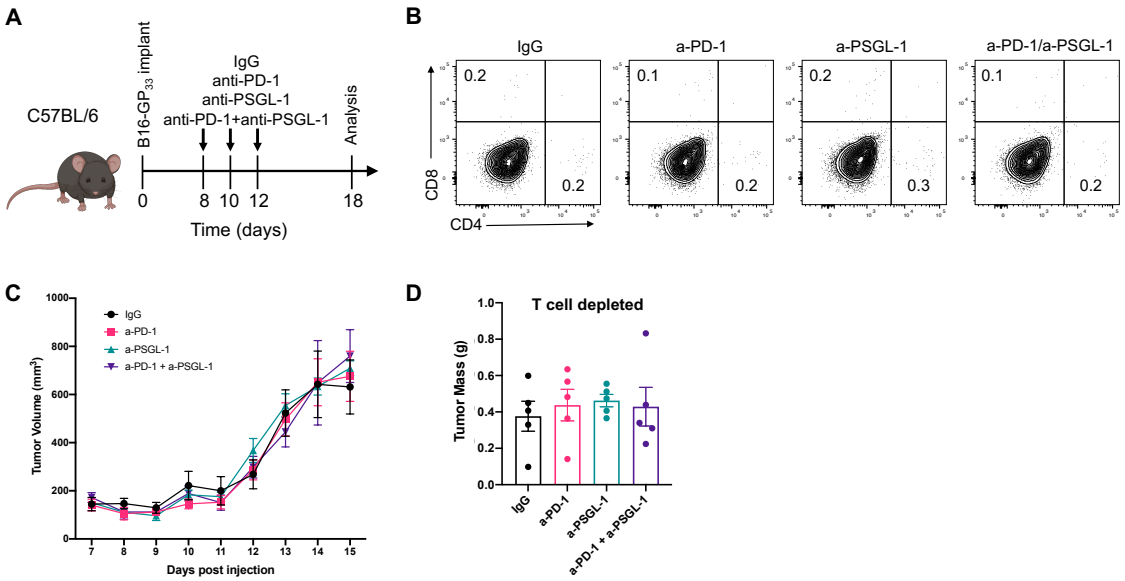

Figure S2.7 Combination treatment and tumor volume in T cell-depleted mice. Strategy showing combination treatments in melanoma tumor-bearing mice (**A**). WT mice were injected s.c. with ($1x10^6$) B16-GP_{33} melanoma cells, T cells were depleted using depleting antibodies, and mice were treated with IgG, anti-PD-1, anti-PSGL-1, or anti-PD-1/anti-PSGL-1 at 8, 10, 12 days after melanoma cell injections. FACS plots showing T cell depletion from each treatment group (**B**). Tumor growth kinetic in treatment groups that were T cell-depleted (**C**) and tumor mass at 15dpi (**D**). Data are representative of two independent experiments (n≥5 mice/group).

CHAPTER THREE

Cell-intrinsic CD38 expression sustains exhausted CD8$^+$ T cells by regulating their survival and metabolism during chronic viral infection

Julia M. DeRogatis[1], Emily N. Neubert[1,2], Karla M. Viramontes[1], Monique L. Henriquez[1], Dequina A. Nicholas[1], and Roberto Tinoco[1,2]

[1]Department of Molecular Biology and Biochemistry, School of Biological Sciences, University of California Irvine, Irvine, CA 92697, USA

[2]Center for Virus Research, University of California Irvine, Irvine, CA 92697, USA

Published in *The Journal of Virology*. DeRogatis JM, Neubert EN, Viramontes KM, Henriquez ML, Nicholas DA, Tinoco R. 2023. Cell-Intrinsic CD38 Expression Sustains Exhausted CD8(+) T Cells by Regulating Their Survival and Metabolism during Chronic Viral Infection. J Virol doi:10.1128/jvi.00225-23:e0022523 (275)

ABSTRACT

Acute and chronic viral infections result in the differentiation of effector and exhausted T cells with functional and phenotypic differences that dictate whether the infection is cleared or progresses to chronicity. High CD38 expression has been observed on $CD8^+$ T cells across various viral infections and tumors in patients, suggesting an important regulatory function for CD38 on responding T cells. Here we show that CD38 expression was increased and sustained on exhausted $CD8^+$ T cells following chronic LCMV infection, with lower levels observed on T cells from acute LCMV infection. We uncovered a cell-intrinsic role for CD38 expression in regulating the survival of effector and exhausted $CD8^+$ T cells. We observed increased proliferation and function of *Cd38*$^{-/-}$ $CD8^+$ progenitor exhausted T cells compared to WT cells. Furthermore, decreased oxidative phosphorylation and glycolytic potential were observed in *Cd38*$^{-/-}$ $CD8^+$ T cells during chronic but not acute LCMV infection. Our studies reveal that CD38 has a dual cell-intrinsic function in $CD8^+$ T cells where it decreases proliferation and function yet supports their survival and metabolism. These findings show that CD38 is not only a marker of T cell activation but also has regulatory functions on effector and exhausted $CD8^+$ T cells.

INTRODUCTION

CD38 is an ectoenzyme expressed on the surface of most innate and adaptive immune cells and is upregulated during T cell activation (167). Upon contact between antigen-presenting cells (APCs) and $CD8^+$ T cells *in vitro*, CD38 localizes to the immunological synapse where its enzymatic functions increase intracellular Ca^{2+} signaling (216, 276). As an ectoenzyme, CD38 converts nicotinamide adenine dinucleotide (NAD^+) to ADP-ribose (ADPR), cyclic-ADPR (cADPR), and $NAADP^+$ (167, 168, 170, 171). CD38 enzymatic activity has numerous physiological impacts, as ADPR, cADPR, and $NAADP^+$ all regulate cytoplasmic Ca^{2+} levels while NAD^+, which is consumed by CD38, is a modulator of cellular metabolism, stress response, and circadian rhythms (167, 168). Additionally, CD38 acts as a receptor on the surface of T cells, the ligation of which can further increase T cell activation through Lck-mediated activation of MAP kinase and CD3**ζ** signaling pathways (177). CD38 continues to be of interest as it is highly expressed on T cells during numerous viral infections and cancers (276). CD38 is a key indicator of T cell activation during viral infection, and $CD38^{hi}CD8^+$ T cells have been detected in patients infected with HCV, HIV, Dengue, H1N1 IAV, H7N9, Ebola, and SARS-CoV-2 (191-199). However, the functional role of CD38 in the anti-viral T cell response remains to be fully investigated.

While CD38 is upregulated with T cell activation during chronic infection and cancer, it is known to promote immunosuppression. CD38 negatively regulates inflammatory responses through the CD38/CD203/CD73 axis by converting NAD^+ to adenosine (172, 213). Adenosine signaling through the adenosine A2A receptor (A2AR) on T cells diminishes effector T cell functions, resulting in a loss of tumor control (277). Further, upregulation of CD38 on tumor cells increases adenosine production and limits T cell proliferation and responses to PD-1/PD-L1 checkpoint blockade (211).

However, adenosine-driven resistance to immunotherapy can be overcome by dual blockade of A2AR and PD-1, which enhances tumor-infiltrating $CD8^+$ T cell IFN-γ and GranzymeB production (278).

Recently, there has been increased interest regarding the role of CD38 in T cell exhaustion, as CD38 expression was found to mark terminally exhausted T cells in tumors (217). Prolonged T cell receptor (TCR) stimulation, as in the case of chronic viral infections and cancer, leads T cells towards a dysfunctional state known as T cell exhaustion (279, 280). Exhausted T cells can differentiate into two distinct populations: progenitor exhausted T cells (Tpex) and terminally exhausted T cells (Tex) (37, 38, 281). The Tpex population is capable of self-renewal and can respond to immune checkpoint blockade (ICB), while the Tex population retains some effector functions but is short-lived and unresponsive to ICB. Delineating these populations is of clinical interest, as patient response to ICB can be driven by the presence or absence of Tpex and Tex cells. CD38, along with CD101, has emerged as a marker for the $CD8^+$ Tex population, which has a fixed epigenetic chromatin state that prevents these cells from regaining effector functions (217). Further, resistance to PD-1 ICB is driven by a population of suboptimally primed, dysfunctional PD-$1^+CD38^{hi}CD8^+$ T cells (219).

While CD38 is an established marker of terminal T cell exhaustion, whether CD38 has a role in promoting exhaustion is still being investigated. In a murine melanoma model, both CD38 deletion and overexpression in antigen-specific $CD8^+$ T cells were not sufficient to alter the exhaustion phenotype of tumor-infiltrating lymphocytes (222). In the case of chronic viral infections, such as HIV, CD38 expression is correlated with disease severity (200). As patients develop acquired immune deficiency syndrome (AIDS), the frequency of CD38 expressing $CD8^+$ T cells increases, and then declines with antiretroviral treatment (201, 204, 205). However, the impact of CD38 expression on the phenotype and function of exhausted T cells in chronic viral infection is currently unknown (200). In this study, we used acute Armstrong (Arm) and chronic Clone 13 (Cl13) lymphocytic

choriomeningitis virus (LCMV) to investigate the cell-intrinsic role of CD38 on virus-specific T cells during acute and chronic infection. In a co-transfer model of virus-specific WT and *Cd38*$^{-/-}$ P14^{+} CD8^{+} T cells, we show that *Cd38*$^{-/-}$ P14^{+} CD8^{+} T cells had decreased survival in both acute and chronic infection. We show that CD38 expression maintained transferred P14^{+} Tpex and Tex populations in Cl13 infected mice, but also restrained proliferation and GranzymeB production in Tpex cells. We found that CD38 did not alter oxidative phosphorylation and glycolysis of adoptively transferred effector T cells generated during Arm infection, but exhausted *Cd38*$^{-/-}$ P14^{+} T cells showed reduced metabolic function in both pathways. Taken together, our study shows that CD38 is an important regulator of virus-specific CD8^{+} T cell survival in both acute and chronic infection. Our work presents an interesting paradigm for CD38 on CD8^{+} Tpex cells, in which CD38 hinders their proliferation and GranzymeB production, but also ensures their survival.

MATERIALS AND METHODS

Mice

Experimental male C57BL/6J (no. 000664) mice were obtained from The Jackson Laboratory and were used at 6-9 weeks of age. B6.129P2-*Cd38*^{tm1Lnd}/J (*Cd38*$^{-/-}$, no. 003727) mice were obtained from The Jackson Laboratory and bred for experiments. P14^{+} mice were obtained from The Scripps Research Institute (originally from Dr. Charles D. Surh) and were crossed with *Cd38*$^{-/-}$ mice to obtain P14^{+} *Cd38*$^{-/-}$ mice. Mice were used at ≥6 weeks of age. Animal care was in accordance with the UC Irvine Institutional Animal Care and Use Committees.

Virus Infection

Lymphocytic choriomeningitis (LCMV) Armstrong and Cl13 strains were propagated in baby-hamster kidney cells and titrated on Vero African-green-monkey kidney cells. Frozen stocks were diluted in Vero cell media and 2x10^{5} plaque-forming units (PFUs) of LCMV Armstrong were injected intraperitoneally (i.p.) or 2x10^{6} PFUs of LCMV Cl13 were injected intravenously (i.v.). For seahorse metabolism studies, mice were infected with Arm (i.p.) or Cl13 retro-orbitally (r.o.).

T Cell Adoptive Transfer

CD8^{+} T cells were enriched from spleens and lymph nodes (LNs) of WT or *Cd38*$^{-/-}$ P14^{+} transgenic mice by column-free magnetic negative selection. Single cell suspensions from pooled spleen and LNs were incubated with biotinylated antibodies purchased from Biolegend against CD4 (GK1.5), B220 (RA3-6B2), CD19 (6D5), CD24 (M1/69), CD11b (M1/70), and CD11c (N418). Labeled cells were removed by mixing cell suspension with Streptavidin RapidSpheres (Stemcell technologies) at RT for 5min, followed by two-5min incubations in an EasyEights™ EasySep™ Magnet (Stemcell technologies). Enriched CD8^{+} T cells were washed in sterile PBS (1x) with FBS (2%), and purity determined by flow cytometry. For uninfected co-transfer experiments, WT P14^{+}

(CD45.1$^+$) and *Cd38*$^{-/-}$ P14$^+$ (CD45.1$^+$CD45.2$^+$) T cells normalized (CD8a$^+$Va2$^+$) and mixed at a 1:1 ratio (1x10^4 cells/genotype) and injected retro-orbitally into WT (CD45.2$^+$) recipient mice. Blood, spleen, and LNs were analyzed for adoptively transferred populations 24h after injection. For infected co-transfer experiments, live WT P14$^+$ (CD45.1$^+$) or *Cd38*$^{-/-}$ P14$^+$ (CD45.1$^+$CD45.2$^+$) T cells were normalized (CD8a$^+$Va2$^+$) and mixed at a 1:1 ratio (1x10^3 cells/genotype) and injected into WT (CD45.2$^+$) recipient mice i.v. These mice were infected with LCMV one day later. Mice were bled r.o. and spleens and lymph nodes were isolated at the indicated time points. Schematic of co-transfer was created with BioRender.com.

Flow Cytometry

For cell surface staining, 2x10^6 cells were incubated with antibodies in staining buffer (PBS, 2% FBS and 0.01% NaN_3) and fixed in PBS with 1.85% formaldehyde for 20 min on ice. For LCMV tetramer staining, cells were incubated with H-2D^b-GP$_{33–41}$, H-2D^b-GP$_{276-286}$, H-2D^b-NP$_{396–404}$, or IA^b-$_{66–77}$ tetramers (NIH core facility) for 1 hr 15 min at room temperature in staining buffer and then fixed with PBS with 1.85% formaldehyde for 20 min on ice. For intracellular cytokine stimulation and staining, cells were resuspended in complete RPMI-1640 (containing 10 mM HEPES, 1% nonessential amino acids and L-glutamine, 1 mM sodium pyruvate, 10% heat inactivated fetal bovine serum (FBS), and antibiotics) supplemented with 50 U/mL IL-2 (NCI) and 1 mg/mL brefeldin A (BFA, Sigma), and then incubated with 2mg/mL LCMV GP$_{33-41}$ peptide (AnaSpec) at 37°C for 4h. Cells were then fixed and permeabilized using a Cytofix/Cytoperm Kit (BD Biosciences) before staining. For intranuclear transcription factor and Ki67 staining, cells were fixed and permeabilized using a Foxp3/transcription factor fixation/permeabilization kit (Fisher) and then stained with anti-human GranzymeB (GB12) from Thermo Fisher and Ki67 (B56) from BD Bioscience. Fluorochrome-conjugated antibodies CD44 (IM7), CD45.1 (A20), CD45.2 (104), CD8α (53-6.7), CD4 (RM4-5),

CD38 (90), CD160 (7H1), CD223 (C9B7W), CD279 (RMP1-30), CD366 (RMT3-23), CD244.2 (m2B4 (B6) 458.1), KLRG1 (2FI/KLRG1), and CD69 (H1.2F3) were purchased from BioLegend. Fluorochrome-conjugated Ly-108 (13G3) was purchased from BD Biosciences. Fluorochrome-conjugated TCF-1 (C63D9) was purchased from Cell Signaling Technology. Surface stains were performed at a 1:200 dilution, while intracellular and intranuclear stains performed at a 1:100 dilution. Caspase3 staining was done using PI (Sigma-Aldrich) and CaspGLOW Fluorescein Active Caspase-3 staining kit (ThermoFisher) and following manufacturer's instructions. All data were collected on a Novocyte3000 (Agilent) and analyzed using FlowJo Software (Tree Star).

Seahorse assay

Co-transferred WT or *Cd38*$^{-/-}$ P14^{+} T cells were isolated from spleens of host mice at 8 days post Armstrong or Cl13 infection. CD8^{+} T cells were purified by negative selection (see methods in T Cell Adoptive Transfer), stained for 10 minutes with propidium iodide (PI) in complete media RPMI-1640 (containing 10 mM HEPES, 1% nonessential amino acids and L-glutamine, 1 mM sodium pyruvate, 10% heat inactivated fetal bovine serum (FBS), and 1% antibiotics (Penicillin, Streptomycin, L-Glutamine) from Corning) surface stained with CD8 BV785 (53-6.7), CD45.1 PB (A20), and CD45.2 FITC(104) from BioLegend, and sorted on a BD FACSAria Fusion at >95% purity. FACS was used to isolate WT P14^{+} (PI^{-}CD8^{+}CD45.1^{+}CD45.2^{-}) and *Cd38*$^{-/-}$ P14^{+} (PI^{-}CD8^{+}CD45.1^{+}CD45.2^{+}) T cells. Live cells were counted immediately after sorting and adhered onto the wells of a poly-D-lysine coated XF96 plate at between 500,000-550,000 cells/well (exact counts were noted and used for normalization). The Seahorse XF Mito Stress Test was performed to measure OCR and ECAR of cells plated in XF media (non-buffered DMEM containing 10 mM glucose, 4 mM L-glutamine, and 2 mM sodium pyruvate) under basal conditions and in response to 1 μM oligomycin (Calbiochem), 1.5 μM fluoro-carbonyl cyanide phenylhydrazone (FCCP) (Enzo) and 1 μM rotenone + 1 μM antimycin

A (Enzo) with the XF96 Extracellular Flux Analyzer (Seahorse Bioscience). Data were normalized using Wave software (Agilent). Basal respiration values were determined as the mean OCR of the last 3 baseline data points minus the median of the 3 OCR data points after antimycin A and rotenone addition (282). Maximal OCR values were determined as the max of the three OCR values after FCCP addition minus the median of the last 3 values after rotenone and antimycin A addition. Basal ECAR values were determined as the mean of the last 3 baseline points. Maximal ECAR values were determined as the highest ECAR point after addition of FCCP. Basal OCR:ECAR was determined as the mean OCR of the last 3 baseline data points divided by the mean of the ECAR of the last 3 baseline data points. Maximal OCR:ECAR was determined as the highest of the 3 OCR values after the addition of FCCP divided by the corresponding ECAR value.

Quantification and Statistical Analysis

Flow cytometry data were analyzed with FlowJo software (TreeStar). Graphs of flow cytometry data and Seahorse data were prepared with GraphPad Prism software. GraphPad Prism was used for statistical analysis to compare outcomes using a two-tailed unpaired Student's *t*-test, Mann Whitney, or a two-tailed paired *t*-test where indicated; significance was set to $P \leq 0.05$ and represented as $*P \leq 0.05$, $**P \leq 0.01$, $***P \leq 0.001$, and $****P \leq 0.0001$. Error bars show SEM.

RESULTS

CD38 expression is upregulated on exhausted CD8$^+$ T cells during chronic viral infection

To assess how CD38 is regulated during acute and chronic viral infections, we infected WT mice with either LCMV Arm or Cl13 and measured PD-1 and CD38 expression on virus-specific T cells over the course of infection. Consistent with previous studies, PD-1 was highly expressed on LCMV MHC class I tetramer$^+$ CD8$^+$ T cells early in chronic Cl13 infection and remained higher than acute infection, albeit to a lower level, over the course of infection (**Fig. 3.1A**). While PD-1 was also expressed during acute Arm infection, it remained significantly lower on virus-specific T cells when compared to Cl13 (**Fig. 3.1A**). As with PD-1, CD38 was also highly upregulated on LCMV MHC class I tetramer$^+$ CD8$^+$ T cells from Cl13 infected mice, peaking at 17 days post infection (dpi) and remaining elevated throughout infection (**Fig. 3.1B**). CD38 was also upregulated on tetramer$^+$ CD8$^+$ T cells during Arm infection, however levels were significantly lower compared to Cl13 infection. We next determined whether cells upregulate PD-1 and CD38 together during infection (**Fig. 3.1C**). In Cl13 infected mice, the majority of LCMV MHC class I tetramer$^+$ CD8$^+$ T cells co-expressed PD-1 and CD38 (**Fig. 3.1C**). In contrast, acutely infected mice had low frequencies of PD-1$^+$CD38$^+$ tetramer$^+$ CD8$^+$ T cells (**Fig. 3.1C**). Next, we examined the regulation of CD38 during chronic viral infection in patients, using a previously published dataset from Hensel, N. *et al.*, 2021 (GSE150345) (35). We analyzed HCV-specific CD8$^+$ T cell *CD38* expression in patients both during chronic HCV (cHCV) infection and after these patients received direct-acting antiviral (DAA) treatment which cured their infection. In data collected from three separate patients, *CD38* expression was high during cHCV infection and levels decreased when these patients were cured from persistent infection (**Fig. 3.1D**). These findings showed that CD38 is expressed on virus-specific CD8$^+$ T cells during acute and chronic viral infection but high expression is sustained on exhausted CD8$^+$ T cells.

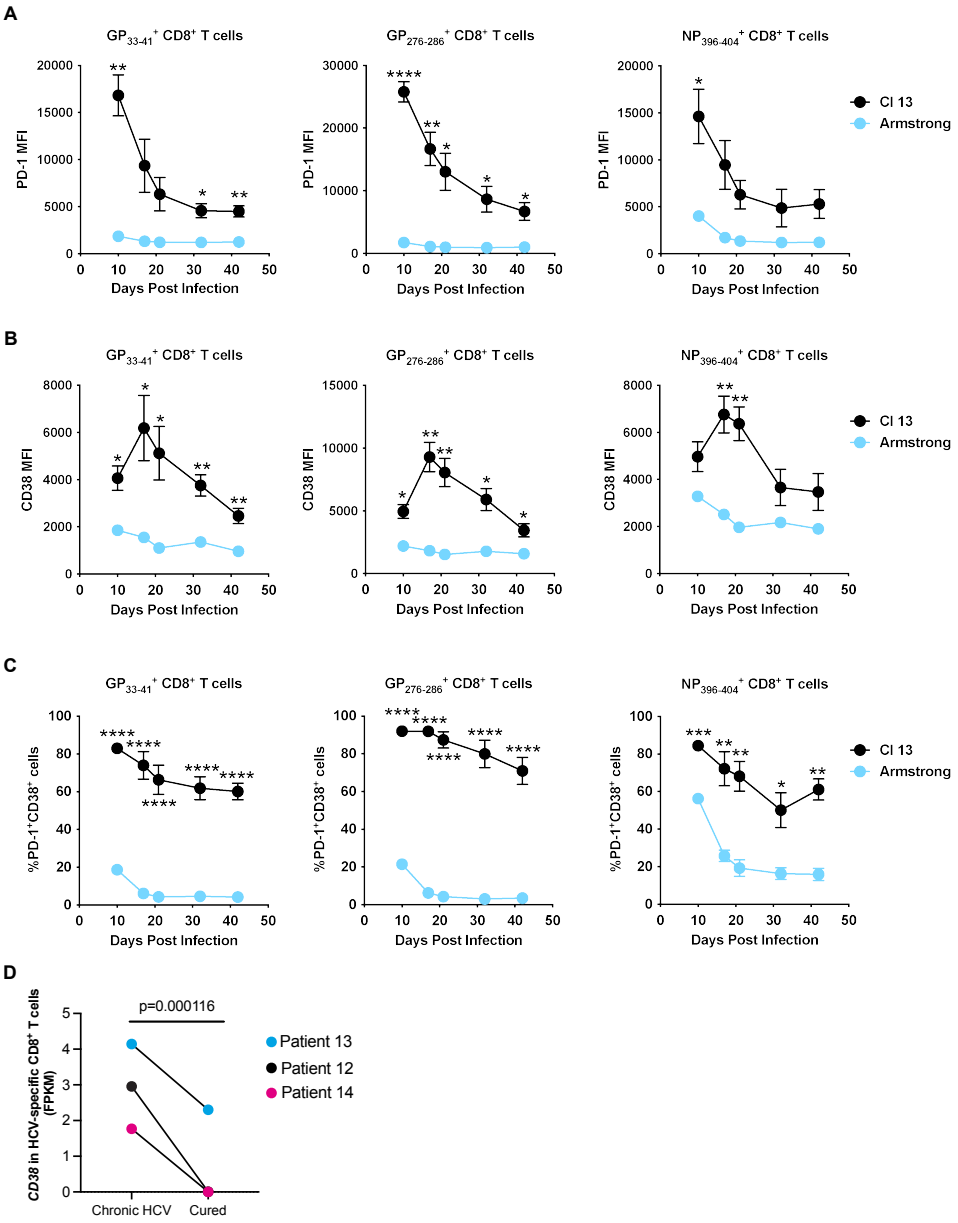

Figure 3.1 CD38 expression and co-regulation with PD-1 during acute and chronic infection. WT mice were infected with 2x10^5 PFU LCMV Armstrong i.p. or 2x10^6 PFU LCMV Cl13 i.v. Geometric mean fluorescence intensity (MFI) of PD-1 on GP_{33-41}, $GP_{276-286}$, and $NP_{396-404}$ tetramer-specific CD8$^+$ T cells in blood of Arm or Cl13-infected mice (**A**). Geometric mean fluorescence intensity (MFI) of CD38 on GP_{33-41}, $GP_{276-286}$, and $NP_{396-404}$ tetramer-specific CD8$^+$ T cells in blood of Arm or Cl13-infected mice (**B**). Frequency of PD-1$^+$CD38$^+$ GP_{33-41}, $GP_{276-286}$, and $NP_{396-404}$ tetramer-specific CD8$^+$ T cells in blood of Arm or Cl13-infected mice (**C**). Virus-specific CD8$^+$ T cells were isolated from patients with hepatitis C infection and low-input RNA-sequencing was performed by Hensel, N. *et al.*,2021 (GSE150345). This data was used to graph the average normalized *CD38* expression in human HCV-specific CD8$^+$ T cells both during cHCV infection and after direct-acting antiviral (DAA)-cure (**D**). Significance was assessed by differential analysis with multi-factor design of paired samples using DESeq2. Data are representative of 3 independent experiments with ≥ 5 mice per group. Data show mean ± s.e.m. *P ≤ 0.05, ***P ≤ 0.001, ****P ≤ 0.0001, multiple unpaired t-test.

Cell-intrinsic CD38 expression supports the survival of virus-specific CD8$^+$ T cells during acute and chronic viral infection

Since we saw CD38 expression on T cells during LCMV infection, we evaluated the cell-intrinsic role of CD38 in CD8$^+$ T cells during acute and chronic viral infection. We co-injected small numbers (1x10^3 cells/each) of WT and *Cd38*$^{-/-}$ P14$^+$ T cell receptor (TCR) transgenic CD8$^+$ T cells specific for LCMV peptide GP_{33-41} into WT mice (**Fig. 3.2A**). WT host mice (CD45.2$^+$) received WT P14$^+$ (CD45.1$^+$) and *Cd38*$^{-/-}$ P14$^+$ (CD45.1$^+$CD45.2$^+$) T cells at a 1:1 ratio, and one day later were infected with LCMV Arm or Cl13. At 8 days post Arm infection the frequencies and numbers of *Cd38*$^{-/-}$ P14$^+$ T cells in the spleen were significantly lower than WT P14$^+$ T cells (**Fig. 3.2B-D**). Over the course of infection, this phenotype persisted, with *Cd38*$^{-/-}$ P14$^+$ T cells present at lower frequencies and numbers out to 30dpi (**Fig. 3.2B,E,F**). *Cd38*$^{-/-}$ P14$^+$ T cells were also present at lower levels than WT P14$^+$ T cells in the blood at 8 and 30dpi (**Fig. S3.1A,B)** and trended toward lower levels in the lymph nodes (**Fig. S3.1B**). Since lower frequencies of *Cd38*$^{-/-}$ P14$^+$ T cells were observed, we next investigated the survival of the co-transferred cells. At day 6 post Arm infection, *Cd38*$^{-/-}$ P14$^+$ T cells had significantly decreased frequencies of cleaved Caspase3$^+$ apoptotic cells (**Fig. 3.2G**). However, by 8dpi and continuing to 30dpi, this trend had reversed and *Cd38*$^{-/-}$ P14$^+$ T cells showed significantly increased frequencies of Caspase3$^+$ apoptotic cells (**Fig. 3.2G**).

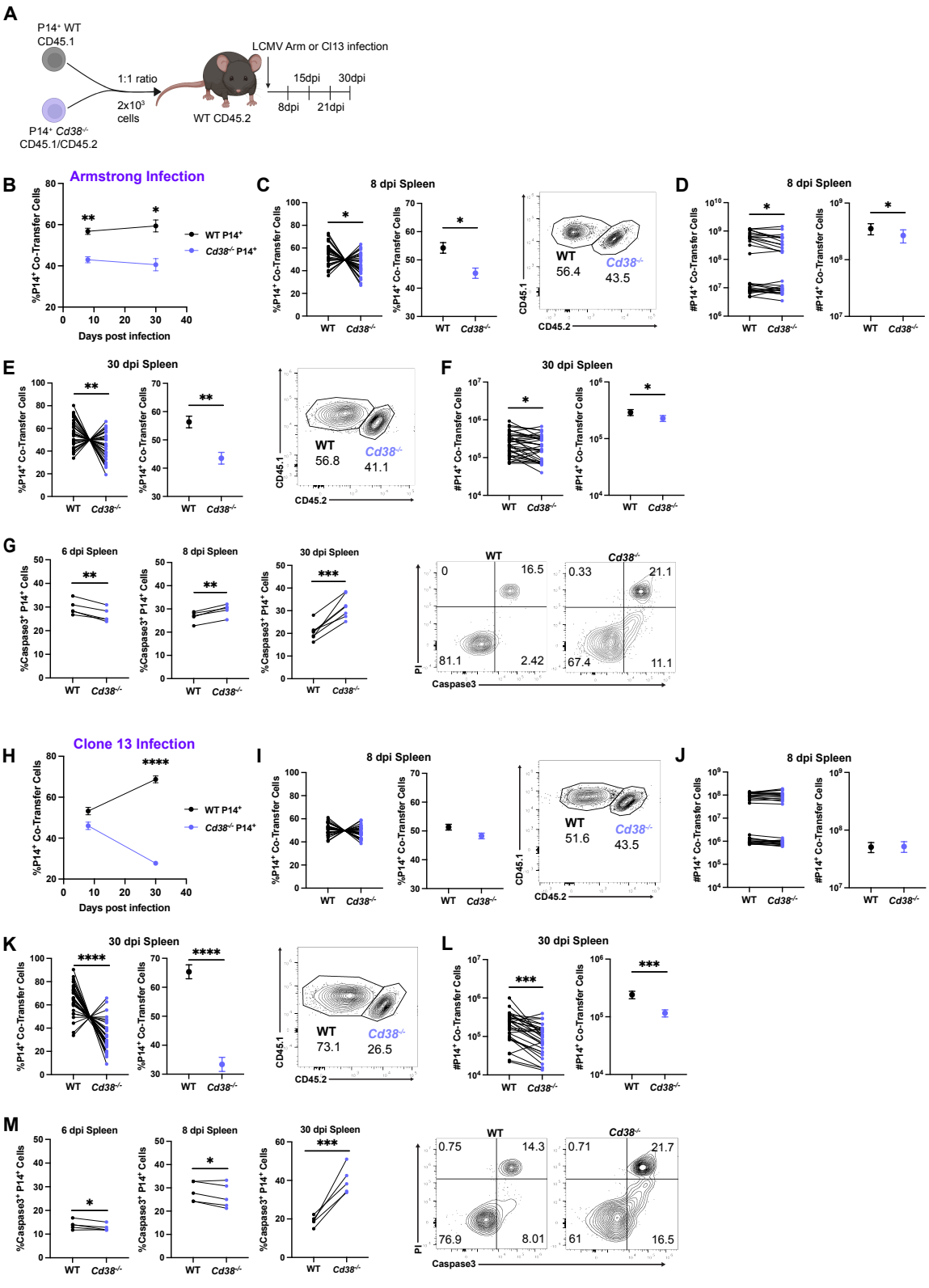
A
P14+ WT CD45.1
P14+ Cd38-/- CD45.1/CD45.2
1:1 ratio
2x10^3 cells
WT CD45.2
LCMV Arm or Cl13 infection
15dpi
30dpi
8dpi
21dpi
B
Armstrong Infection
%P14+ Co-Transfer Cells
WT P14+
Cd38-/- P14+
Days post infection
C
8 dpi Spleen
WT
56.4
Cd38-/-
43.5
CD45.1
CD45.2
D
8 dpi Spleen
#P14+ Co-Transfer Cells
E
30 dpi Spleen
WT
56.8
41.1
F
30 dpi Spleen
G
6 dpi Spleen
8 dpi Spleen
30 dpi Spleen
%Caspase3+ P14+ Cells
0
16.5
81.1
2.42
0.33
21.1
67.4
11.1
PI
Caspase3
H
Clone 13 Infection
I
8 dpi Spleen
WT
51.6
43.5
J
8 dpi Spleen
K
30 dpi Spleen
WT
73.1
26.5
L
30 dpi Spleen
M
6 dpi Spleen
8 dpi Spleen
30 dpi Spleen
0.75
14.3
76.9
8.01
0.71
21.7
61
16.5

Figure 3.2 Cell-intrinsic kinetics and survival of WT and *Cd38*$^{-/-}$ P14^{+} T cells during acute and chronic LCMV infection. WT and *Cd38*$^{-/-}$ P14^{+} CD8^{+} T cells were transferred at a 1:1 ratio (1x10^{3} each) into WT naïve mice, followed by LCMV Arm or Cl13 infection a day later (**A**). Ratio of co-transferred WT and *Cd38*$^{-/-}$ P14^{+} T cells in the spleen at 8 and 30dpi in Arm-infected mice (**B**). Individual ratios (left) and averaged ratio (right) of co-transferred WT or *Cd38*$^{-/-}$ P14^{+} T cells from six experiments at 8dpi in the spleen of Arm-infected mice (**C**). Representative FACS plots of co-transferred WT or *Cd38*$^{-/-}$ P14^{+} T cells at 8dpi in the spleen of Arm-infected mice (**C**). Individual numbers (left) and averaged numbers (right) of co-transferred WT or *Cd38*$^{-/-}$ P14^{+} T cells at 8dpi in the spleen of Arm-infected mice (**D**). Individual ratios (left) and averaged ratio (right) of co-transferred WT or *Cd38*$^{-/-}$ P14^{+} T cells from six experiments at 30dpi in the spleen of Arm-infected mice (**E**). Representative FACS plots (**E**), individual numbers (**F**, left) and averaged numbers (**F**, right) of co-transferred WT or *Cd38*$^{-/-}$ P14^{+} T cells at 30dpi in the spleen of Arm-infected mice. Frequencies of Caspase3^{+} apoptotic WT or *Cd38*$^{-/-}$ P14^{+} T cells at 6, 8, and 30dpi in the spleen of Arm-infected mice and representative FACS plots (**G**). Ratio of co-transferred WT and *Cd38*$^{-/-}$ P14^{+} T cells in the spleen at 8 and 30dpi in Cl13-infected mice (**H**). Individual ratios (left) and averaged ratio (right) of co-transferred WT or *Cd38*$^{-/-}$ P14^{+} T cells from six experiments at 8dpi in the spleen of Cl13-infected mice (**I**). Representative FACS plots of co-transferred WT or *Cd38*$^{-/-}$ P14^{+} T cells at 8dpi in the spleen of Cl13-infected mice (**I**). Individual numbers (left) and averaged numbers (right) of co-transferred WT or *Cd38*$^{-/-}$ P14^{+} T cells at 8dpi in the spleen of Cl13-infected mice (**J**). Individual ratios (left) and averaged ratio (right) of co-transferred WT or *Cd38*$^{-/-}$ P14^{+} T cells from six experiments at 30dpi in the spleen of Cl13-infected mice (**K**). Representative FACS plots (**K**), individual numbers (**L**, left) and averaged numbers (**L**, right) of co-transferred WT or *Cd38*$^{-/-}$ P14^{+} T cells at 30dpi in the spleen of Cl13-infected mice. Frequency of Caspase3^{+} apoptotic WT or *Cd38*$^{-/-}$ P14^{+} T cells at 6, 8, and 30dpi in the spleen of Cl13-infected mice and representative FACS plots (**M**). Data are representative of 6 independent experiments with ≥ 5 mice per group. Data show mean ± s.e.m. *P ≤ 0.05, ***P ≤ 0.001, ****P ≤ 0.0001, paired t-test.

Next, we investigated the role of CD38 in virus-specific T cells during chronic infection, using the same co-transfer set-up described above. Adoptively transferred *Cd38*$^{-/-}$ P14^{+} T cells were present at similar frequencies to WT P14^{+} T cells at 8dpi in the spleen, and then dropped to significantly lower frequencies over the course of Cl13 infection (**Fig. 3.2H,I,K**). This was true of the number of *Cd38*$^{-/-}$ P14^{+} T cells as well, which were present at similar numbers to WT P14^{+} T cells at 8dpi (**Fig. 3.2J**), and then significantly lower numbers at 30dpi (**Fig. 3.2L**). *Cd38*$^{-/-}$ P14^{+} T cells were present at lower levels than WT P14^{+} T cells in the blood at 8 dpi (**Fig. S3.1C)** and similar levels to WT P14^{+} T cells in the blood and lymph nodes at 30dpi (**Fig. S3.1D**). When apoptosis of adoptively transferred subsets was analyzed, *Cd38*$^{-/-}$ P14^{+} T cells initially had reduced Caspase3^{+} frequencies at 6 and 8dpi, and then significantly higher frequencies of Caspase3^{+} apoptotic cells than WT P14^{+} T cells at 30dpi (**Fig. 3.2M**). Because we saw a reduction of *Cd38*$^{-/-}$ P14^{+} T cells at multiple timepoints during acute and chronic infection, we wondered how these cells faired in competition with WT P14^{+} T cells in uninfected mice. When WT and *Cd38*$^{-/-}$ P14^{+} populations were examined in lymph nodes and spleens 24h after adoptive transfer, there was a significant decrease in the frequencies of *Cd38*$^{-/-}$ P14^{+} T cells (**Fig. S3.1E,F**). These findings showed a cell-intrinsic role for CD38 both in promoting initial residence in uninfected mice, as well as survival of CD8^{+} T cells during acute and chronic viral infection.

Cd38$^{-/-}$ CD8^{+} T cells are activated after acute and chronic LCMV infection

Because we saw that CD38 deletion impacted the survival phenotype of CD8^{+} T cells during LCMV infection, we wanted to examine whether loss of CD38 also impacted the effector phenotype of CD8^{+} T cells at 8 days post Arm and Cl13 infection. WT P14^{+} (CD45.1) and *Cd38*$^{-/-}$ P14^{+} (CD45.1^{+}/CD45.2^{+}) cells were co-transferred in small numbers (2x10^{3}) into mice at a 1:1 ratio, and one day later mice were infected with LCMV Arm or Cl13. The frequency of co-transferred

GranzymeB$^+$ cells was increased in *Cd38*$^{-/-}$ P14$^+$ T cells (**Fig. 3.3A**), while proliferating Ki67$^+$ P14$^+$ cell frequencies were similar between WT and *Cd38*$^{-/-}$ P14$^+$ T cells at 8 days post Arm infection (**Fig. 3.3B**). We next evaluated inhibitory receptor expression in WT and *Cd38*$^{-/-}$ P14$^+$ T cells and observed low frequencies of PD-1$^+$TIM-3$^+$ at 8 days post Arm infection, with a slight increase in *Cd38*$^{-/-}$ cells (**Fig. 3.3C**). CD39, a marker of antigen-specific T cell engagement and an ectoenzyme capable of converting ATP to adenosine, was also analyzed on transferred P14$^+$ T cells and observed to be present at significantly higher frequencies in *Cd38*$^{-/-}$ than in WT P14$^+$ T cells (**Fig. 3.3D**) (283). When cytokine production was investigated, we observed similar frequencies of IFN-γ^+ and a small but significant increase of IFN-γ^+TNF-α^+ *Cd38*$^{-/-}$ P14$^+$ T cells compared to WT at day 8 post Arm infection (**Fig. S3.2A**). At day 8 post Cl13 infection, *Cd38*$^{-/-}$ P14$^+$ T cells had a small but significant increase in GranzymeB production (**Fig. 3.3E**) and similar frequencies of Ki67$^+$ cells (**Fig. 3.3F**) when compared to WT P14$^+$ T cells. At 8dpi, most transferred cells were PD-1$^+$, with significantly more PD-1$^+$TIM-3$^+$ *Cd38*$^{-/-}$ P14$^+$ T cells than WT (**Fig. 3.3G**). The frequency of CD39$^+$ cells was also higher in transferred *Cd38*$^{-/-}$ P14$^+$ T cells than in WT P14$^+$ T cells (**Fig. 3.3H**). Compared to Arm infection, overall cytokine production was lower at 8 days post Cl13 infection, although *Cd38*$^{-/-}$ P14$^+$ T cells had increased frequencies of IFN-γ^+ and IFN-γ^+TNF-α^+ cells compared to WT (**Fig. S3.2B**). Together, these findings demonstrate that while CD38 deletion did not alter proliferation in co-transferred P14$^+$ CD8$^+$ T cells at 8dpi, loss of CD38 did promote an increase in GranzymeB$^+$, PD-1$^+$TIM-3$^+$, and CD39$^+$ cells in both Arm and Cl13 infection.

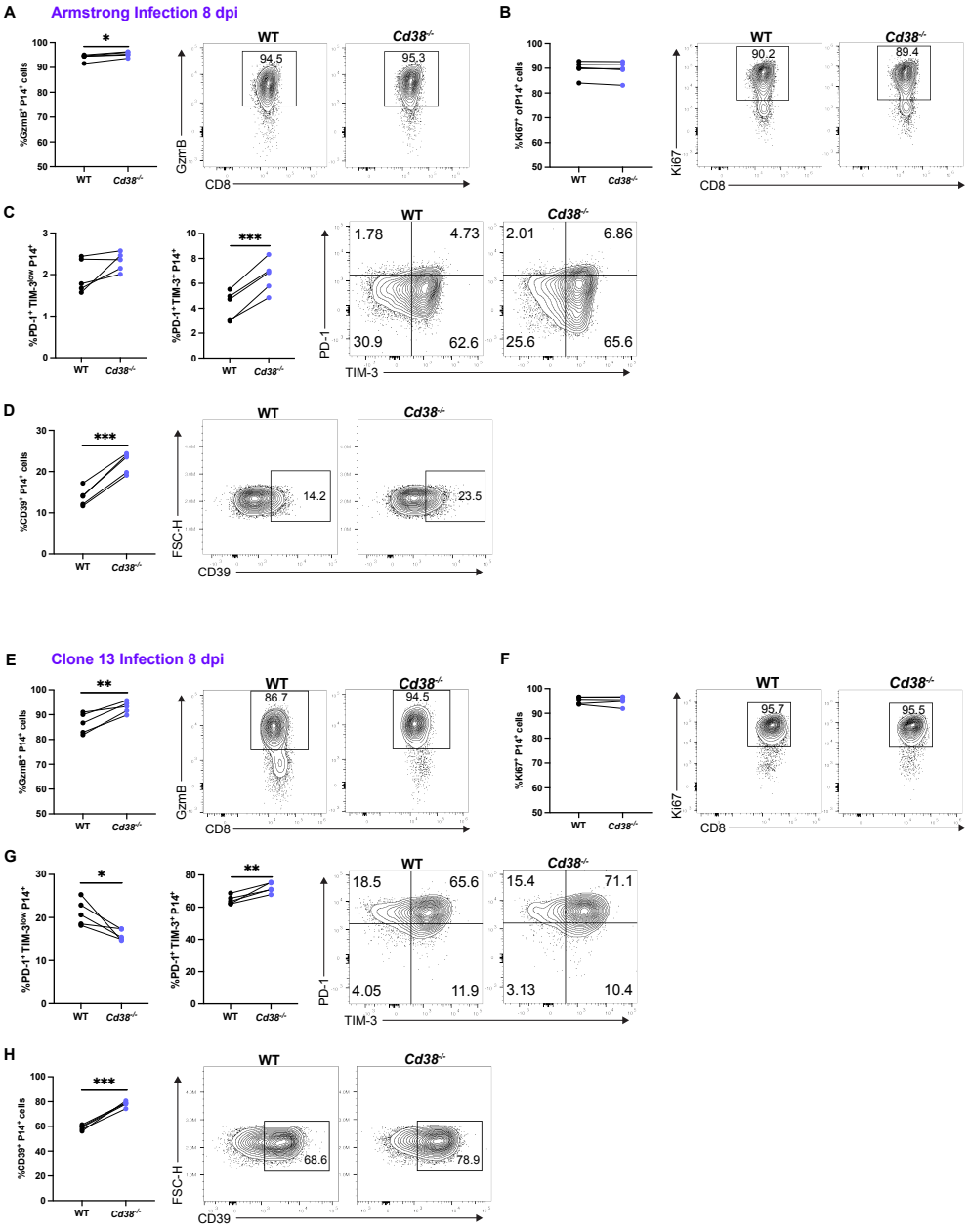

Figure 3.3 Effector phenotype and function of WT and *Cd38*$^{-/-}$ P14^{+} T cells at day 8 of acute or chronic LCMV infection. WT and *Cd38*$^{-/-}$ P14^{+} CD8^{+} T cells were transferred at a 1:1 ratio (1x10^{3} each) into WT naïve mice, followed by LCMV Arm or Cl13 infection a day later. Frequency and representative FACS plots of GranzymeB^{+} co-transferred WT and *Cd38*$^{-/-}$ P14^{+} T cells at 8dpi from spleens of Arm-infected mice (**A**). Frequency and representative FACS plots of Ki67^{+} (**B**) PD-1^{+}TIM-3^{low} (**C**, left), PD-1^{+}TIM-3^{+} (**C,** right) and CD39^{+} (**D**) co-transferred WT and *Cd38*$^{-/-}$ P14^{+} T cells from spleens of Arm-infected mice at 8dpi. Frequency and representative FACS plots of GranzymeB^{+} co-transferred WT and *Cd38*$^{-/-}$ P14^{+} T cells from spleens of Cl13-infected mice at 8dpi (**E**). Frequency and representative FACS plots of Ki67^{+} (**F**) PD-1^{+}TIM-3^{low} (**G**, left), PD-1^{+}TIM-3^{+} (**G,** right) and CD39^{+} (**H**) co-transferred WT and *Cd38*$^{-/-}$ P14^{+} T cells from spleens of Cl13-infected mice at 8dpi. Data are representative of 3 independent experiments with ≥ 5 mice per group. Data show mean ± s.e.m. *P ≤ 0.05, ***P ≤ 0.001, ****P ≤ 0.0001, paired t-test.

Cd38$^{-/-}$ CD8^{+} T cell proliferation is increased at late stages of Cl13 infection

While we observed similar frequencies of Ki67^{+} WT and *Cd38*$^{-/-}$ P14^{+} T cells at 8 days post Arm and Cl13 infection, we wanted to examine whether any differences occurred at 30dpi. WT P14^{+} (CD45.1) and *Cd38*$^{-/-}$ P14^{+} (CD45.1^{+}/CD45.2^{+}) cells were co-transferred in small numbers (2x10^{3}) into mice at a 1:1 ratio, and one day later mice were infected with LCMV Arm or Cl13 and spleens were analyzed at 30dpi. The frequency of GranzymeB^{+} and Ki67^{+} cells were ~10% in both WT and *Cd38*$^{-/-}$ P14^{+} T cells at 30 days post Arm infection (**Fig. 3.4A,B**). At 30dpi, most WT and *Cd38*$^{-/-}$ P14^{+} T cells were PD-1^{-}TIM3^{-} (**Fig. 3.4C**). The majority of WT and *Cd38*$^{-/-}$ P14^{+} T cells at 30dpi were IFN-γ^{+}TNF-α^{+}, with no differences in cytokine production observed (**Fig. S3.2C**). With Cl13 infection, we observed similar frequencies of GranzymeB^{+} co-transferred cells at 30dpi (**Fig. 3.4D**). However, *Cd38*$^{-/-}$ P14^{+} T cells had a significant increase in their proliferation as shown by the increase in Ki67^{+} cells at 30dpi (**Fig. 3.4E**). Most transferred cells were PD-1^{+}TIM-3^{low} at 30dpi, and no differences were apparent in PD-1^{+}TIM-3^{+} populations between WT and *Cd38*$^{-/-}$ P14^{+} T cells (**Fig. 3.4F**). Compared to Arm infection, there were decreased frequencies of IFN-γ^{+}TNF-α^{+} transferred cells at day 30 post Cl13 infection, however, no differences were observed between WT and *Cd38*$^{-/-}$ P14^{+} T cells (**Fig. S3.2D**). These findings showed that CD38 expression limited the proliferation of exhausted CD8^{+} T cells while having minimal impact on cytokine production and inhibitory receptor expression.

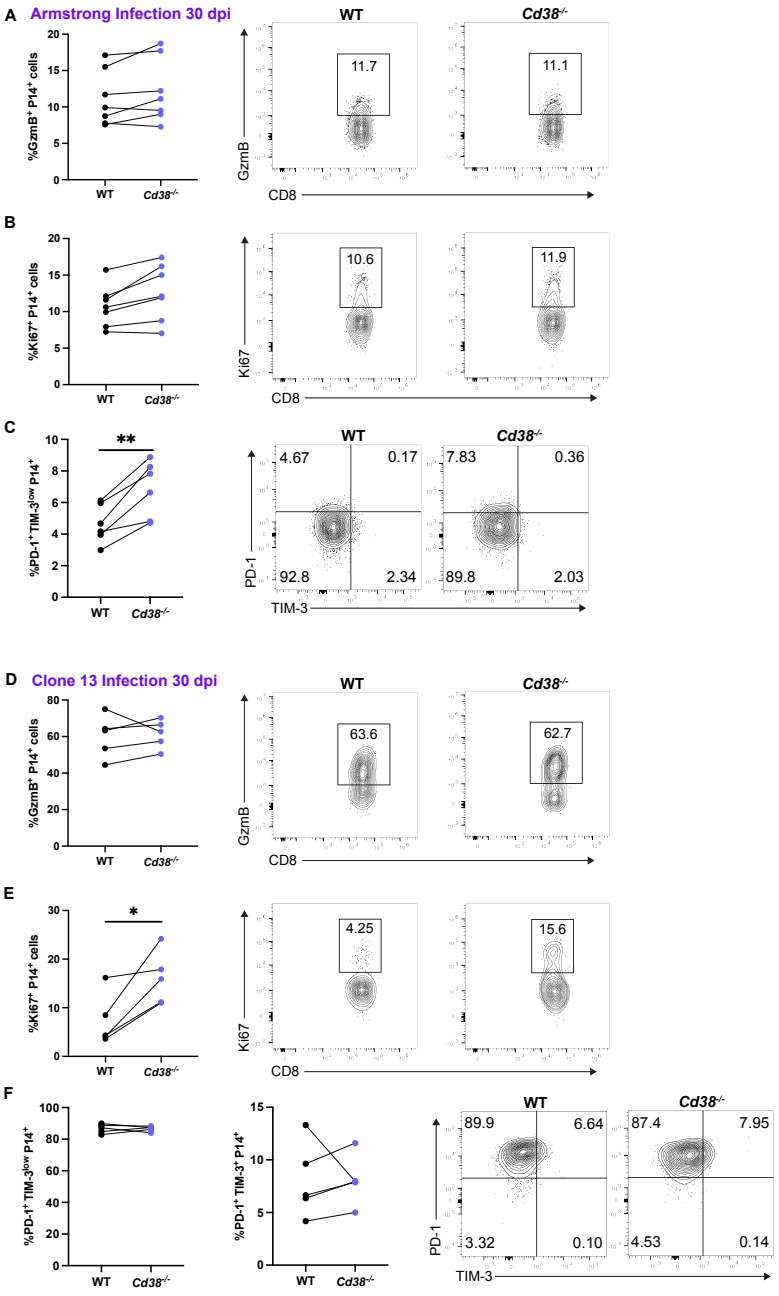

Figure 3.4 Effector phenotype and function of WT and *Cd38*$^{-/-}$ P14^{+} T cells at day 30 of acute or chronic LCMV. WT and *Cd38*$^{-/-}$ P14^{+} CD8^{+} T cells were transferred at a 1:1 ratio (1x10^{3} each) into WT naïve mice, followed by LCMV Arm or Cl13 infection a day later. Frequency and representative FACS plots of GranzymeB^{+} co-transferred WT and *Cd38*$^{-/-}$ P14^{+} T cells from spleens of Arm-infected mice at 30dpi (**A**). Frequency and representative FACS plots of Ki67^{+} (**B**) and PD-1^{+}TIM-3^{low} (**C**) co-transferred WT and *Cd38*$^{-/-}$ P14^{+} T cells from spleens of Arm-infected mice at 30dpi. Frequency and representative FACS plots of GranzymeB^{+} co-transferred WT and *Cd38*$^{-/-}$ P14^{+} T cells from spleens of Cl13-infected mice at 30dpi (**D**). Frequency and representative FACS plots of Ki67^{+} (**E**) PD-1^{+}TIM-3^{low} (**F**, left), PD-1^{+}TIM-3^{+} (**F,** right) co-transferred WT and *Cd38*$^{-/-}$ P14^{+} T cells from spleens of Cl13-infected mice at 30dpi. Data are representative of 6 independent experiments with ≥ 4 mice per group. Data show mean ± s.e.m. *P ≤ 0.05, ***P ≤ 0.001, ****P ≤ 0.0001, paired t-test.

CD38 expression promotes the maintenance of Tpex and Tex subsets during chronic infection

During chronic viral infection and cancer, exhausted T cells form two distinct populations, progenitor (Tpex) and terminal (Tex) exhausted T cells (281). Tpex cells are characterized by expression of the transcription factor TCF-1 and are capable of self-renewal and seeding of the Tex population, which retain better effector function but are short-lived (38, 281). To assess how CD38 may impact Tpex and Tex populations, we co-transferred small numbers ($2x10^3$) of WT $P14^+$ and *Cd38*$^{-/-}$ $P14^+$ T cells into mice at a 1:1 ratio, infected mice with Cl13 one day later, then analyzed Tpex and Tex populations in the $CD45.1^+$ transferred cells in the spleen at 8 and 30dpi. Although both WT and *Cd38*$^{-/-}$ $P14^+$ T cells differentiated into Tpex and Tex subsets at 8dpi, the frequencies and numbers of *Cd38*$^{-/-}$ $P14^+$ Tpex were significantly decreased compared to WT (**Fig. 3.5A**). In contrast, the Tex population was composed of similar frequencies and numbers of WT and *Cd38*$^{-/-}$ $P14^+$ T cells at 8dpi (**Fig. 3.5B**). On day 30 post Cl13 infection, the *Cd38*$^{-/-}$ $P14^+$ Tpex and Tex frequencies and numbers were significantly lower than WT $P14^+$ (**Fig. 3.5C,D**). When the frequencies of Tpex and Tex were tracked over the course of chronic infection, we found that *Cd38*$^{-/-}$ $P14^+$ T cells were more terminal than WT at 8dpi (**Fig. 3.5E**). We next evaluated apoptosis in the transferred Tpex and Tex populations during infection and found that *Cd38*$^{-/-}$ $P14^+$ Tpex had more $Caspase3^+$ cells at 6 and 8dpi and trended toward more at 30dpi than WT $P14^+$ Tpex (**Fig. 3.5F**). *Cd38*$^{-/-}$ $P14^+$ Tex showed reduced $Caspase3^+$ cells at 6 and 8dpi, and increased $Caspase3^+$ cells at 30dpi compared to WT $P14^+$ Tex (**Fig. 3.5F**). Further analysis of exhausted *Cd38*$^{-/-}$ $P14^+$ T cells showed increased frequencies of effector markers such CD69 and KLRG1 when compared to WT (**Fig. 3.5G,H**) (34). Expression of the terminal marker $2B4^+$ was similar in *Cd38*$^{-/-}$ and WT $P14^+$ T cells at 8 and 30dpi (**Fig. 3.5G,H**). The frequencies of $TCF\text{-}1^+$ cells were reduced at 8 and 30dpi with CD38 deletion (**Fig. 3.5G,H).** These findings showed that CD38 expression is important for the survival and maintenance of Tpex and Tex cells,

as well as TCF-1 expression, over the course of chronic infection. Additionally, cells lacking CD38 show increased expression of markers associated with effector-like exhausted populations.

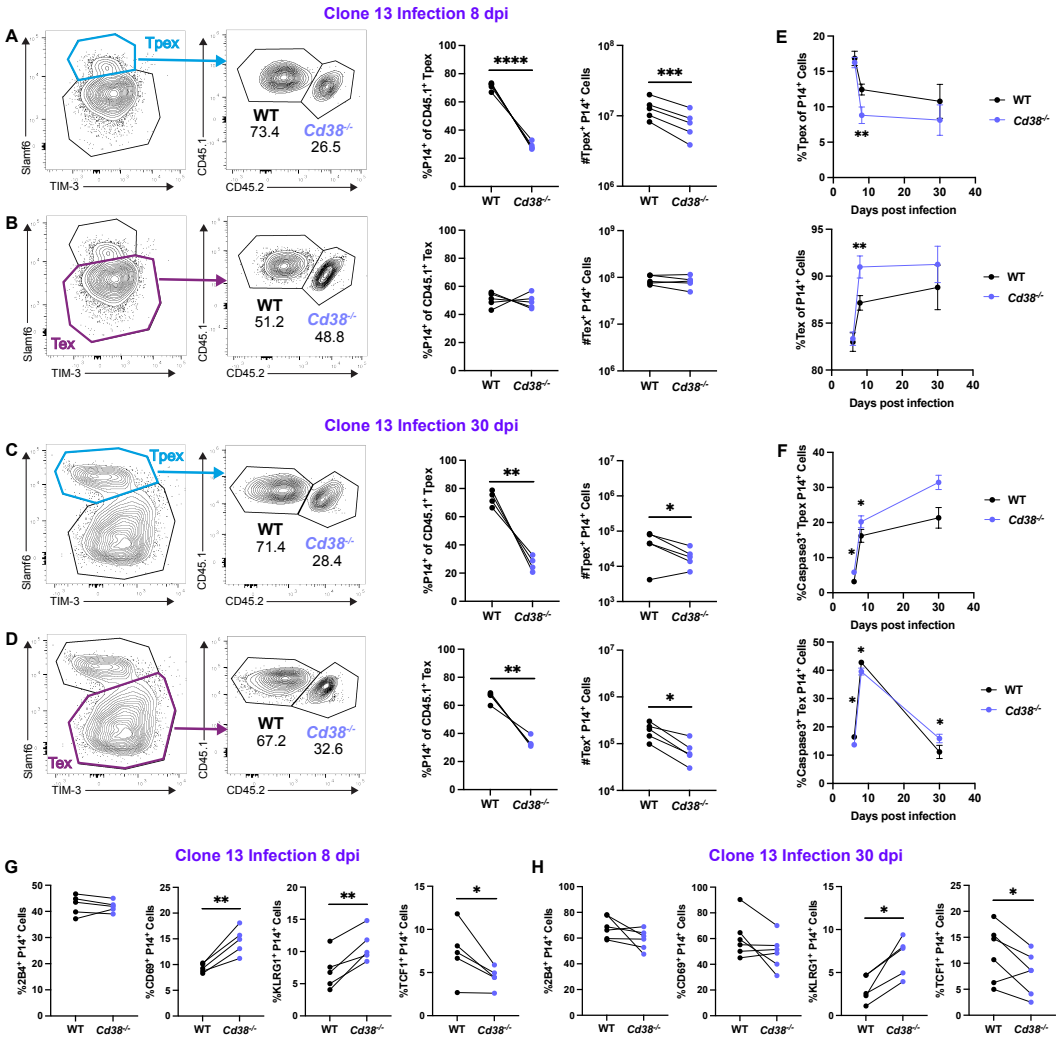

Figure 3.5 Analysis of exhausted populations in WT and *Cd38*$^{-/-}$ P14^{+} T cells during Cl13 infection. WT and *Cd38*$^{-/-}$ P14^{+} CD8^{+} T cells were transferred at a 1:1 ratio (1x10^{3} each) into WT naïve mice, followed by LCMV Cl13 infection a day later. Frequencies of WT or *Cd38*$^{-/-}$ P14^{+} T cells of total co-transferred Tpex cells, representative FACS plots, and numbers of total Tpex at 8dpi in spleen (**A**). Frequencies of WT or *Cd38*$^{-/-}$ P14^{+} T cells of total co-transferred Tex cells, representative FACS plots, and numbers of total Tex at 8dpi in spleen (**B**). Frequencies of WT or *Cd38*$^{-/-}$ P14^{+} T cells of total co-transferred Tpex cells, representative FACS plots, and total numbers of Tpex at 30dpi in spleen (**C**). Frequencies of WT or *Cd38*$^{-/-}$ P14^{+} CD8^{+} T of total co-transferred Tex cells, representative FACS plots, and total numbers of Tex at 30dpi in spleen (**D**). Frequencies of co-transferred Tpex and Tex cells in the spleen over the course of Cl13 infection (**E**). Frequencies of apoptotic Caspase3^{+} co-transferred Tpex and Tex in the spleen over the course of Cl13 infection (**F**). Frequencies of 2B4^{+}, CD69^{+}, KLRG1^{+} and TCF1^{+} co-transfer cells at 8dpi (**G**) and 30dpi (**H**) in the spleen. Data are representative of 3 (8dpi spleen), 6 (30dpi spleen), or 2 (2B4 and CD69 expression) independent experiments with ≥ 4 mice per group. Data show mean ± s.e.m. *P ≤ 0.05, ***P ≤ 0.001, ****P ≤ 0.0001, paired t-test.

CD38 negatively regulates the proliferation and function of progenitor exhausted CD8$^+$ T cells

Because we saw an increase in surface markers indicative of effector-like exhausted cells, we next examined the impact of CD38 deletion on the effector functions of Tpex and Tex transferred cells. On day 8 post Cl13 infection, the frequency of GranzymeB$^+$ Tpex cells was significantly increased in *Cd38*$^{-/-}$ P14$^+$ T cells compared to WT (**Fig. 3.6A**), whereas Ki67$^+$ cells were similar (**Fig. 3.6B**). *Cd38*$^{-/-}$ P14$^+$ Tex cells had a small but significant increase in GranzymeB$^+$ cells and similar Ki67$^+$ cells compared to WT P14$^+$ Tex cells (**Fig. 3.6C**). At 30dpi, *Cd38*$^{-/-}$ P14$^+$ Tpex had significantly more GranzymeB production and Ki67 than WT (**Fig. 3.6D,E**). *Cd38*$^{-/-}$ P14$^+$ Tex had similar GranzymeB and increased Ki67 production compared to WT P14$^+$ Tex (**Fig. 3.6F**). These findings showed that CD38 expression restrained GranzymeB production and proliferation of Tpex cells during chronic infection.

CD38 increased the metabolic fitness of CD8$^+$ T cells during chronic infection

Since CD38 has enzymatic functions, we next examined whether metabolic changes occurred in *Cd38*$^{-/-}$ P14$^+$ T cells. To examine the impact of CD38 expression on mitochondrial respiration and glycolysis during LCMV infection, we carried out the Seahorse XF Cell Mito Stress Test on live-sorted WT and *Cd38*$^{-/-}$ P14$^+$ T cells from Arm or Cl13-infected mice at 8dpi. CD38 deletion during Arm infection did not impact the P14$^+$ cell oxidative phosphorylation (**Fig. 3.7A,B**). Basal and maximal oxygen consumption rate (OCR; a proxy for oxidative phosphorylation) and extracellular acidification rate (ECAR; a proxy for glycolysis) were indistinguishable between WT and *Cd38*$^{-/-}$ P14$^+$ T cells from Arm-infected mice (**Fig. 3.7C,D**). The ratio of OCR:ECAR was also quantified to gain a relative measure of cellular preference for oxidative phosphorylation or glycolysis (**Fig. 3.7E**). At 8 days post Arm infection, CD38 deletion did not significantly impact the OCR:ECAR ratio. In contrast to Arm infection, CD38 deletion in P14$^+$ T cells from mice infected with Cl13 resulted in decreased oxidative

phosphorylation and glycolysis (**Fig. 3.7F,G**). The basal and maximal OCR of *Cd38*$^{-/-}$ P14^{+} T cells were decreased compared to WT P14^{+} T cells from Cl13 infected mice (**Fig. 3.7H**). Basal and maximal ECAR levels were also significantly decreased with CD38 deletion (**Fig. 3.7I**). Basal and maximal OCR:ECAR ratios were similar between WT and *Cd38*$^{-/-}$ P14^{+} T cells from Cl13 infected mice (**Fig. 3.7J**). Relative to Arm infection, the larger OCR:ECAR ratios in Cl13 samples demonstrated a preference for oxidative phosphorylation (**Fig. 3.7J**). These findings showed that cell intrinsic CD38 expression sustained the basal and maximal metabolic function of exhausted CD8^{+} T cells during Cl13 infection.

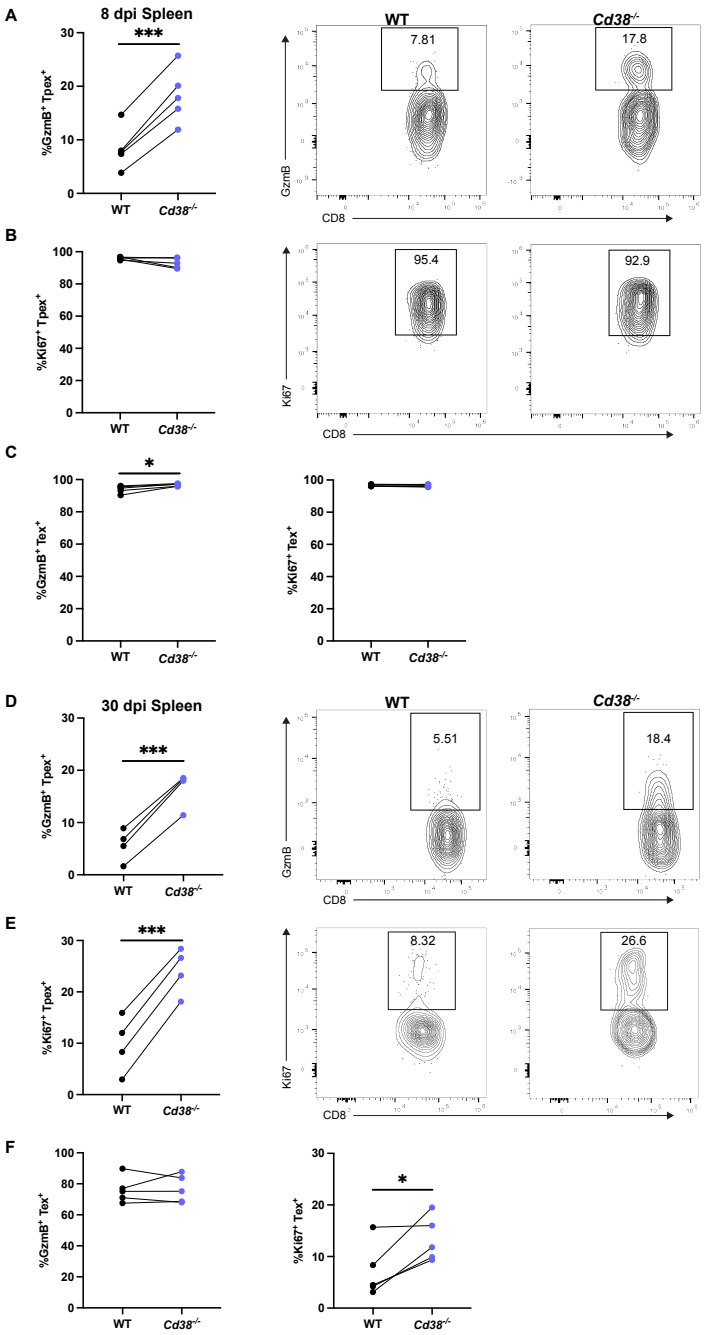

Figure 3.6 *Cd38*$^{-/-}$ P14^{+} Tpex and Tex cell phenotypes in Cl13 infection. WT and *Cd38*$^{-/-}$ P14^{+} CD8^{+} T cells were transferred at a 1:1 ratio (1x10^{3} each) into WT naïve mice, followed by LCMV Cl13 infection a day later. Frequencies of GranzymeB^{+} WT or *Cd38*$^{-/-}$ Tpex cells at 8dpi in spleen and representative FACS plots (**A**). Frequencies of Ki67^{+} WT or *Cd38*$^{-/-}$ Tpex cells at 8dpi in spleen and representative FACS plots (**B**). Frequencies of GranzymeB^{+} and Ki67^{+} co-transferred WT or *Cd38*$^{-/-}$ Tex P14^{+} T cells in the spleen (**C**). 8dpi frequencies of GranzymeB^{+} WT or *Cd38*$^{-/-}$ Tpex cells at 30dpi in spleen and representative FACS plots (**D**). Frequencies of Ki67^{+} WT or *Cd38*$^{-/-}$ Tpex cells at 30dpi in spleen and representative FACS plots (**E**). 30dpi frequencies of GranzymeB^{+} and Ki67^{+} co-transferred WT or *Cd38*$^{-/-}$ Tex P14^{+} T cells in the spleen (**F**). Data are representative of 3 (8dpi spleen) or 6 (30dpi spleen) independent experiments with ≥ 4 mice per group. Data show mean ± s.e.m. *P ≤ 0.05, ***P ≤ 0.001, ****P ≤ 0.0001, paired t-test.

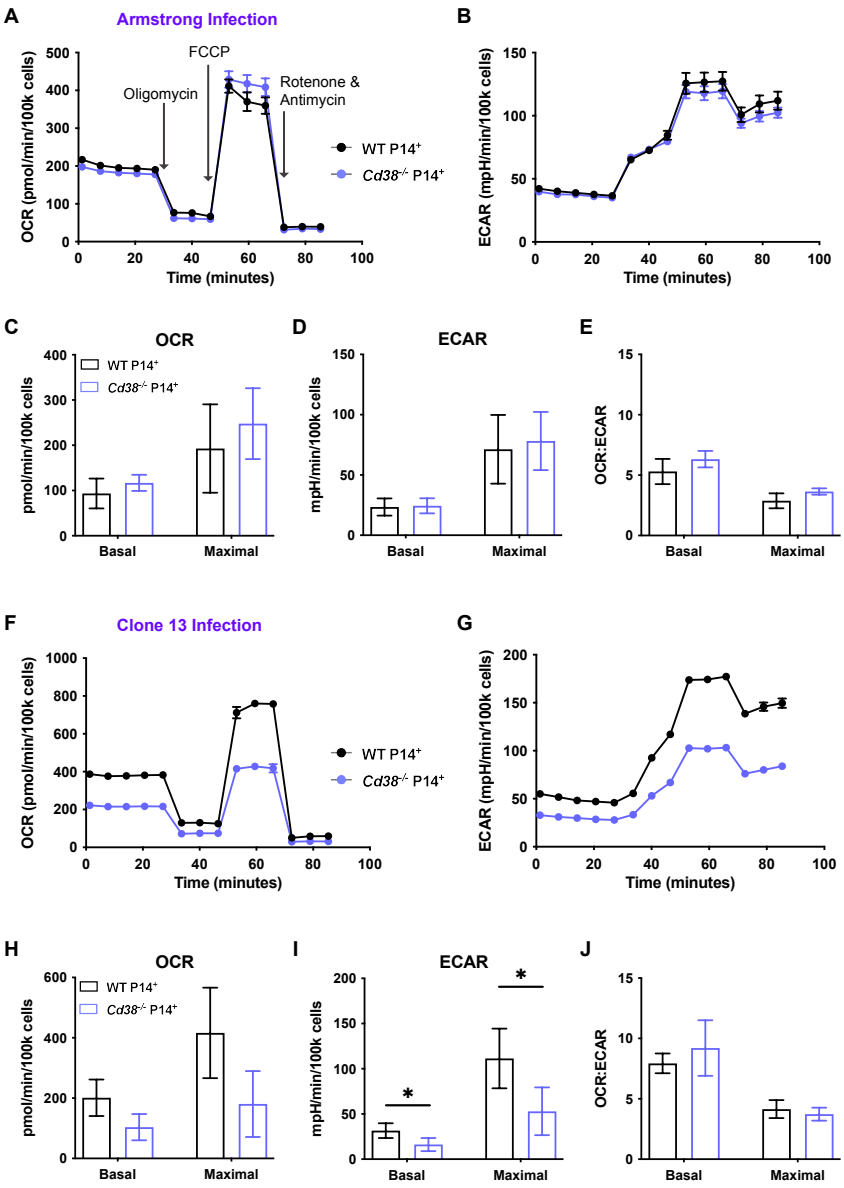

Figure 3.7 Metabolism of *Cd38*$^{-/-}$ virus-specific CD8^{+} T cells. WT and *Cd38*$^{-/-}$ P14^{+} CD8^{+} T cells were transferred at a 1:1 ratio (1x10^{3} each) into WT naïve mice, followed by LCMV Arm or Cl13 infection a day later. Live WT and *Cd38*$^{-/-}$ P14^{+} CD8^{+} T cells were isolated from host mice at 8dpi and a Seahorse XF Cell Mito Stress Test was performed. Oxygen consumption rate (OCR) of live WT and *Cd38*$^{-/-}$ P14^{+} T cells from Arm-infected mice at baseline and after addition of Oligomycin, FCCP, and Rotenone & Antimycin A (**A**). Extracellular acidification rate (ECAR) of live WT and *Cd38*$^{-/-}$ P14^{+} T cells from Arm-infected mice at baseline and after addition of Mito Stress Test compounds (**B**). Basal and maximal OCR and ECAR rates, and quantified OCR:ECAR ratio for isolated WT and *Cd38*$^{-/-}$ P14^{+} T cells from Arm-infected mice (**C-E**). Seahorse XF Cell Mito Stress Test OCR and ECAR values from live WT and *Cd38*$^{-/-}$ P14^{+} T cells isolated from Cl13-infected mice at 8dpi (**F,G**). Basal and maximal OCR and ECAR rates, and quantified OCR:ECAR ratio for isolated WT and *Cd38*$^{-/-}$ P14^{+} T cells from Cl13-infected mice (**H-J**). Seahorse data presented are median values of a representative biological replicate. Data are representative of 3 independent experiments with ≥ 5 mice per group for Arm and ≥ 15 mice for Cl13 infection. Data show mean ± s.e.m. *P ≤ 0.05, ***P ≤ 0.001, ****P ≤ 0.0001 by paired t-test.

DISCUSSION

CD38 upregulation on activated T cells has been associated with response to infections (200). More recently, CD38 was found to mark terminal T cell dysfunction and has gained interest as a possible pharmacological target for the enhancement of T cell responses (217, 220). However, the functional role of CD38 on T cells in response to acute and chronic viral infection remains largely undefined. In this study, we used an adoptive co-transfer of *Cd38*$^{-/-}$ P14^{+} and WT P14^{+} CD8^{+} T cells to investigate the cell-intrinsic role of CD38 on virus-specific T cells. We found that CD38 promotes the survival of CD8^{+} T cells during LCMV infection. In an acute infection, proliferation and GranzymeB production were not limited by CD38 expression. While CD38 expression seems to play a relatively minor role in shaping the effector response of CD8^{+} T cells to acute infection, we found that CD38 is an important regulator of cell proliferation and GranzymeB production, Tpex and Tex phenotype and maintenance, and metabolism during chronic infection.

During HIV infection, CD38 is upregulated on T cells and can serve as a marker of disease progression (201-203). In cases of H7N9 avian influenza, a larger population of CD38^{+}HLA-DR^{+}CD8^{+} T cells are found in patients who succumb to flu (196). In both Dengue and Ebola-infected patients, CD8^{+}CD38^{+} T cells are upregulated in febrile patients (194, 196, 206). In concurrence with these data, we found that CD38 levels were elevated on T cells during Arm and Cl13 infection, although to a much higher extent in Cl13. Our study and others have shown that CD38 is co-expressed with PD-1 and correlates with activation as well as exhaustion (196). As with PD-1, CD38 is expressed during activation in response to acute infection, and CD38 levels are elevated and sustained on exhausted T cells during chronic infection. This differential expression is a result of divergent chromatin accessibility in T cells during acute and chronic infection (284). Regions of the *Pdcd1* locus become uniquely accessible at day 5 and onward during tumorigenesis and at day 8 post infection and

onward during chronic infection (29, 217, 284). Similarly, the *Cd38* locus is uniquely open in both virus and tumor-specific exhausted T cells (39, 217). The expression patterns and chromatin accessibility of CD38 make it a particularly good marker of chronic T cell stimulation and raises the question of how CD38 signaling may shape the phenotype of activated T cells. Interestingly, our analysis of the Hansel *et al.* study showed that CD38 gene expression levels were high on $CD8^+$ T cells from patients with chronic HCV, but these were decreased when the same patients were cured from their infection, suggesting that CD38 expression may be linked to persistent TCR stimulation.

As an ecto-enzyme, the immunosuppressive function of CD38 has been well established through its contribution in regulating extracellular adenosine levels. CD38, in conjunction with CD203a and CD73 enzymatic activities, converts extracellular NAD^+ to adenosine (172). In the tumor microenvironment, CD38-expressing tumor cells and myeloid-derived suppressor cells produce adenosine to limit cytotoxic T cell function through the adenosine receptor (211, 215, 285). Blocking the immunosuppressive adenosine pathway through targeting of the adenosine (A2A) receptor or CD73 has proven beneficial to anti-tumor T cell responses (278, 285, 286). While less is known about the cell-intrinsic role of CD38 on virus- or tumor-specific T cells, evidence suggests CD38 as a possible inhibitor of T cell function (194, 217, 219). We found that CD38 deletion did not impact cytokine production of $CD8^+$ T cells during Arm and Cl13 infection. While CD38 deletion did promote increased PD-1 and TIM-3 expression at 8dpi, by 30dpi the impact of deletion on inhibitory receptor expression was minimal. These findings are consistent with a recent study showing that over-expression or deletion of CD38 on tumor-specific T cells did not alter their exhaustion phenotype (222). CD73 is downstream of CD39, another ecto-enzyme capable of initiating conversion of ATP to adenosine (287, 288). The limited impact of CD38 deletion on virus-specific T cells at 8 days post LCMV infection may be partially due to the redundancy of enzymatic functions of CD39, CD73, and CD203 in adenosine formation (172). This is relevant, as we saw an increase in $CD39^+$ cells in *Cd38*$^{-/-}$

P14$^+$ T cells. This indicates that CD38 deletion alone may not be enough to alter immunosuppressive adenosine signaling.

While effector functions were largely similar in co-transferred WT and *Cd38*$^{-/-}$ P14$^+$ CD8$^+$ T cells at 30dpi, we discovered an important cell-intrinsic role for CD38 expression in the survival of virus-specific CD8$^+$ T cells. We found that adoptively transferred *Cd38*$^{-/-}$ P14$^+$ T cells were significantly decreased by day 30 post Arm and Cl13 infection due in part to increased apoptosis. Interestingly, when we performed co-transfers of naïve *Cd38*$^{-/-}$ and WT P14$^+$ T cells into uninfected mice, cells lacking CD38 had diminished frequencies by 24 hours. This indicated that CD38 may also play a cell-intrinsic role of homing of naïve T cells. Our data indicate that *Cd38*$^{-/-}$ P14$^+$ T cells can expand in response to viral infection (as indicated by the similar frequencies in spleens of Cl13-infected mice at 8dpi), however these cells are unable to persist over the course of infection. A similar loss of adoptively transferred *Cd38*$^{-/-}$ tumor-specific T cells compared to WT was seen in tumors 14 days after transfer (222). Interestingly, the decreased frequency of *Cd38*$^{-/-}$ T cells was not attributed to apoptosis in the tumor model, whereas in the LCMV model, *Cd38*$^{-/-}$ P14$^+$ T cells had increased Caspase3 expression. Further research is needed to define the cell-intrinsic mechanism that drives the loss of *Cd38*$^{-/-}$ T cells in uninfected mice and in tumor models. TCR signaling has been shown to regulate CD38, and a corresponding role for CD38 in promoting survival could explain its persistent expression on memory and exhausted T cells in mice and in patients with viral infections and autoimmune disorders (176, 206, 289-291). Given its upregulation on activated and memory T cells, and considering we show that transferred *Cd38*$^{-/-}$ P14$^+$ T cells undergo significantly more apoptosis than WT P14$^+$ T cells, it appears that CD38 expression promotes maintenance and survival of activated T cells. *In vitro*, CD38 limits proliferation of activated T cells, and small interfering RNA targeting of CD38 can increase T cell proliferation (176, 219). In accordance with this, we found that proliferation of adoptively transferred

WT P14$^+$ T cells was significantly constrained during Cl13 infection when compared to *Cd38*$^{-/-}$ P14$^+$ T cells at 30dpi.

While we found that CD38 expression did not alter the development of T cell exhaustion, both Tpex and Tex frequencies and numbers were reduced during Cl13 infection with CD38 deletion. Phenotypically, we observed an increased effector response in *Cd38*$^{-/-}$ P14$^+$ Tpex cells, as shown by more proliferation and GranzymeB production. The Tpex population is defined by high expression of the TCF-1 transcription factor and is vital for anti-viral and anti-tumor T cell responses, as Tpex cells are stem-like, able to expand into the Tex population, and can respond to ICB (37, 281). Compared to Tpex cells, Tex cells are more effector-like, having higher cytokine and GranzymeB production, as well as increased proliferation (38). In this context, it appears that CD38 may have a cell-intrinsic role in limiting an effector-like Tpex phenotype. However, while CD38 deletion promoted proliferation and KLRG1 expression, the overall frequencies of *Cd38*$^{-/-}$ Tpex and Tex cells were decreased in co-transfer experiments, and Tpex cells lacking CD38 had higher apoptotic frequencies than their WT counterparts. Further, we found that cells expressing CD38 maintained higher TCF-1 frequencies over time, an important factor in Tpex formation. Our data presents an interesting paradigm, in which CD38 hinders proliferation and GranzymeB production in CD8$^+$ T cells, particularly in the Tpex subset, but also ensures their survival.

Since we saw that CD38 deletion impacted survival of transferred P14$^+$ T cells during viral infection, we wanted to investigate whether cellular metabolism was also impacted by loss of CD38. The enzymatic activities of CD38 have been reviewed at length (180, 200, 276, 292, 293), establishing CD38 as a prominent regulator of cellular NAD$^+$, NAADP, ADPR and cADPR levels. The consumption of NAD$^+$ by CD38 has the potential to limit T cell metabolism and effector functions, as NAD$^+$ is a key substrate of the immunomodulatory proteins ART, PARP, and SIRT which are

involved in T cell fate, survival, and metabolism (276, 293). *In vitro*, CD38 deletion supports increased oxidative phosphorylation in $CD4^+$ T cells and supports NAD^+ levels in cultures of $CD8^+$ T cells (212, 222). Interestingly, our analysis of virus-specific $CD8^+$ T cell metabolism *ex vivo* revealed similar metabolic profiles in WT and *Cd38*$^{-/-}$ $P14^+$ T cells from Arm-infected mice. Given the established NADase activity of CD38, along with previous *in vitro* findings, we anticipated that CD38 deletion would increase the metabolic capabilities of transferred $P14^+$ T cells. To our surprise, we discovered that *Cd38*$^{-/-}$ $P14^+$ T cells from Cl13 infection had reduced oxidative phosphorylation and glycolysis both at basal and maximal conditions. This is opposite of the predicted phenotype arising from NAD^+ depletion. However, given that WT and *Cd38*$^{-/-}$ $P14^+$ T cells were transferred into C57BL/6 hosts with functional CD38, along with the recent finding that NAD^+ levels are similar in B16-F10 tumors of WT and *Cd38*$^{-/-}$ mice, the impaired metabolism seen in *Cd38*$^{-/-}$ $P14^+$ T cells may be a result of cell-intrinsic CD38 signaling rather than enzymatic activity (222). Additionally, the impact of CD38 on metabolism appears to be correlated with expression levels, as WT $P14^+$ T cells from Arm infection expressed much lower levels of CD38 than from Cl13 and were spared metabolic impacts upon CD38 deletion. This represents an exciting potential role for CD38 signaling in the mitochondrial fitness of $P14^+$ T cells during Cl13 infection.

Our study shows the regulation of CD38 expression in effector and exhausted $CD8^+$ T cells during viral infection. We found that CD38 is upregulated and expressed at higher levels on $CD8^+$ T cells in Cl13 compared to Arm infection. We showed that CD38 deletion has a cell-intrinsic role in regulating the survival of virus-specific $CD8^+$ T cells throughout the course of viral infection. We found no differences in the metabolism of WT and *Cd38*$^{-/-}$ $P14^+$ T cells from Arm infected mice, but *Cd38*$^{-/-}$ cells arising during Cl13 infection had decreased oxidative phosphorylation and glycolysis. *Cd38*$^{-/-}$ $P14^+$ Tpex and Tex cells were decreased, and *Cd38*$^{-/-}$ Tpex cells were more proliferative and functional than WT cells, indicating an inhibitory function of CD38 in this cell type. Further,

exhausted *Cd38*$^{-/-}$ T cells were decreased in TCF-1^{+} populations and increased in apoptotic Tpex cells during chronic infection. Our studies show a dual cell-intrinsic role for CD38 in limiting proliferation of virus-specific T cells, while also promoting their survival. These data uncover important roles of CD38 in virus-specific T cell responses to infection and highlight new avenues for research into the mechanisms through which CD38 regulates the survival, effector function, and metabolism of exhausted CD8^{+} T cells.

ACKNOWLEDGEMENTS

We would like to thank all current and former members in the Tinoco Laboratory (Twitter: @Tinoco_Lab) for all their constructive comments and advice during this project. This work was supported by the NIH (R01 AI137239 to R. Tinoco), and (R00 HD098330 to D. Nicholas), T32 Training Program for Interdisciplinary Cancer Research IDCR (T32CA009054 to J.M. DeRogatis), T32 virus-host interactions: a multi-scale training program (T32AI007319 to E.N. Neubert), and T32 Microbiology and Infectious Diseases training grant (T32AI141346 to K.M. Viramontes). The authors would like to thank Dr. Jie Wu (UCI Genomics High Throughput Facility) for human HCV RNAseq analysis, which is a Chao Family Comprehensive Cancer Center (CFCCC) shared resource supported by the Cancer Center Support Grant (P30CA062203). We would like to thank Dr. Jennifer Atwood at the UCI Institute for Immunology Flow Core, a shared resource of the Cancer Center Support Grant (CA-62203) at the University of California, Irvine, for assistance with FACS. This study was also supported by the UCI Stem Cell Research Center with additional support from California Institute for Regenerative Medicine grant CL1-00520-1.2 to Vanessa Scarfone and the UC Irvine Stem Cell FACS Core.

SUPPLEMENTARY FIGURES

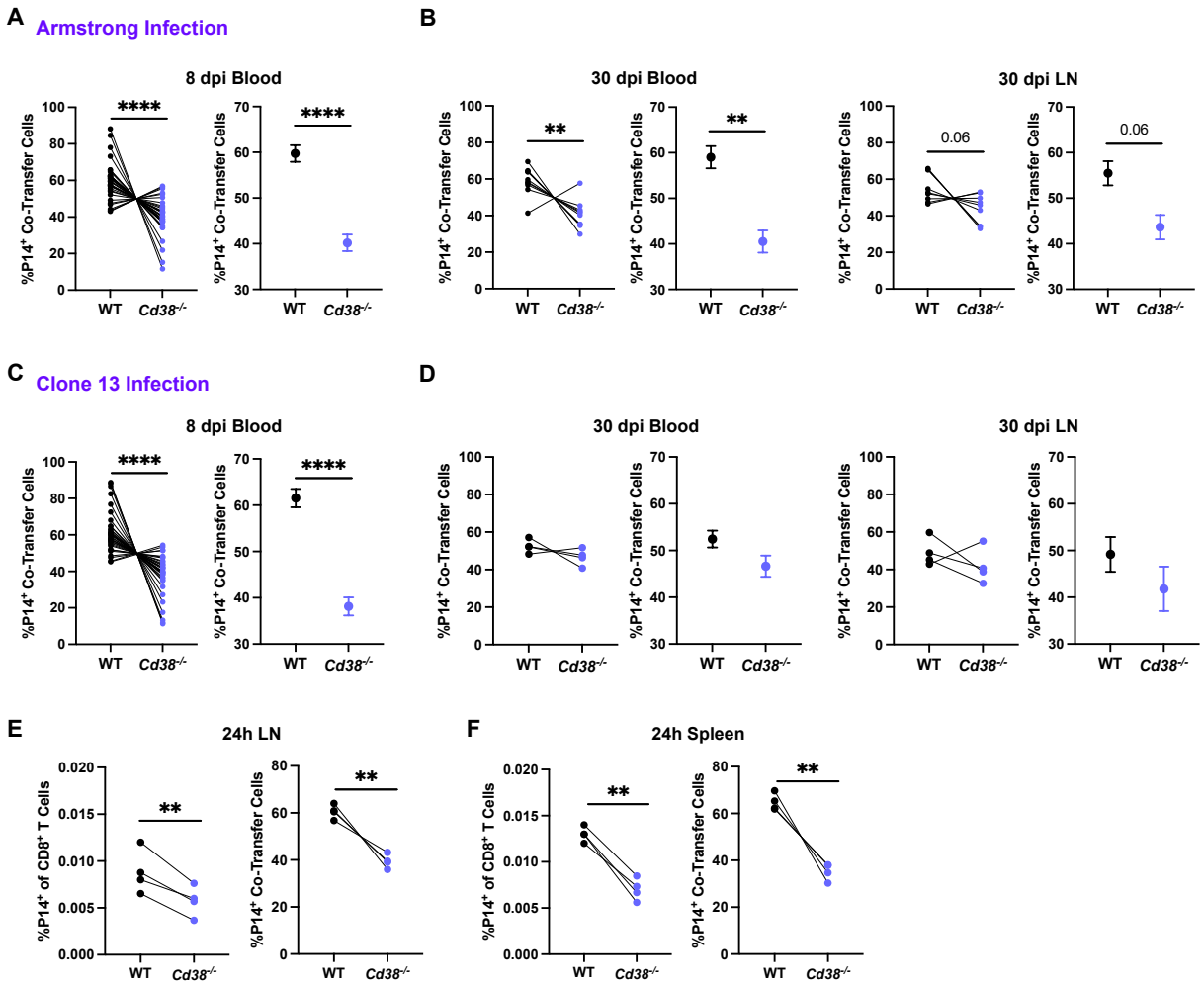

Figure S3.1 Frequencies of WT and *Cd38*$^{-/-}$ P14^{+} co-transfer populations in infected and uninfected mice. WT and *Cd38*$^{-/-}$ P14^{+} CD8^{+} T cells were transferred at a 1:1 ratio (1x10^{3} each) into WT naïve mice, followed by LCMV Arm or Cl13 infection a day later. Individual (**A**, left) and average (**A**, right) ratios of co-transferred cells in the blood of Arm-infected mice at 8dpi. Individual and average ratios of co-transferred cells in the blood (**B**, left) and LNs (**B**, right) of Arm-infected mice at 30dpi (**B**). Individual (**C,** left) and average (**C,** right) ratios of co-transferred cells in the blood of Cl13-infected mice at 8dpi. Individual and average ratios of co-transferred cells in the blood (**D**, left) and LNs (**D**, right) of Cl13-infected mice at 30dpi (**D**). WT and *Cd38*$^{-/-}$ P14^{+} T cells were transferred at a 1:1 ratio (1x10^{4} each) into WT naïve mice with no infection. Spleen and LN were collected 24h after co-transfer. Frequency of CD8^{+} T cells and comparative ratio of WT and *Cd38*$^{-/-}$ P14^{+} co-transferred cells in the LN (**E**) and spleen (**F**) at 24h in uninfected mice. Data are representative of 6 (8dpi blood) or 2 (24h timepoint, 30dpi LN and blood) independent experiments with ≥ 5 mice per group. Data show mean ± s.e.m. *P ≤ 0.05, ***P ≤ 0.001, ****P ≤ 0.0001, paired t-test.

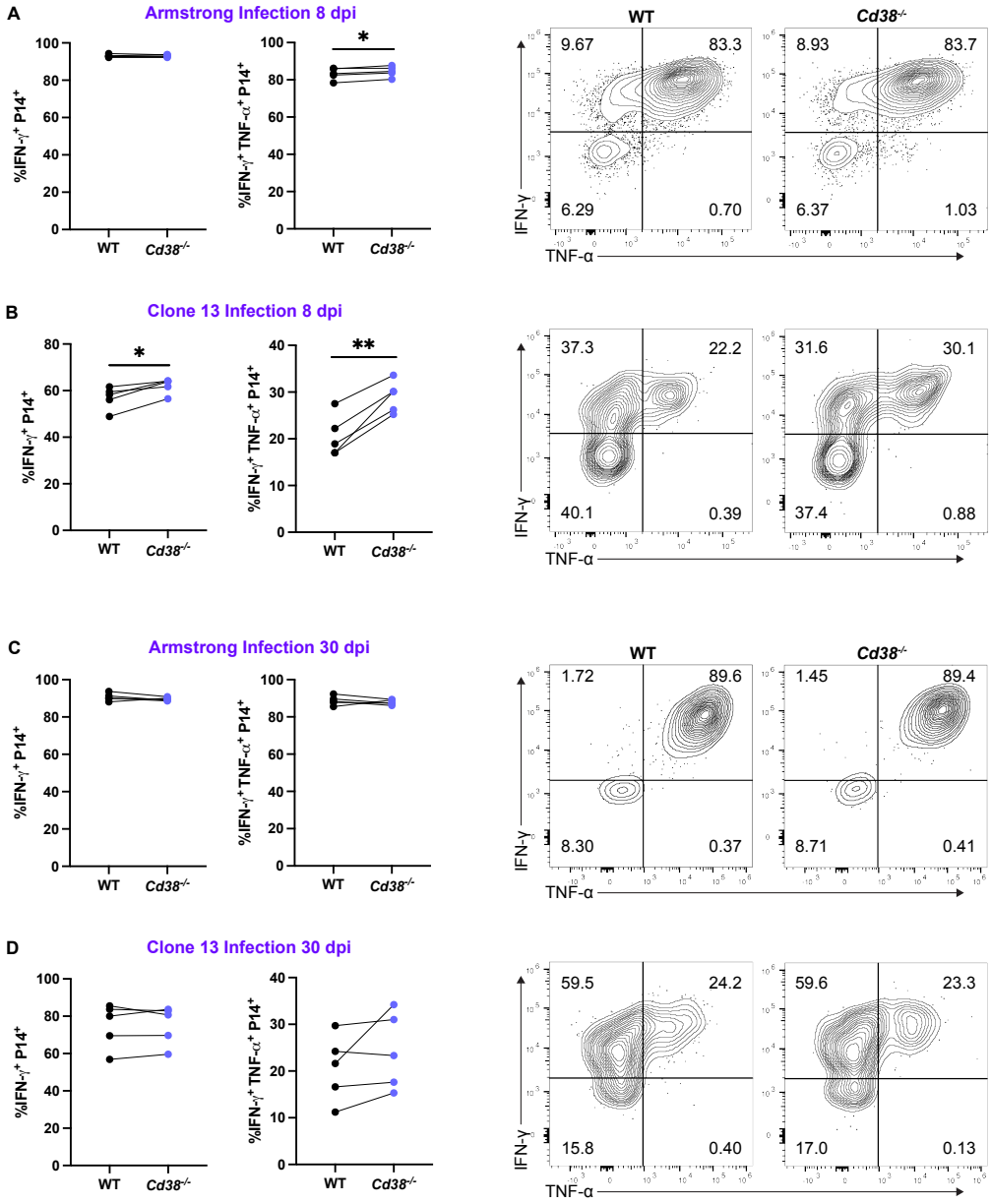

Figure S3.2 Cytokine production in WT and *Cd38*$^{-/-}$ P14^{+} T cells during LCMV infection. WT and *Cd38*$^{-/-}$ P14^{+} CD8^{+} T cells were transferred at a 1:1 ratio (1x10^{3} each) into WT naïve mice, followed by LCMV Arm or Cl13 infection a day later. Splenic P14^{+} CD8^{+} T were stimulated *ex vivo* with the LCMV GP$_{33-41}$ peptide and cytokine production was measured. Quantification of IFN-γ and TNF-α production and representative FACS plots for splenic WT and *Cd38*$^{-/-}$ P14^{+} T cells at day 8 post Arm infection (**A**). Quantification of IFN-γ and TNF-α production and representative FACS plots for splenic WT and *Cd38*$^{-/-}$ P14^{+} T cells at day 8 post Cl13 infection (**B**). Quantification of IFN-γ and TNF-α production and representative FACS plots for splenic WT and *Cd38*$^{-/-}$ P14^{+} T cells at day 30 post Arm infection (**C**). Quantification of IFN-γ and TNF-α production and representative FACS plots for splenic WT and *Cd38*$^{-/-}$ P14^{+} T cells at day 30 post Cl13 infection (**D**). Data are representative of 3 independent experiments with ≥ 5 mice per group. Data show mean ± s.e.m. *P ≤ 0.05, ***P ≤ 0.001, ****P ≤ 0.0001, paired t-test.

CHAPTER 4

SUMMARY AND FUTURE DIRECTIONS

PSGL-1 as a new therapeutic target (Chapter 2)

In our studies, we found that PSGL-1 was highly upregulated on tumor-infiltrating lymphocytes. Upon antibody targeting of PSGL-1, mice had smaller melanoma tumors than their counterpart IgG-treated mice. The murine melanoma cell line used in these experiments is a highly aggressive, PD-1 blockade-resistant cell line (271, 294), making this result an exciting new therapeutic strategy for aggressive melanoma control. Our studies provided new insight into the phenotypic and functional impact of targeting PSGL-1 on tumor-infiltrating lymphocytes (TILs). Anti-PSGL-1 treated TILs retained more effector functions, particularly in their proliferation and granzyme production, than IgG treated TILs. One of the most notable findings of this project was that anti-PSGL-1 treatment caused a significant decrease in the presence of Tregulatory (Treg) cells within the tumor. This separates anti-PSGL-1 treatment from other immunotherapies, as PD-1 blockade promotes Treg function and proliferation, and CTLA-4 blockade promotes expansion of the Treg population and can lead to worse anti-tumor immunity (295-297). Accordingly, when treatment groups were expanded to include anti-PD-1, anti-PSGL-1, and a combination of anti-PD-1 and anti-PSGL-1 treatments, only treatments with anti-PSGL-1 were able to decrease tumor Treg numbers.

The observed decrease in intratumoral Treg cells after anti-PSGL-1 treatment opens many avenues for future research. One important question that arises is whether targeting PSGL-1 with a monoclonal antibody or through gene deletion alters the trafficking of Tregs. To delve into this question, we could follow the same tumor implantation and anti-PSGL-1 treatment timeline that was done in our paper, and perform sequential mouse analysis at 10, 13, and 18dpi to examine Treg frequencies in the LN, TdLN, and tumor. This will allow us to track whether the Treg presence in the

LNs and tumor are changed over time by anti-PSGL-1 treatment, as a possible explanation for the diminished Treg presence in the tumor at 18dpi could be a result of slowed Treg entry. Proliferation and apoptosis will also have to be examined at each time point using a Foxp3-GFP reporter mouse, as an alternative explanation for the decreased tumoral Treg population could be reduced division or increased cell death.

Further questions remain about the impact of PSGL-1 blockade on the Treg phenotype, as Tregs are the highest expressor of PSGL-1 in both the TdLN and tumor. Our studies found that the expression of the inhibitory receptors PD-1, TIM-3, and LAG3 were not altered on Tregs at 18dpi with anti-PSGL-1 treatment. However, these markers are only a small window into the Treg phenotype, as suppressive Tregs express high levels of CD25, CD39, CTLA-4, Helios, LAP and TGF-β, and IL-10 in the tumor microenvironment (298, 299). In the future, we should resolve the role that PSGL-1 plays in shaping the Treg phenotype, particularly in the tumor microenvironment, as Tregs are a key immunosuppressive player in deciding the outcome of immune checkpoint blockade (295, 300). This could include taking out Tregs from anti-PSGL-1 treated tumors and evaluating their suppressive function *in vitro*. Utilizing the melanoma models and treatment approach we took in our study and including earlier timepoints and a more in-depth Treg analysis could help to uncover the impact of PSGL-1 blockade on the Treg phenotype. Tregs should be analyzed for rates of cell death through a caspase stain, for proliferation and phenotype markers through flow cytometry analysis, and for production of immunosuppressive cytokines through intracellular staining and/or ELISA. Further, we could isolate and perform bulk RNAseq on Tregs isolated from tumors during early and late time points. This would allow us to analyze transcriptome changes that occur in Tregs due to anti-PSGL-1 treatment. These experiments could help to elucidate the impact of targeting PSGL-1 on Tregs and highlight a previously unknown role for PSGL-1 in the modulation of Treg phenotype and function in tumors.

Another route to determining the role of PSGL-1 on Tregs in the anti-tumor T cell response is to use our *Selplg*$^{fl/fl}$ FOXP3ERT2^{Cre} line. This mouse line allows us to selectively delete PSGL-1 only on Treg cells with the injection of tamoxifen. By performing *in vivo* tumor studies in this line, it will allow us to determine whether the slowed melanoma tumor growth and increased T cell functions observed in our published study are reliant on PSGL-1 inhibition on Tregs. This inducible deletion mouse model allows us to investigate whether targeting PSGL-1 on Tregs alone promotes tumor control in multiple models of melanoma, and how the timing of PSGL-1 deletion alters the intratumoral Treg phenotype and/or functions. As Tregs are such an important player in shaping the TME, understanding the role of PSGL-1 on their movement, phenotype and function will provide important fundamental knowledge as well as provide new mechanistic insight into the therapeutic potential of targeting PSGL-1.

In addition to its ability to reduce Treg numbers, PSGL-1 blockade is different from PD-1 blockade in its ability to promote robust proliferation of $CD8^+$ T cells and $CD4^+$ T cells, as well as increase granzymeB production in $CD8^+$ T cells. Further, the antigen-specific population of T cells was significantly increased in the tumors of anti-PSGL-1-treated mice. While our paper concluded that targeting PSGL-1 reinvigorates exhausted T cells, we did not delve into the impact of anti-PSGL-1 treatment on the differentiation of Tpex and Tex subsets of exhausted T cells.

The balance of Tpex and Tex cells in the tumor microenvironment and draining lymph node can impact the outcome of immunotherapeutic treatments (38, 301). Therefore, understanding the factors that shape the Tpex and Tex populations is of great clinical interest. A natural extension for our project is then to determine what role PSGL-1 may have in the formation and phenotype of Tpex and Tex populations. Tpex cells express the transcription factor TCF1, are high for Slamf6, CXCR3, CXCR5, express relatively low levels of effector cytokines and granzymes, and are long-lived and

capable of self-renewal and respond to immune checkpoint blockade (34, 38). Tex cells, on the other hand, are defined by the transcription factor TOX, express high levels of PD-1, TIM-3, CD101, CD69, and can produce more cytokines and granzymes than Tpex cells, although not nearly as much as effector T cells. Our data showed that most tumor-infiltrating T cells treated with anti-PSGL-1 antibody were PD-1^{hi}TIM-3^{+}, which indicates a highly stimulated, more terminal T cell phenotype (302). We also observed increased proliferation and granzymeB after anti-PSGL-1 treatment. While we did not use SlamF6 and TCF1 to examine the progenitor exhausted (Tpex) and terminal exhausted (Tex) populations in our published study, the high expression of inhibitory receptors, in combination with an increase in granzymeB production and proliferation, indicate that targeting PSGL-1 promotes a more terminal phenotype. In agreement with our published data, which indicates that anti-PSGL-1 treatment results in a more terminal T cell phenotype, data collected from D4M melanoma tumors support this hypothesis, as targeting PSGL-1 on TILs resulted in a significant decrease in Tpex population and an increased in the Tex population at 19dpi (**Fig. 4.1**).

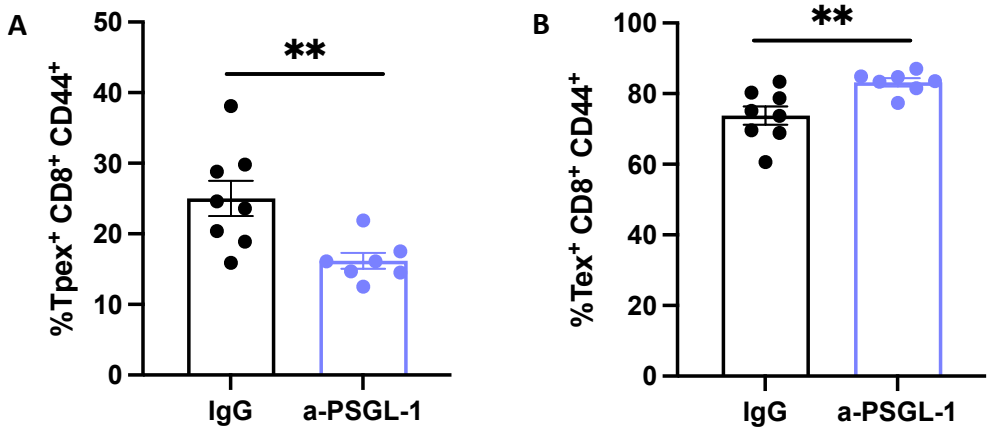

Figure 4.1 Tpex and Tex frequencies in D4M tumors. WT mice were injected with (1×10^6) D4M-3A melanoma cells s.c. and injected with IgG or anti–PSGL-1 antibodies at 8, 10, and 12 dpi. Frequency of Tpex cells (**A**) and Tex cells (**B**) at 19dpi. Graphs show the mean ± SEM. *, $P < 0.05$; **, $P < 0.005$; ***, $P < 0.001$ by two-tailed *t* test or Mann–Whitney *U* test.

The impact of PSGL-1 expression on the formation and phenotype of Tpex and Tex cells should be further studied. To understand the impact of therapeutic targeting of PSGL-1 on these exhausted subsets, the *in vivo* approach outlined in our paper could be utilized, with the addition of earlier end timepoints (11dpi and 13dpi), to investigate the Tpex and Tex populations present in the tumor and TdLN during and after anti-PSGL-1 treatment. Our preliminary data indicate that targeting PSGL-1 drives T cells towards a more terminal fate (**Fig 4.1**). This is supported by the fact that tumor-infiltrating, antigen-specific *Selplg*$^{-/-}$ CD8^{+} T cells have significantly higher frequencies of Tex cells than their WT counterparts (166). Given our knowledge that stronger activation signals drive the more terminal Tex population, our findings that blocking PSGL-1 drives a more terminal fate make sense in the context of PSGL-1 as an immune checkpoint molecule (34, 302). It appears that relieving T cells of PSGL-1 inhibitory signals allows them to be more activated and more functional, but also more terminal than T cells with intact PSGL-1 signaling. This hypothesis can explain the lack of survival benefit seen in our PSGL-1 study, where administration of the PSGL-1 antibody alone did not support significant survival benefit over IgG treatment, despite slower tumor growth. Anti-PSGL-1 treatment may promote a burst of increased effector function as the TILs become more terminal, however they then undergo apoptosis and long-term therapeutic benefit is lost. This is another avenue for future study, as we should investigate whether longer duration of anti-PSGL-1 treatment, sequential administration of anti-PSGL-1 and then anti-PD-1, or a new combination of anti-PSGL-1 and an additional immunotherapy can promote increased long-term survival over IgG treatment.

Our paper demonstrated a strong phenotype, however the full mechanism through which targeting anti-PSGL-1 promotes improved tumor control is still unknown. V-domain suppressor of T cell function (VISTA) is a ligand for PSGL-1 at pH 6 and is a known suppressor of T cell proliferation and function (129). We hypothesize that a portion of the therapeutic benefit of targeting PSGL-1 is coming from the blockade of PSGL-1-VISTA interactions. The available *in vitro* reagents

to study the PSGL-1-VISTA interactions are currently limited, however it would be interesting to perform *in vivo* studies with an additional anti-VISTA therapy to determine if there are additive effects of blocking VISTA and PSGL-1 together. If we see no additional therapeutic benefit with the addition of an anti-VISTA reagent, then this will provide more evidence that the 4RA10 anti-PSGL-1 antibody used in our studies was effectively blocking PSGL-1 signaling through VISTA and vice-versa.

A final avenue of future study for this project is the role of PSGL-1 in metastasis. In our studies, we did not investigate whether PSGL-1 deletion or therapeutic targeting impacted metastasis rates or phenotype. In multiple myeloma, prostate cancer, lung cancer, and gastric cancer, PSGL-1 promotes metastasis of cancer cells through interactions with selectins and chemokines, as well as through alterations of infiltrating immune cells (146-151). PSGL-1 suppresses T cell function in the tumor microenvironment, but we have yet to uncover the impact of PSGL-1 expression on tumor infiltrating myeloid cells, as well as the tumor cells themselves. Understanding how PSGL-1 signals in these cells, as well as how cancer cells may use it as an adhesion molecule, will increase our understanding of the immune-cancer cell dynamics in the TME, as well as the factors that cancer cells use to extravasate and spread. We should first determine the expression of PSGL-1 in our lab murine melanoma lines (D4M, Yummer, B16-F10), perform *in vitro* studies to observe if anti-PSGL-1 treatment alters growth kinetics of the melanoma cells, and then perform *in vivo* studies and treat the cancer cells with anti-PSGL-1 prior to tail vein injection for metastasis studies.

Our work studying PSGL-1 provides important insight not only into the basic biological consequences of targeting PSGL-1 on T cells, but also into the feasibility of PSGL-1 as a new therapeutic agent. Anti-PSGL-1 treatment resulted in slower melanoma tumor growth, decreased immunosuppressive Tregs, and bolstered T cell functions in the TME. We reveal anti-PSGL-1 treatment to be a novel way to improve anti-tumor immunity in PD-1 resistant tumors and open doors

to impactful future projects regarding the impact of PSGL-1 expression on Tpex and Tex cells, on Tregs, on tumor metastasis, and on VISTA signaling. While these studies focused on melanoma, it would be relevant to extend our research on targeting PSGL-1 to other tumor types that have shown benefit from immunotherapies, such as lung cancer and colorectal cancer.

CD38 as an immune-modulatory molecule (Chapter 3)

In our CD38 study, we sought to understand the role of CD38 in the virus-specific $CD8^+$ T cell response. CD38 is expressed on activated T cells and is upregulated significantly on antigen-specific T cells responding to chronic infection in mice and humans. We used a co-transfer approach to study the cell-intrinsic function of CD38 on antigen-specific T cells during acute and chronic infection and found that CD38 expression was important for the maintenance of T cells over the course of infection. In both acute and chronic infection, *Cd38*$^{-/-}$ $CD8^+$ T cells had increased apoptosis and decreased numbers when compared to WT cells at 30dpi. Interestingly, when the ratio of WT and *Cd38*$^{-/-}$ $CD8^+$ T cells was examined at 24h post co-transfer, cells lacking CD38 were already present at reduced frequencies in the spleen and lymph nodes. In the context of this study, we did not follow up to determine what factors are causing this reduced homing in *Cd38*$^{-/-}$ $CD8^+$ T cells, however this presents an interesting area for future research. Naïve T cells express CCR7, CD62L, CD31 (a known ligand of CD38), CD27, and CD28, all of which facilitate the homing of naïve T cells to secondary lymphoid organs as well as naïve T cell rolling, adhesion and TCR signaling (303). It is not known how CD38 deletion impacts the expression of these naïve T cell features, however our results indicate that CD38 deletion likely does have an impact on the naïve phenotype, given the significant reduction of *Cd38*$^{-/-}$ $CD8^+$ T cells in secondary lymphoid organs after adoptive transfer.

When *Cd38*$^{-/-}$ $CD8^+$ T cells were examined during chronic infection, they were found to retain more granzymeB at 8dpi and more Ki67 at 30dpi when compared to WT $CD8^+$ T cells. This indicated

a more effector-like phenotype, which was consistent with the increased frequency of CD69^{+} *Cd38*$^{-/-}$ CD8^{+} T cells at 8dpi and increased frequency of KLRG-1^{+} *Cd38*$^{-/-}$ CD8^{+} T cells compared to WT at 8 and 30dpi, both markers of activation and effector function (34, 39, 304). Interestingly, this increase in effector function was even more prominent in the Tpex subset of exhausted T cells. *Cd38*$^{-/-}$ Tpex cells had significantly increased proliferation and granzymeB production than WT Tpex cells at 30dpi. However, apoptosis was also significantly increased in *Cd38*$^{-/-}$ CD8^{+} T cells at 30dpi, indicating that CD38 deletion is a double edged-sword; it boosts effector function while diminishing survival of virus-specific T cells. Currently, this result indicates that it would be unwise to try and block CD38 on CD8^{+} T cells, as it ultimately would hinder the anti-viral T cell response by decreasing the pool of responding T cells. However, given that CD38 deletion does promote effector function in exhausted T cells, there are numerous interesting questions that arise as to how CD38 limits effector function and support survival in WT CD8^{+} T cells. There is not much known about cell intrinsic CD38 signaling, and it would provide new knowledge to the field to perform experiments with a CD38 agonist compound/antibody to see the impact that CD38 ligation has on TCR signaling and pro-survival pathways. This experiment could be performed *in vitro* initially. Western blotting and qPCR could be done on T cells treated with a CD38 agonist to investigate the impact of CD38 engagement on mRNA and genes involved in TCR activation pathways as well as anti-apoptosis proteins. Further, it would be interesting to see what impact CD38 engagement has on Tpex and Tex genes, TOX and TCF1, as the frequency of TCF1^{+} CD8^{+} T cells were reduced with CD38 deletion.

While our study found that CD38 deletion did not drastically alter the development of exhaustion, this may in part be due to the redundancy of signaling and/or enzymatic functions in the CD38/CD39/CD203/CD73 ectoenzymes (305). Indeed, CD39 was upregulated on *Cd38*$^{-/-}$ CD8^{+} T cells compared to WT at 8 dpi in both acute and chronic infection and may be compensating for the loss of CD38. CD39 is a marker of terminally exhausted T cells and has been implicated in

maintenance of the T cell dysfunction and immune suppression (306, 307). The cell-intrinsic role of CD39 in shaping T cell exhaustion is still being investigated, however CD39, like CD38, can facilitate production of immunosuppressive adenosine. Given the similarly high expression of CD38 and CD39 on terminally exhausted T cells, as well as their role in adenosine production, it would be worthwhile to try a two-pronged approach of blocking both CD38 and CD39. Monoclonal antibody targeting of CD38 and CD39, in addition to duel genetic knockout T cell models, would be interesting to investigate as combination therapies. Targeting CD38 and CD39 may have a larger impact on the T cell exhaustion phenotype than targeting either alone and could provide interesting fundamental insight into the overlap in functionality between the two ectoenzymes. Further, CD38 deletion could be combined with anti-PD-1 treatment to determine whether the increased Tpex and Tex effector functions seen with CD38 deletion could be enhanced with PD-1 blockade, and whether PD-1 blockade could promote increased survival and maintenance of *Cd38*$^{-/-}$ CD8^{+} T cells. If survival and metabolism remain hindered in *Cd38*$^{-/-}$ CD8^{+} T cells even with the use of immune checkpoint blockade, perhaps a monoclonal antibody targeting CD38 should be investigated for therapeutic efficacy. It may be that blocking CD38 only at earlier timepoints or only at later infection timepoints may enhance T cell effector function while limiting the negative impacts on survival and metabolism seen in *Cd38*$^{-/-}$ CD8^{+} T cells.

Our study found that CD38 deletion led to impaired oxidative phosphorylation and glycolysis in T cells from chronically infected mice. This metabolic impairment was unique to *Cd38*$^{-/-}$ CD8^{+} T cells from chronic infection, as *Cd38*$^{-/-}$ CD8^{+} T cells from Arm-infected mice performed oxidative phosphorylation and glycolysis similarly to WT CD8^{+} T cells. The reduced capacity of *Cd38*$^{-/-}$ CD8^{+} T cells from chronic infection to perform both oxidative phosphorylation and glycolysis indicates a global mitochondrial dysfunction in these cells and would be a worthwhile to investigate further. MitoTracker Green dye can be used to measure total mitochondrial mass, MitoTracker Deep Red to

measure intact mitochondrial membrane potential, and gating by flow cytometry on Green^{hi} Deep Red^{lo} can indicate mitochondrial damage (220). While our data indicated that lack of CD38 results in mitochondrial impairment in chronic infection, CD38^{hi}CD8^{+} T cells from systemic lupus erythematosus (SLE) patients showed increased mitochondrial mass with increased reactive oxygen species (MitoSOX^{+}) and damaged cristae (220). These data indicate that while high expression of CD38 promotes mitochondrial abnormalities and defects in patients with SLE, lack of any CD38 limits mitochondrial respiration at 8dpi in virus-specific T cells. More work needs to be done to understand how these results fit together, and whether the reduced mitochondrial respiration we found was due to reduced mitochondrial numbers or mass, or results of structural damage or abnormalities. Understanding the impact of CD38 expression on the mitochondrial function in T cells from chronic infection will provide important knowledge, as well provide insight into the outcomes of therapeutically targeting CD38.

Overall, our work on CD38 found a new role for CD38 in promoting the survival of virus-specific T cells in both acute and chronic infection, as well as promoting proper homing of naïve CD8^{+} T cells. We showed that CD38 expression limits apoptosis in CD8^{+} T cells over the course of acute and chronic infection, but that it also limits granzyme production and proliferation in exhausted T cells during chronic infection. Finally, we found that CD38 deletion diminished mitochondrial respiration in CD8^{+} T cells during chronic infection. Our work provides insight into some of the roles that CD38 plays on virus-specific CD8^{+} T cells and provides more information as to why CD38 is so significantly upregulated on CD8^{+} T cells during acute and chronic infection. This chapter is an exciting first step into understanding the complex enzymatic and cell-intrinsic roles that the ectoenzyme CD38 plays on CD8^{+} T cells and provides direction for further research.

Sources

1. Butz EA, Bevan MJ. 1998. Massive expansion of antigen-specific CD8+ T cells during an acute virus infection. Immunity 8:167-75.
2. Murali-Krishna K, Altman JD, Suresh M, Sourdive DJ, Zajac AJ, Miller JD, Slansky J, Ahmed R. 1998. Counting antigen-specific CD8 T cells: a reevaluation of bystander activation during viral infection. Immunity 8:177-87.
3. Zajac AJ, Blattman JN, Murali-Krishna K, Sourdive DJ, Suresh M, Altman JD, Ahmed R. 1998. Viral immune evasion due to persistence of activated T cells without effector function. J Exp Med 188:2205-13.
4. Ahmed R, Salmi A, Butler LD, Chiller JM, Oldstone MB. 1984. Selection of genetic variants of lymphocytic choriomeningitis virus in spleens of persistently infected mice. Role in suppression of cytotoxic T lymphocyte response and viral persistence. J Exp Med 160:521-40.
5. Utzschneider DT, Legat A, Fuertes Marraco SA, Carrie L, Luescher I, Speiser DE, Zehn D. 2013. T cells maintain an exhausted phenotype after antigen withdrawal and population reexpansion. Nat Immunol 14:603-10.
6. Pauken KE, Sammons MA, Odorizzi PM, Manne S, Godec J, Khan O, Drake AM, Chen Z, Sen DR, Kurachi M, Barnitz RA, Bartman C, Bengsch B, Huang AC, Schenkel JM, Vahedi G, Haining WN, Berger SL, Wherry EJ. 2016. Epigenetic stability of exhausted T cells limits durability of reinvigoration by PD-1 blockade. Science 354:1160-1165.
7. Abdel-Hakeem MS, Manne S, Beltra JC, Stelekati E, Chen Z, Nzingha K, Ali MA, Johnson JL, Giles JR, Mathew D, Greenplate AR, Vahedi G, Wherry EJ. 2021. Epigenetic scarring of exhausted T cells hinders memory differentiation upon eliminating chronic antigenic stimulation. Nat Immunol 22:1008-1019.
8. Hensel N, Gu Z, Sagar, Wieland D, Jechow K, Kemming J, Llewellyn-Lacey S, Gostick E, Sogukpinar O, Emmerich F, Price DA, Bengsch B, Boettler T, Neumann-Haefelin C, Eils R, Conrad C, Bartenschlager R, Grun D, Ishaque N, Thimme R, Hofmann M. 2021. Memory-like HCV-specific CD8(+) T cells retain a molecular scar after cure of chronic HCV infection. Nat Immunol 22:229-239.
9. Yates KB, Tonnerre P, Martin GE, Gerdemann U, Al Abosy R, Comstock DE, Weiss SA, Wolski D, Tully DC, Chung RT, Allen TM, Kim AY, Fidler S, Fox J, Frater J, Lauer GM, Haining WN, Sen DR. 2021. Epigenetic scars of CD8(+) T cell exhaustion persist after cure of chronic infection in humans. Nat Immunol 22:1020-1029.
10. Hor JL, Whitney PG, Zaid A, Brooks AG, Heath WR, Mueller SN. 2015. Spatiotemporally Distinct Interactions with Dendritic Cell Subsets Facilitates CD4+ and CD8+ T Cell Activation to Localized Viral Infection. Immunity 43:554-65.
11. Wei SC, Sharma R, Anang NAS, Levine JH, Zhao Y, Mancuso JJ, Setty M, Sharma P, Wang J, Pe'er D, Allison JP. 2019. Negative Co-stimulation Constrains T Cell Differentiation by Imposing Boundaries on Possible Cell States. Immunity 50:1084-1098 e10.
12. McLane LM, Abdel-Hakeem MS, Wherry EJ. 2019. CD8 T Cell Exhaustion During Chronic Viral Infection and Cancer. Annu Rev Immunol 37:457-495.
13. Pauken KE, Wherry EJ. 2015. Overcoming T cell exhaustion in infection and cancer. Trends Immunol 36:265-76.
14. Hui E, Cheung J, Zhu J, Su X, Taylor MJ, Wallweber HA, Sasmal DK, Huang J, Kim JM, Mellman I, Vale RD. 2017. T cell costimulatory receptor CD28 is a primary target for PD-1-mediated inhibition. Science 355:1428-1433.
15. Topalian SL, Drake CG, Pardoll DM. 2015. Immune checkpoint blockade: a common denominator approach to cancer therapy. Cancer Cell 27:450-61.
16. Wherry EJ, Blattman JN, Murali-Krishna K, van der Most R, Ahmed R. 2003. Viral persistence alters CD8 T-cell immunodominance and tissue distribution and results in distinct stages of functional impairment. J Virol 77:4911-27.

17. Wherry EJ, Ha SJ, Kaech SM, Haining WN, Sarkar S, Kalia V, Subramaniam S, Blattman JN, Barber DL, Ahmed R. 2007. Molecular signature of CD8+ T cell exhaustion during chronic viral infection. Immunity 27:670-84.
18. Ahmadzadeh M, Johnson LA, Heemskerk B, Wunderlich JR, Dudley ME, White DE, Rosenberg SA. 2009. Tumor antigen-specific CD8 T cells infiltrating the tumor express high levels of PD-1 and are functionally impaired. Blood 114:1537-44.
19. Fuller MJ, Zajac AJ. 2003. Ablation of CD8 and CD4 T cell responses by high viral loads. J Immunol 170:477-86.
20. Bengsch B, Ohtani T, Herati RS, Bovenschen N, Chang KM, Wherry EJ. 2018. Deep immune profiling by mass cytometry links human T and NK cell differentiation and cytotoxic molecule expression patterns. J Immunol Methods 453:3-10.
21. Utzschneider DT, Charmoy M, Chennupati V, Pousse L, Ferreira DP, Calderon-Copete S, Danilo M, Alfei F, Hofmann M, Wieland D, Pradervand S, Thimme R, Zehn D, Held W. 2016. T Cell Factor 1-Expressing Memory-like CD8(+) T Cells Sustain the Immune Response to Chronic Viral Infections. Immunity 45:415-27.
22. Schmitz JE, Kuroda MJ, Santra S, Sasseville VG, Simon MA, Lifton MA, Racz P, Tenner-Racz K, Dalesandro M, Scallon BJ, Ghrayeb J, Forman MA, Montefiori DC, Rieber EP, Letvin NL, Reimann KA. 1999. Control of viremia in simian immunodeficiency virus infection by CD8+ lymphocytes. Science 283:857-60.
23. Barber DL, Wherry EJ, Masopust D, Zhu B, Allison JP, Sharpe AH, Freeman GJ, Ahmed R. 2006. Restoring function in exhausted CD8 T cells during chronic viral infection. Nature 439:682-7.
24. Leach DR, Krummel MF, Allison JP. 1996. Enhancement of antitumor immunity by CTLA-4 blockade. Science 271:1734-6.
25. Pardoll DM. 2012. The blockade of immune checkpoints in cancer immunotherapy. Nat Rev Cancer 12:252-64.
26. Utzschneider DT, Alfei F, Roelli P, Barras D, Chennupati V, Darbre S, Delorenzi M, Pinschewer DD, Zehn D. 2016. High antigen levels induce an exhausted phenotype in a chronic infection without impairing T cell expansion and survival. J Exp Med 213:1819-34.
27. Man K, Gabriel SS, Liao Y, Gloury R, Preston S, Henstridge DC, Pellegrini M, Zehn D, Berberich-Siebelt F, Febbraio MA, Shi W, Kallies A. 2017. Transcription Factor IRF4 Promotes CD8(+) T Cell Exhaustion and Limits the Development of Memory-like T Cells during Chronic Infection. Immunity 47:1129-1141 e5.
28. Martinez GJ, Pereira RM, Aijo T, Kim EY, Marangoni F, Pipkin ME, Togher S, Heissmeyer V, Zhang YC, Crotty S, Lamperti ED, Ansel KM, Mempel TR, Lahdesmaki H, Hogan PG, Rao A. 2015. The transcription factor NFAT promotes exhaustion of activated CD8(+) T cells. Immunity 42:265-278.
29. Scott-Browne JP, Lopez-Moyado IF, Trifari S, Wong V, Chavez L, Rao A, Pereira RM. 2016. Dynamic Changes in Chromatin Accessibility Occur in CD8(+) T Cells Responding to Viral Infection. Immunity 45:1327-1340.
30. Kallies A, Zehn D, Utzschneider DT. 2020. Precursor exhausted T cells: key to successful immunotherapy? Nat Rev Immunol 20:128-136.
31. Alfei F, Kanev K, Hofmann M, Wu M, Ghoneim HE, Roelli P, Utzschneider DT, von Hoesslin M, Cullen JG, Fan Y, Eisenberg V, Wohlleber D, Steiger K, Merkler D, Delorenzi M, Knolle PA, Cohen CJ, Thimme R, Youngblood B, Zehn D. 2019. TOX reinforces the phenotype and longevity of exhausted T cells in chronic viral infection. Nature 571:265-269.
32. Khan O, Giles JR, McDonald S, Manne S, Ngiow SF, Patel KP, Werner MT, Huang AC, Alexander KA, Wu JE, Attanasio J, Yan P, George SM, Bengsch B, Staupe RP, Donahue G, Xu W, Amaravadi RK, Xu X, Karakousis GC, Mitchell TC, Schuchter LM, Kaye J, Berger SL, Wherry EJ. 2019. TOX transcriptionally and epigenetically programs CD8(+) T cell exhaustion. Nature 571:211-218.
33. Seo H, Chen J, Gonzalez-Avalos E, Samaniego-Castruita D, Das A, Wang YH, Lopez-Moyado IF, Georges RO, Zhang W, Onodera A, Wu CJ, Lu LF, Hogan PG, Bhandoola A, Rao A. 2019. TOX and TOX2 transcription factors cooperate with NR4A transcription factors to impose CD8(+) T cell exhaustion. Proc Natl Acad Sci U S A 116:12410-12415.

34. Dolina JS, Van Braeckel-Budimir N, Thomas GD, Salek-Ardakani S. 2021. CD8(+) T Cell Exhaustion in Cancer. Front Immunol 12:715234.
35. Collier JL, Weiss SA, Pauken KE, Sen DR, Sharpe AH. 2021. Not-so-opposite ends of the spectrum: CD8(+) T cell dysfunction across chronic infection, cancer and autoimmunity. Nat Immunol 22:809-819.
36. Blank CU, Haining WN, Held W, Hogan PG, Kallies A, Lugli E, Lynn RC, Philip M, Rao A, Restifo NP, Schietinger A, Schumacher TN, Schwartzberg PL, Sharpe AH, Speiser DE, Wherry EJ, Youngblood BA, Zehn D. 2019. Defining 'T cell exhaustion'. Nat Rev Immunol 19:665-674.
37. Im SJ, Hashimoto M, Gerner MY, Lee J, Kissick HT, Burger MC, Shan Q, Hale JS, Lee J, Nasti TH, Sharpe AH, Freeman GJ, Germain RN, Nakaya HI, Xue HH, Ahmed R. 2016. Defining CD8+ T cells that provide the proliferative burst after PD-1 therapy. Nature 537:417-421.
38. Miller BC, Sen DR, Al Abosy R, Bi K, Virkud YV, LaFleur MW, Yates KB, Lako A, Felt K, Naik GS, Manos M, Gjini E, Kuchroo JR, Ishizuka JJ, Collier JL, Griffin GK, Maleri S, Comstock DE, Weiss SA, Brown FD, Panda A, Zimmer MD, Manguso RT, Hodi FS, Rodig SJ, Sharpe AH, Haining WN. 2019. Subsets of exhausted CD8(+) T cells differentially mediate tumor control and respond to checkpoint blockade. Nat Immunol 20:326-336.
39. Beltra JC, Manne S, Abdel-Hakeem MS, Kurachi M, Giles JR, Chen Z, Casella V, Ngiow SF, Khan O, Huang YJ, Yan P, Nzingha K, Xu W, Amaravadi RK, Xu X, Karakousis GC, Mitchell TC, Schuchter LM, Huang AC, Wherry EJ. 2020. Developmental Relationships of Four Exhausted CD8(+) T Cell Subsets Reveals Underlying Transcriptional and Epigenetic Landscape Control Mechanisms. Immunity 52:825-841 e8.
40. He R, Hou S, Liu C, Zhang A, Bai Q, Han M, Yang Y, Wei G, Shen T, Yang X, Xu L, Chen X, Hao Y, Wang P, Zhu C, Ou J, Liang H, Ni T, Zhang X, Zhou X, Deng K, Chen Y, Luo Y, Xu J, Qi H, Wu Y, Ye L. 2016. Follicular CXCR5- expressing CD8(+) T cells curtail chronic viral infection. Nature 537:412-428.
41. Ley K, Kansas GS. 2004. Selectins in T-cell recruitment to non-lymphoid tissues and sites of inflammation. Nat Rev Immunol 4:325-35.
42. Silvan J, Gonzalez-Tajuelo R, Vicente-Rabaneda E, Perez-Frias A, Espartero-Santos M, Munoz-Callejas A, Garcia-Lorenzo E, Gamallo C, Castaneda S, Urzainqui A. 2018. Deregulated PSGL-1 Expression in B Cells and Dendritic Cells May Be Implicated in Human Systemic Sclerosis Development. J Invest Dermatol 138:2123-2132.
43. Borges E, Tietz W, Steegmaier M, Moll T, Hallmann R, Hamann A, Vestweber D. 1997. P-Selectin Glycoprotein Ligand-1 (PSGL-1) on T Helper 1 but Not on T Helper 2 Cells Binds to P-Selectin and Supports Migration into Inflamed Skin. The Journal of Experimental Medicine 185:573-578.
44. Poholek AC, Hansen K, Hernandez SG, Eto D, Chandele A, Weinstein JS, Dong X, Odegard JM, Kaech SM, Dent AL, Crotty S, Craft J. 2010. In vivo regulation of Bcl6 and T follicular helper cell development. J Immunol 185:313-26.
45. Angiari S, Rossi B, Piccio L, Zinselmeyer BH, Budui S, Zenaro E, Bianca VD, Bach SD, Scarpini E, Bolomini-Vittori M, Piacentino G, Dusi S, Laudanna C, Cross AH, Miller MJ, Constantin G. 2013. Regulatory T Cells Suppress the Late Phase of the Immune Response in Lymph Nodes through P-Selectin Glycoprotein Ligand-1. The Journal of Immunology 191:5489-5500.
46. Vachino G, Chang X-J, Veldman GM, Kumar R, Sako D, Fouser LA, Berndt MC, Cumming DA. 1995. P-selectin Glycoprotein Ligand-1 Is the Major Counter-receptor for P-selectin on Stimulated T Cells and Is Widely Distributed in Non-functional Form on Many Lymphocytic Cells. Journal of Biological Chemistry 270:21966-21974.
47. Vachino G, Chang XJ, Veldman GM, Kumar R, Sako D, Fouser LA, Berndt MC, Cumming DA. 1995. P-selectin glycoprotein ligand-1 is the major counter-receptor for P-selectin on stimulated T cells and is widely distributed in non-functional form on many lymphocytic cells. J Biol Chem 270:21966-74.
48. Yang J, Furie BC, Furie B. 1999. The biology of P-selectin glycoprotein ligand-1: its role as a selectin counterreceptor in leukocyte-endothelial and leukocyte-platelet interaction. Thrombosis and Haemostasis 81:1-7.

49. Sako D, Chang XJ, Barone KM, Vachino G, White HM, Shaw G, Veldman GM, Bean KM, Ahern TJ, Furie B. 1993. Expression cloning of a functional glycoprotein ligand for P-selectin. Cell 75:1179-1186.
50. Cummings RD. 1999. Structure and function of the selectin ligand PSGL-1. Brazilian Journal of Medical and Biological Research 32:519-528.
51. Xia L, Ramachandran V, McDaniel JM, Nguyen KN, Cummings RD, McEver RP. 2003. N-terminal residues in murine P-selectin glycoprotein ligand-1 required for binding to murine P-selectin. Blood 101:552-559.
52. Baïsse B, Galisson F, Giraud S, Schapira M, Spertini O. 2007. Evolutionary conservation of P-selectin glycoprotein ligand-1 primary structure and function. BMC Evolutionary Biology 7:166.
53. Zheng P-S, Vais D, LaPierre D, Liang Y-Y, Lee V, Yang BL, Yang BB. 2004. PG-M/versican binds to P-selectin glycoprotein ligand-1 and mediates leukocyte aggregation. Journal of Cell Science 117:5887-5895.
54. Leppänen A, Mehta P, Ouyang Y-B, Ju T, Helin J, Moore KL, Die Iv, Canfield WM, McEver RP, Cummings RD. 1999. A Novel Glycosulfopeptide Binds to P-selectin and Inhibits Leukocyte Adhesion to P-selectin. Journal of Biological Chemistry 274:24838-24848.
55. Leppänen A, White SP, Helin J, McEver RP, Cummings RD. 2000. Binding of Glycosulfopeptides to P-selectin Requires Stereospecific Contributions of Individual Tyrosine Sulfate and Sugar Residues. Journal of Biological Chemistry 275:39569-39578.
56. Somers WS, Tang J, Shaw GD, Camphausen RT. 2000. Insights into the Molecular Basis of Leukocyte Tethering and Rolling Revealed by Structures of P- and E-Selectin Bound to SLeX and PSGL-1. Cell 103:467-479.
57. Jandus C, Simon H-U, von Gunten S. 2011. Targeting Siglecs—A novel pharmacological strategy for immuno- and glycotherapy. Biochemical Pharmacology 82:323-332.
58. Erbani J, Tay J, Barbier V, Levesque J-P, Winkler IG. 2020. Acute Myeloid Leukemia Chemo-Resistance Is Mediated by E-selectin Receptor CD162 in Bone Marrow Niches. Frontiers in Cell and Developmental Biology 8.
59. Goetz DJ, Greif DM, Ding H, Camphausen RT, Howes S, Comess KM, Snapp KR, Kansas GS, Luscinskas FW. 1997. Isolated P-selectin glycoprotein ligand-1 dynamic adhesion to P- and E-selectin. J Cell Biol 137:509-19.
60. Spertini O, Cordey AS, Monai N, Giuffre L, Schapira M. 1996. P-selectin glycoprotein ligand 1 is a ligand for L-selectin on neutrophils, monocytes, and CD34+ hematopoietic progenitor cells. J Cell Biol 135:523-31.
61. Xia L, Ramachandran V, McDaniel JM, Nguyen KN, Cummings RD, McEver RP. 2003. N-terminal residues in murine P-selectin glycoprotein ligand-1 required for binding to murine P-selectin. Blood 101:552-9.
62. Mehta P, Cummings RD, McEver RP. 1998. Affinity and kinetic analysis of P-selectin binding to P-selectin glycoprotein ligand-1. J Biol Chem 273:32506-13.
63. Krishnamurthy VR, Sardar MY, Ying Y, Song X, Haller C, Dai E, Wang X, Hanjaya-Putra D, Sun L, Morikis V, Simon SI, Woods RJ, Cummings RD, Chaikof EL. 2015. Glycopeptide analogues of PSGL-1 inhibit P-selectin in vitro and in vivo. Nat Commun 6:6387.
64. Somers WS, Tang J, Shaw GD, Camphausen RT. 2000. Insights into the molecular basis of leukocyte tethering and rolling revealed by structures of P- and E-selectin bound to SLe(X) and PSGL-1. Cell 103:467-79.
65. Martinez M, Joffraud M, Giraud S, Baisse B, Bernimoulin MP, Schapira M, Spertini O. 2005. Regulation of PSGL-1 interactions with L-selectin, P-selectin, and E-selectin: role of human fucosyltransferase-IV and -VII. J Biol Chem 280:5378-90.
66. Moore KL. 1998. Structure and function of P-selectin glycoprotein ligand-1. Leuk Lymphoma 29:1-15.
67. Ouyang Y, Lane WS, Moore KL. 1998. Tyrosylprotein sulfotransferase: purification and molecular cloning of an enzyme that catalyzes tyrosine O-sulfation, a common posttranslational modification of eukaryotic proteins. Proc Natl Acad Sci U S A 95:2896-901.
68. Abadier M, Ley K. 2017. P-selectin glycoprotein ligand-1 in T cells. Curr Opin Hematol 24:265-273.

69. Austrup F, Vestweber D, Borges E, Lohning M, Brauer R, Herz U, Renz H, Hallmann R, Scheffold A, Radbruch A, Hamann A. 1997. P- and E-selectin mediate recruitment of T-helper-1 but not T-helper-2 cells into inflammed tissues. Nature 385:81-3.
70. Mangan PR, O'Quinn D, Harrington L, Bonder CS, Kubes P, Kucik DF, Bullard DC, Weaver CT. 2005. Both Th1 and Th2 cells require P-selectin glycoprotein ligand-1 for optimal rolling on inflamed endothelium. Am J Pathol 167:1661-75.
71. Nolz JC, Harty JT. 2014. IL-15 regulates memory CD8+ T cell O-glycan synthesis and affects trafficking. J Clin Invest 124:1013-26.
72. Haddad W, Cooper CJ, Zhang Z, Brown JB, Zhu Y, Issekutz A, Fuss I, Lee HO, Kansas GS, Barrett TA. 2003. P-selectin and P-selectin glycoprotein ligand 1 are major determinants for Th1 cell recruitment to nonlymphoid effector sites in the intestinal lamina propria. J Exp Med 198:369-77.
73. Nunez-Andrade N, Lamana A, Sancho D, Gisbert JP, Gonzalez-Amaro R, Sanchez-Madrid F, Urzainqui A. 2011. P-selectin glycoprotein ligand-1 modulates immune inflammatory responses in the enteric lamina propria. J Pathol 224:212-21.
74. Yang J, Hirata T, Croce K, Merrill-Skoloff G, Tchernychev B, Williams E, Flaumenhaft R, Furie BC, Furie B. 1999. Targeted gene disruption demonstrates that P-selectin glycoprotein ligand 1 (PSGL-1) is required for P-selectin-mediated but not E-selectin-mediated neutrophil rolling and migration. J Exp Med 190:1769-82.
75. Ramachandran V, Yago T, Epperson TK, Kobzdej MM, Nollert MU, Cummings RD, Zhu C, McEver RP. 2001. Dimerization of a selectin and its ligand stabilizes cell rolling and enhances tether strength in shear flow. Proc Natl Acad Sci U S A 98:10166-71.
76. Ramos-Sevillano E, Urzainqui A, de Andres B, Gonzalez-Tajuelo R, Domenech M, Gonzalez-Camacho F, Sanchez-Madrid F, Brown JS, Garcia E, Yuste J. 2016. PSGL-1 on Leukocytes is a Critical Component of the Host Immune Response against Invasive Pneumococcal Disease. PLoS Pathog 12:e1005500.
77. Ferris ST, Durai V, Wu R, Theisen DJ, Ward JP, Bern MD, Davidson JTt, Bagadia P, Liu T, Briseno CG, Li L, Gillanders WE, Wu GF, Yokoyama WM, Murphy TL, Schreiber RD, Murphy KM. 2020. cDC1 prime and are licensed by CD4(+) T cells to induce anti-tumour immunity. Nature 584:624-629.
78. Urzainqui A, Hoyo GMd, Lamana A, Fuente Hdl, Barreiro O, Olazabal IM, Martin P, Wild MK, Vestweber D, González-Amaro R, Sánchez-Madrid F. 2007. Functional Role of P-Selectin Glycoprotein Ligand 1/P-Selectin Interaction in the Generation of Tolerogenic Dendritic Cells. The Journal of Immunology 179:7457-7465.
79. Luo J. 2018. PI3K Is a Linker Between L-selectin and PSGL-1 Signaling to IL-18 Transcriptional Activation at the Promoter Level. Inflammation 41:555-561.
80. Tinoco R, Carrette F, Barraza ML, Otero DC, Magaña J, Bosenberg MW, Swain SL, Bradley LM. 2016. PSGL-1 Is an Immune Checkpoint Regulator that Promotes T Cell Exhaustion. Immunity 44:1190-203.
81. Rossi FM, Corbel SY, Merzaban JS, Carlow DA, Gossens K, Duenas J, So L, Yi L, Ziltener HJ. 2005. Recruitment of adult thymic progenitors is regulated by P-selectin and its ligand PSGL-1. Nat Immunol 6:626-34.
82. Veerman KM, Williams MJ, Uchimura K, Singer MS, Merzaban JS, Naus S, Carlow DA, Owen P, Rivera-Nieves J, Rosen SD, Ziltener HJ. 2007. Interaction of the selectin ligand PSGL-1 with chemokines CCL21 and CCL19 facilitates efficient homing of T cells to secondary lymphoid organs. Nat Immunol 8:532-9.
83. Veldkamp CT, Kiermaier E, Gabel-Eissens SJ, Gillitzer ML, Lippner DR, DiSilvio FA, Mueller CJ, Wantuch PL, Chaffee GR, Famiglietti MW, Zgoba DM, Bailey AA, Bah Y, Engebretson SJ, Graupner DR, Lackner ER, LaRosa VD, Medeiros T, Olson ML, Phillips AJ, Pyles H, Richard AM, Schoeller SJ, Touzeau B, Williams LG, Sixt M, Peterson FC. 2015. Solution Structure of CCL19 and Identification of Overlapping CCR7 and PSGL-1 Binding Sites. Biochemistry 54:4163-6.
84. Steen A, Larsen O, Thiele S, Rosenkilde MM. 2014. Biased and g protein-independent signaling of chemokine receptors. Front Immunol 5:277.

85. Forster R, Schubel A, Breitfeld D, Kremmer E, Renner-Muller I, Wolf E, Lipp M. 1999. CCR7 coordinates the primary immune response by establishing functional microenvironments in secondary lymphoid organs. Cell 99:23-33.
86. Gunn MD, Kyuwa S, Tam C, Kakiuchi T, Matsuzawa A, Williams LT, Nakano H. 1999. Mice lacking expression of secondary lymphoid organ chemokine have defects in lymphocyte homing and dendritic cell localization. J Exp Med 189:451-60.
87. Potsch C, Vohringer D, Pircher H. 1999. Distinct migration patterns of naive and effector CD8 T cells in the spleen: correlation with CCR7 receptor expression and chemokine reactivity. Eur J Immunol 29:3562-70.
88. Yasuda T, Kuwabara T, Nakano H, Aritomi K, Onodera T, Lipp M, Takahama Y, Kakiuchi T. 2007. Chemokines CCL19 and CCL21 promote activation-induced cell death of antigen-responding T cells. Blood 109:449-56.
89. Schakel K, Kannagi R, Kniep B, Goto Y, Mitsuoka C, Zwirner J, Soruri A, von Kietzell M, Rieber E. 2002. 6-Sulfo LacNAc, a novel carbohydrate modification of PSGL-1, defines an inflammatory type of human dendritic cells. Immunity 17:289-301.
90. Chang MY, Chan CK, Braun KR, Green PS, O'Brien KD, Chait A, Day AJ, Wight TN. 2012. Monocyte-to-macrophage differentiation: synthesis and secretion of a complex extracellular matrix. J Biol Chem 287:14122-35.
91. Wight TN, Kang I, Evanko SP, Harten IA, Chang MY, Pearce OMT, Allen CE, Frevert CW. 2020. Versican-A Critical Extracellular Matrix Regulator of Immunity and Inflammation. Front Immunol 11:512.
92. Zheng PS, Vais D, Lapierre D, Liang YY, Lee V, Yang BL, Yang BB. 2004. PG-M/versican binds to P-selectin glycoprotein ligand-1 and mediates leukocyte aggregation. J Cell Sci 117:5887-95.
93. Snyder JM, Washington IM, Birkland T, Chang MY, Frevert CW. 2015. Correlation of Versican Expression, Accumulation, and Degradation during Embryonic Development by Quantitative Immunohistochemistry. J Histochem Cytochem 63:952-67.
94. Lemire JM, Merrilees MJ, Braun KR, Wight TN. 2002. Overexpression of the V3 variant of versican alters arterial smooth muscle cell adhesion, migration, and proliferation in vitro. J Cell Physiol 190:38-45.
95. Zhang Y, Cao L, Yang BL, Yang BB. 1998. The G3 domain of versican enhances cell proliferation via epidermial growth factor-like motifs. J Biol Chem 273:21342-51.
96. Zhang Y, Cao L, Kiani CG, Yang BL, Yang BB. 1998. The G3 domain of versican inhibits mesenchymal chondrogenesis via the epidermal growth factor-like motifs. J Biol Chem 273:33054-63.
97. Kawashima H, Atarashi K, Hirose M, Hirose J, Yamada S, Sugahara K, Miyasaka M. 2002. Oversulfated chondroitin/dermatan sulfates containing GlcAbeta1/IdoAalpha1-3GalNAc(4,6-O-disulfate) interact with L- and P-selectin and chemokines. J Biol Chem 277:12921-30.
98. Kawashima H, Hirose M, Hirose J, Nagakubo D, Plaas AH, Miyasaka M. 2000. Binding of a large chondroitin sulfate/dermatan sulfate proteoglycan, versican, to L-selectin, P-selectin, and CD44. J Biol Chem 275:35448-56.
99. Kim S, Takahashi H, Lin WW, Descargues P, Grivennikov S, Kim Y, Luo JL, Karin M. 2009. Carcinoma-produced factors activate myeloid cells through TLR2 to stimulate metastasis. Nature 457:102-6.
100. Tang M, Diao J, Gu H, Khatri I, Zhao J, Cattral MS. 2015. Toll-like Receptor 2 Activation Promotes Tumor Dendritic Cell Dysfunction by Regulating IL-6 and IL-10 Receptor Signaling. Cell Rep 13:2851-64.
101. Wang W, Xu GL, Jia WD, Ma JL, Li JS, Ge YS, Ren WH, Yu JH, Liu WB. 2009. Ligation of TLR2 by versican: a link between inflammation and metastasis. Arch Med Res 40:321-3.
102. Xu L, Xue T, Zhang J, Qu J. 2016. Knockdown of versican V1 induces a severe inflammatory response in LPS-induced acute lung injury via the TLR2-NF-kappaB signaling pathway in C57BL/6J mice. Mol Med Rep 13:5005-12.
103. Chang MY, Kang I, Gale M, Jr., Manicone AM, Kinsella MG, Braun KR, Wigmosta T, Parks WC, Altemeier WA, Wight TN, Frevert CW. 2017. Versican is produced by Trif- and type I interferon-

dependent signaling in macrophages and contributes to fine control of innate immunity in lungs. Am J Physiol Lung Cell Mol Physiol 313:L1069-L1086.
104. Chang MY, Tanino Y, Vidova V, Kinsella MG, Chan CK, Johnson PY, Wight TN, Frevert CW. 2014. Reprint of: A rapid increase in macrophage-derived versican and hyaluronan in infectious lung disease. Matrix Biol 35:162-73.
105. Du WW, Yang W, Yee AJ. 2013. Roles of versican in cancer biology--tumorigenesis, progression and metastasis. Histol Histopathol 28:701-13.
106. Ricciardelli C, Sakko AJ, Ween MP, Russell DL, Horsfall DJ. 2009. The biological role and regulation of versican levels in cancer. Cancer Metastasis Rev 28:233-45.
107. Theocharis AD, Skandalis SS, Tzanakakis GN, Karamanos NK. 2010. Proteoglycans in health and disease: novel roles for proteoglycans in malignancy and their pharmacological targeting. FEBS J 277:3904-23.
108. Derynck R, Goeddel DV, Ullrich A, Gutterman JU, Williams RD, Bringman TS, Berger WH. 1987. Synthesis of messenger RNAs for transforming growth factors alpha and beta and the epidermal growth factor receptor by human tumors. Cancer Res 47:707-12.
109. Kodama J, Hasengaowa, Kusumoto T, Seki N, Matsuo T, Nakamura K, Hongo A, Hiramatsu Y. 2007. Versican expression in human cervical cancer. Eur J Cancer 43:1460-6.
110. Kodama J, Hasengaowa, Kusumoto T, Seki N, Matsuo T, Ojima Y, Nakamura K, Hongo A, Hiramatsu Y. 2007. Prognostic significance of stromal versican expression in human endometrial cancer. Ann Oncol 18:269-74.
111. Gao D, Vahdat LT, Wong S, Chang JC, Mittal V. 2012. Microenvironmental regulation of epithelial-mesenchymal transitions in cancer. Cancer Res 72:4883-9.
112. Gorter A, Zijlmans HJ, van Gent H, Trimbos JB, Fleuren GJ, Jordanova ES. 2010. Versican expression is associated with tumor-infiltrating CD8-positive T cells and infiltration depth in cervical cancer. Mod Pathol 23:1605-15.
113. Hartley G, Regan D, Guth A, Dow S. 2017. Regulation of PD-L1 expression on murine tumor-associated monocytes and macrophages by locally produced TNF-alpha. Cancer Immunol Immunother 66:523-535.
114. Schauer R. 2009. Sialic acids as regulators of molecular and cellular interactions. Curr Opin Struct Biol 19:507-14.
115. Chang YC, Nizet V. 2014. The interplay between Siglecs and sialylated pathogens. Glycobiology 24:818-25.
116. Macauley MS, Crocker PR, Paulson JC. 2014. Siglec-mediated regulation of immune cell function in disease. Nat Rev Immunol 14:653-66.
117. Mahajan VS, Pillai S. 2016. Sialic acids and autoimmune disease. Immunol Rev 269:145-61.
118. Pearce OM, Laubli H. 2016. Sialic acids in cancer biology and immunity. Glycobiology 26:111-28.
119. Pepin M, Mezouar S, Pegon J, Muczynski V, Adam F, Bianchini EP, Bazaa A, Proulle V, Rupin A, Paysant J, Panicot-Dubois L, Christophe OD, Dubois C, Lenting PJ, Denis CV. 2016. Soluble Siglec-5 associates to PSGL-1 and displays anti-inflammatory activity. Sci Rep 6:37953.
120. Ali SR, Fong JJ, Carlin AF, Busch TD, Linden R, Angata T, Areschoug T, Parast M, Varki N, Murray J, Nizet V, Varki A. 2014. Siglec-5 and Siglec-14 are polymorphic paired receptors that modulate neutrophil and amnion signaling responses to group B Streptococcus. J Exp Med 211:1231-42.
121. Cornish AL, Freeman S, Forbes G, Ni J, Zhang M, Cepeda M, Gentz R, Augustus M, Carter KC, Crocker PR. 1998. Characterization of siglec-5, a novel glycoprotein expressed on myeloid cells related to CD33. Blood 92:2123-32.
122. Duan S, Koziol-White CJ, Jester WF, Jr., Nycholat CM, Macauley MS, Panettieri RA, Jr., Paulson JC. 2019. CD33 recruitment inhibits IgE-mediated anaphylaxis and desensitizes mast cells to allergen. J Clin Invest 129:1387-1401.
123. Lock K, Zhang J, Lu J, Lee SH, Crocker PR. 2004. Expression of CD33-related siglecs on human mononuclear phagocytes, monocyte-derived dendritic cells and plasmacytoid dendritic cells. Immunobiology 209:199-207.

124. Stanczak MA, Siddiqui SS, Trefny MP, Thommen DS, Boligan KF, von Gunten S, Tzankov A, Tietze L, Lardinois D, Heinzelmann-Schwarz V, von Bergwelt-Baildon M, Zhang W, Lenz HJ, Han Y, Amos CI, Syedbasha M, Egli A, Stenner F, Speiser DE, Varki A, Zippelius A, Laubli H. 2018. Self-associated molecular patterns mediate cancer immune evasion by engaging Siglecs on T cells. J Clin Invest 128:4912-4923.
125. Yokoi H, Myers A, Matsumoto K, Crocker PR, Saito H, Bochner BS. 2006. Alteration and acquisition of Siglecs during in vitro maturation of CD34+ progenitors into human mast cells. Allergy 61:769-76.
126. Wang L, Rubinstein R, Lines JL, Wasiuk A, Ahonen C, Guo Y, Lu LF, Gondek D, Wang Y, Fava RA, Fiser A, Almo S, Noelle RJ. 2011. VISTA, a novel mouse Ig superfamily ligand that negatively regulates T cell responses. J Exp Med 208:577-92.
127. Lines JL, Pantazi E, Mak J, Sempere LF, Wang L, O'Connell S, Ceeraz S, Suriawinata AA, Yan S, Ernstoff MS, Noelle R. 2014. VISTA is an immune checkpoint molecule for human T cells. Cancer Res 74:1924-32.
128. Lines JL, Sempere LF, Broughton T, Wang L, Noelle R. 2014. VISTA is a novel broad-spectrum negative checkpoint regulator for cancer immunotherapy. Cancer Immunol Res 2:510-7.
129. Johnston RJ, Su LJ, Pinckney J, Critton D, Boyer E, Krishnakumar A, Corbett M, Rankin AL, Dibella R, Campbell L, Martin GH, Lemar H, Cayton T, Huang RY, Deng X, Nayeem A, Chen H, Ergel B, Rizzo JM, Yamniuk AP, Dutta S, Ngo J, Shorts AO, Ramakrishnan R, Kozhich A, Holloway J, Fang H, Wang YK, Yang Z, Thiam K, Rakestraw G, Rajpal A, Sheppard P, Quigley M, Bahjat KS, Korman AJ. 2019. VISTA is an acidic pH-selective ligand for PSGL-1. Nature 574:565-570.
130. Sako D, Comess KM, Barone KM, Camphausen RT, Cumming DA, Shaw GD. 1995. A sulfated peptide segment at the amino terminus of PSGL-1 is critical for P-selectin binding. Cell 83:323-31.
131. Hidari KIPJ, Weyrich AS, Zimmerman GA, McEver RP. 1997. Engagement of P-selectin Glycoprotein Ligand-1 Enhances Tyrosine Phosphorylation and Activates Mitogen-activated Protein Kinases in Human Neutrophils. Journal of Biological Chemistry 272:28750-28756.
132. Stadtmann A, Germena G, Block H, Boras M, Rossaint J, Sundd P, Lefort C, Fisher CI, Buscher K, Gelschefarth B, Urzainqui A, Gerke V, Ley K, Zarbock A. 2013. The PSGL-1–L-selectin signaling complex regulates neutrophil adhesion under flow. Journal of Experimental Medicine 210:2171-2180.
133. Zarbock A, Abram CL, Hundt M, Altman A, Lowell CA, Ley K. 2008. PSGL-1 engagement by E-selectin signals through Src kinase Fgr and ITAM adapters DAP12 and FcRγ to induce slow leukocyte rolling. The Journal of Experimental Medicine 205:2339-2347.
134. Zarbock A, Lowell CA, Ley K. 2007. Spleen tyrosine kinase Syk is necessary for E-selectin-induced alpha(L)beta(2) integrin-mediated rolling on intercellular adhesion molecule-1. Immunity 26:773-783.
135. Yago T, Shao B, Miner JJ, Yao L, Klopocki AG, Maeda K, Coggeshall KM, McEver RP. 2010. E-selectin engages PSGL-1 and CD44 through a common signaling pathway to induce integrin αLβ2-mediated slow leukocyte rolling. Blood 116:485-494.
136. Mueller H, Stadtmann A, Van Aken H, Hirsch E, Wang D, Ley K, Zarbock A. 2010. Tyrosine kinase Btk regulates E-selectin–mediated integrin activation and neutrophil recruitment by controlling phospholipase C (PLC) γ2 and PI3Kγ pathways. Blood 115:3118-3127.
137. Block H, Herter JM, Rossaint J, Stadtmann A, Kliche S, Lowell CA, Zarbock A. 2012. Crucial role of SLP-76 and ADAP for neutrophil recruitment in mouse kidney ischemia-reperfusion injury. Journal of Experimental Medicine 209:407-421.
138. Kuwano Y, Spelten O, Zhang H, Ley K, Zarbock A. 2010. Rolling on E- or P-selectin induces the extended but not high-affinity conformation of LFA-1 in neutrophils. Blood 116:617-624.
139. Spertini C, Baïsse B, Spertini O. 2012. Ezrin-Radixin-Moesin-binding Sequence of PSGL-1 Glycoprotein Regulates Leukocyte Rolling on Selectins and Activation of Extracellular Signal-regulated Kinases. Journal of Biological Chemistry 287:10693-10702.
140. Alonso-Lebrero JL, Serrador JM, Domínguez-Jiménez C, Barreiro O, Luque A, del Pozo MA, Snapp K, Kansas G, Schwartz-Albiez R, Furthmayr H, Lozano F, Sánchez-Madrid F. 2000. Polarization and interaction of adhesion molecules P-selectin glycoprotein ligand 1 and intercellular adhesion molecule 3 with moesin and ezrin in myeloid cells. Blood 95:2413-2419.

141. Urzainqui A, Serrador JM, Viedma F, Yáñez-Mó Ma, Rodríguez A, Corbí AL, Alonso-Lebrero JL, Luque A, Deckert M, Vázquez J, Sánchez-Madrid F. 2002. ITAM-Based Interaction of ERM Proteins with Syk Mediates Signaling by the Leukocyte Adhesion Receptor PSGL-1. Immunity 17:401-412.
142. Atarashi K, Hirata T, Matsumoto M, Kanemitsu N, Miyasaka M. 2005. Rolling of Th1 Cells via P-Selectin Glycoprotein Ligand-1 Stimulates LFA-1-Mediated Cell Binding to ICAM-1. The Journal of Immunology 174:1424-1432.
143. Ba X-Q, Chen C-X, Xu T, Cui L-L, Gao Y-G, Zeng X-L. 2005. Engagement of PSGL-1 upregulates CSF-1 transcription via a mechanism that may involve Syk. Cellular Immunology 237:1-6.
144. Chen S-C, Huang C-C, Chien C-L, Jeng C-J, Su H-T, Chiang E, Liu M-R, Wu CHH, Chang C-N, Lin R-H. 2004. Cross-linking of P-selectin glycoprotein ligand-1 induces death of activated T cells. Blood 104:3233-3242.
145. Azab AK, Quang P, Azab F, Pitsillides C, Thompson B, Chonghaile T, Patton JT, Maiso P, Monrose V, Sacco A, Ngo HT, Flores LM, Lin CP, Magnani JL, Kung AL, Letai A, Carrasco R, Roccaro AM, Ghobrial IM. 2012. P-selectin glycoprotein ligand regulates the interaction of multiple myeloma cells with the bone marrow microenvironment. Blood 119:1468-1478.
146. Dimitroff CJ, Descheny L, Trujillo N, Kim R, Nguyen V, Huang W, Pienta KJ, Kutok JL, Rubin MA. 2005. Identification of Leukocyte E-selectin Ligands, P-selectin Glycoprotein Ligand-1 and E-selectin Ligand-1, on Human Metastatic Prostate Tumor Cells. Cancer research 65:5750-5760.
147. Gong L, Cai Y, Zhou X, Yang H. 2012. Activated Platelets Interact with Lung Cancer Cells Through P-Selectin Glycoprotein Ligand-1. Pathology & Oncology Research 18:989-996.
148. Borsig L. 2008. The role of platelet activation in tumor metastasis. Expert Review of Anticancer Therapy 8:1247-1255.
149. Heidemann F, Schildt A, Schmid K, Bruns OT, Riecken K, Jung C, Ittrich H, Wicklein D, Reimer R, Fehse B, Heeren J, Lüers G, Schumacher U, Heine M. 2014. Selectins Mediate Small Cell Lung Cancer Systemic Metastasis. PLoS ONE 9.
150. Chen J-L, Chen W-X, Zhu J-S, Chen N-W, Zhou T, Yao M, Zhang D-Q, Wu Y-L. 2003. Effect of P-selectin monoclonal antibody on metastasis of gastric cancer and immune function. World Journal of Gastroenterology : WJG 9:1607-1610.
151. Hoos A, Protsyuk D, Borsig L. 2014. Metastatic Growth Progression Caused by PSGL-1–Mediated Recruitment of Monocytes to Metastatic Sites. Cancer Research 74:695-704.
152. Zheng Y, Yang J, Qian J, Qiu P, Hanabuchi S, Lu Y, Wang Z, Liu Z, Li H, He J, Lin P, Weber D, Davis RE, Kwak L, Cai Z, Yi Q. 2013. PSGL-1/selectin and ICAM-1/CD18 interactions are involved in macrophage-induced drug resistance in myeloma. Leukemia 27:702-710.
153. Muz B, Azab F, de la Puente P, Rollins S, Alvarez R, Kawar Z, Azab AK. 2015. Inhibition of P-Selectin and PSGL-1 Using Humanized Monoclonal Antibodies Increases the Sensitivity of Multiple Myeloma Cells to Bortezomib. BioMed Research International 2015.
154. Richter U, Schröder C, Wicklein D, Lange T, Geleff S, Dippel V, Schumacher U, Klutmann S. 2011. Adhesion of small cell lung cancer cells to E- and P-Selectin under physiological flow conditions: implications for metastasis formation. Histochemistry and Cell Biology 135:499-512.
155. Spertini C, Baïsse B, Bellone M, Gikic M, Smirnova T, Spertini O. 2019. Acute Myeloid and Lymphoblastic Leukemia Cell Interactions with Endothelial Selectins: Critical Role of PSGL-1, CD44 and CD43. Cancers 11.
156. Nuñez-Andrade N, Lamana A, Sancho D, Gisbert JP, Gonzalez-Amaro R, Sanchez-Madrid F, Urzainqui A. 2011. P-selectin glycoprotein ligand-1 modulates immune inflammatory responses in the enteric lamina propria. The Journal of Pathology 224:212-221.
157. He X, Schoeb TR, Panoskaltsis-Mortari A, Zinn KR, Kesterson RA, Zhang J, Samuel S, Hicks MJ, Hickey MJ, Bullard DC. 2006. Deficiency of P-Selectin or P-Selectin Glycoprotein Ligand-1 Leads to Accelerated Development of Glomerulonephritis and Increased Expression of CC Chemokine Ligand 2 in Lupus-Prone Mice. The Journal of Immunology 177:8748-8756.
158. Karpus WJ, Lukacs NW, Kennedy KJ, Smith WS, Hurst SD, Barrett TA. 1997. Differential CC chemokine-induced enhancement of T helper cell cytokine production. The Journal of Immunology 158:4129-4136.

159. Roth SJ, Carr MW, Springer TA. 1995. C-C chemokines, but not the C-X-C chemokines interleukin-8 and interferon-γ inducible protein-10, stimulate transendothelial chemotaxis of T lymphocytes. European Journal of Immunology 25:3482-3488.
160. Huang D, Wang J, Kivisakk P, Rollins BJ, Ransohoff RM. 2001. Absence of Monocyte Chemoattractant Protein 1 in Mice Leads to Decreased Local Macrophage Recruitment and Antigen-Specific T Helper Cell Type 1 Immune Response in Experimental Autoimmune Encephalomyelitis. Journal of Experimental Medicine 193:713-726.
161. Bakos E, Thaiss CA, Kramer MP, Cohen S, Radomir L, Orr I, Kaushansky N, Ben-Nun A, Becker-Herman S, Shachar I. 2017. CCR2 Regulates the Immune Response by Modulating the Interconversion and Function of Effector and Regulatory T Cells. The Journal of Immunology 198:4659-4671.
162. González-Tajuelo R, Fuente-Fernández Mdl, Morales-Cano D, Muñoz-Callejas A, González-Sánchez E, Silván J, Serrador JM, Cadenas S, Barreira B, Espartero-Santos M, Gamallo C, Vicente-Rabaneda EF, Castañeda S, Pérez-Vizcaíno F, Cogolludo Á, Jiménez-Borreguero LJ, Urzainqui A. 2020. Spontaneous Pulmonary Hypertension Associated With Systemic Sclerosis in P-Selectin Glycoprotein Ligand 1–Deficient Mice. Arthritis & Rheumatology 72:477-487.
163. Pérez-Frías A, González-Tajuelo R, Núñez-Andrade N, Tejedor R, García-Blanco MJ, Vicente-Rabaneda E, Castañeda S, Gamallo C, Silván J, Esteban-Villafruela A, Cubero-Rueda L, García-García C, Muñoz-Calleja C, García-Diez A, Urzainqui A. 2014. Development of an Autoimmune Syndrome Affecting the Skin and Internal Organs in P-Selectin Glycoprotein Ligand 1 Leukocyte Receptor–Deficient Mice. Arthritis & Rheumatology 66:3178-3189.
164. Nasti TH, Bullard DC, Yusuf N. 2015. P-selectin enhances growth and metastasis of mouse mammary tumors by promoting regulatory T cell infiltration into the tumors. Life Sciences 131:11-18.
165. Matsumoto M, Miyasaka M, Hirata T. 2009. P-Selectin Glycoprotein Ligand-1 Negatively Regulates T-Cell Immune Responses. The Journal of Immunology 183:7204-7211.
166. Viramontes KM, Neubert EN, DeRogatis JM, Tinoco R. 2022. PD-1 Immune Checkpoint Blockade and PSGL-1 Inhibition Synergize to Reinvigorate Exhausted T Cells. Front Immunol 13:869768.
167. Malavasi F, Deaglio S, Funaro A, Ferrero E, Horenstein AL, Ortolan E, Vaisitti T, Aydin S. 2008. Evolution and function of the ADP ribosyl cyclase/CD38 gene family in physiology and pathology. Physiol Rev 88:841-86.
168. Canto C, Menzies KJ, Auwerx J. 2015. NAD(+) Metabolism and the Control of Energy Homeostasis: A Balancing Act between Mitochondria and the Nucleus. Cell Metab 22:31-53.
169. Malavasi F, Funaro A, Alessio M, DeMonte LB, Ausiello CM, Dianzani U, Lanza F, Magrini E, Momo M, Roggero S. 1992. CD38: a multi-lineage cell activation molecule with a split personality. Int J Clin Lab Res 22:73-80.
170. Gelman L, Deterre P, Gouy H, Boumsell L, Debre P, Bismuth G. 1993. The lymphocyte surface antigen CD38 acts as a nicotinamide adenine dinucleotide glycohydrolase in human T lymphocytes. Eur J Immunol 23:3361-4.
171. Aarhus R, Graeff RM, Dickey DM, Walseth TF, Lee HC. 1995. ADP-ribosyl cyclase and CD38 catalyze the synthesis of a calcium-mobilizing metabolite from NADP. J Biol Chem 270:30327-33.
172. Horenstein AL, Chillemi A, Zaccarello G, Bruzzone S, Quarona V, Zito A, Serra S, Malavasi F. 2013. A CD38/CD203a/CD73 ectoenzymatic pathway independent of CD39 drives a novel adenosinergic loop in human T lymphocytes. Oncoimmunology 2:e26246.
173. Zocchi E, Daga A, Usai C, Franco L, Guida L, Bruzzone S, Costa A, Marchetti C, De Flora A. 1998. Expression of CD38 increases intracellular calcium concentration and reduces doubling time in HeLa and 3T3 cells. J Biol Chem 273:8017-24.
174. Aksoy P, Escande C, White TA, Thompson M, Soares S, Benech JC, Chini EN. 2006. Regulation of SIRT 1 mediated NAD dependent deacetylation: a novel role for the multifunctional enzyme CD38. Biochem Biophys Res Commun 349:353-9.
175. Aksoy P, White TA, Thompson M, Chini EN. 2006. Regulation of intracellular levels of NAD: a novel role for CD38. Biochem Biophys Res Commun 345:1386-92.

176. Sandoval-Montes C, Santos-Argumedo L. 2005. CD38 is expressed selectively during the activation of a subset of mature T cells with reduced proliferation but improved potential to produce cytokines. J Leukoc Biol 77:513-21.
177. Zubiaur M, Izquierdo M, Terhorst C, Malavasi F, Sancho J. 1997. CD38 ligation results in activation of the Raf-1/mitogen-activated protein kinase and the CD3-zeta/zeta-associated protein-70 signaling pathways in Jurkat T lymphocytes. J Immunol 159:193-205.
178. Lischke T, Heesch K, Schumacher V, Schneider M, Haag F, Koch-Nolte F, Mittrucker HW. 2013. CD38 controls the innate immune response against Listeria monocytogenes. Infect Immun 81:4091-9.
179. Partida-Sanchez S, Cockayne DA, Monard S, Jacobson EL, Oppenheimer N, Garvy B, Kusser K, Goodrich S, Howard M, Harmsen A, Randall TD, Lund FE. 2001. Cyclic ADP-ribose production by CD38 regulates intracellular calcium release, extracellular calcium influx and chemotaxis in neutrophils and is required for bacterial clearance in vivo. Nat Med 7:1209-16.
180. Piedra-Quintero ZL, Wilson Z, Nava P, Guerau-de-Arellano M. 2020. CD38: An Immunomodulatory Molecule in Inflammation and Autoimmunity. Front Immunol 11:597959.
181. Musso T, Deaglio S, Franco L, Calosso L, Badolato R, Garbarino G, Dianzani U, Malavasi F. 2001. CD38 expression and functional activities are up-regulated by IFN-gamma on human monocytes and monocytic cell lines. J Leukoc Biol 69:605-12.
182. Bauvois B, Durant L, Laboureau J, Barthelemy E, Rouillard D, Boulla G, Deterre P. 1999. Upregulation of CD38 gene expression in leukemic B cells by interferon types I and II. J Interferon Cytokine Res 19:1059-66.
183. Tirumurugaan KG, Kang BN, Panettieri RA, Foster DN, Walseth TF, Kannan MS. 2008. Regulation of the cd38 promoter in human airway smooth muscle cells by TNF-alpha and dexamethasone. Respir Res 9:26.
184. Deaglio S, Dianzani U, Horenstein AL, Fernandez JE, van Kooten C, Bragardo M, Funaro A, Garbarino G, Di Virgilio F, Banchereau J, Malavasi F. 1996. Human CD38 ligand. A 120-KDA protein predominantly expressed on endothelial cells. J Immunol 156:727-34.
185. Petri B, Bixel MG. 2006. Molecular events during leukocyte diapedesis. FEBS J 273:4399-407.
186. Herrmann MM, Barth S, Greve B, Schumann KM, Bartels A, Weissert R. 2016. Identification of gene expression patterns crucially involved in experimental autoimmune encephalomyelitis and multiple sclerosis. Dis Model Mech 9:1211-1220.
187. Henriques A, Silva I, Ines L, Souto-Carneiro MM, Pais ML, Trindade H, da Silva JA, Paiva A. 2016. CD38, CD81 and BAFFR combined expression by transitional B cells distinguishes active from inactive systemic lupus erythematosus. Clin Exp Med 16:227-32.
188. Amici SA, Young NA, Narvaez-Miranda J, Jablonski KA, Arcos J, Rosas L, Papenfuss TL, Torrelles JB, Jarjour WN, Guerau-de-Arellano M. 2018. CD38 Is Robustly Induced in Human Macrophages and Monocytes in Inflammatory Conditions. Front Immunol 9:1593.
189. Cole S, Walsh A, Yin X, Wechalekar MD, Smith MD, Proudman SM, Veale DJ, Fearon U, Pitzalis C, Humby F, Bombardieri M, Axel A, Adams H, 3rd, Chiu C, Sharp M, Alvarez J, Anderson I, Madakamutil L, Nagpal S, Guo Y. 2018. Integrative analysis reveals CD38 as a therapeutic target for plasma cell-rich pre-disease and established rheumatoid arthritis and systemic lupus erythematosus. Arthritis Res Ther 20:85.
190. Korver W, Carsillo M, Yuan J, Idamakanti N, Wagoner M, Shi P, Xia CQ, Smithson G, McLean L, Zalevsky J, Fedyk ER. 2019. A Reduction in B, T, and Natural Killer Cells Expressing CD38 by TAK-079 Inhibits the Induction and Progression of Collagen-Induced Arthritis in Cynomolgus Monkeys. J Pharmacol Exp Ther 370:182-196.
191. Radziewicz H, Ibegbu CC, Hon H, Osborn MK, Obideen K, Wehbi M, Freeman GJ, Lennox JL, Workowski KA, Hanson HL, Grakoui A. 2008. Impaired hepatitis C virus (HCV)-specific effector CD8+ T cells undergo massive apoptosis in the peripheral blood during acute HCV infection and in the liver during the chronic phase of infection. J Virol 82:9808-22.

192. Hua S, Lecuroux C, Saez-Cirion A, Pancino G, Girault I, Versmisse P, Boufassa F, Taulera O, Sinet M, Lambotte O, Venet A. 2014. Potential role for HIV-specific CD38-/HLA-DR+ CD8+ T cells in viral suppression and cytotoxicity in HIV controllers. PLoS One 9:e101920.
193. Murray SM, Down CM, Boulware DR, Stauffer WM, Cavert WP, Schacker TW, Brenchley JM, Douek DC. 2010. Reduction of immune activation with chloroquine therapy during chronic HIV infection. J Virol 84:12082-6.
194. Chandele A, Sewatanon J, Gunisetty S, Singla M, Onlamoon N, Akondy RS, Kissick HT, Nayak K, Reddy ES, Kalam H, Kumar D, Verma A, Panda H, Wang S, Angkasekwinai N, Pattanapanyasat K, Chokephaibulkit K, Medigeshi GR, Lodha R, Kabra S, Ahmed R, Murali-Krishna K. 2016. Characterization of Human CD8 T Cell Responses in Dengue Virus-Infected Patients from India. J Virol 90:11259-11278.
195. Fox A, Le NM, Horby P, van Doorn HR, Nguyen VT, Nguyen HH, Nguyen TC, Vu DP, Nguyen MH, Diep NT, Bich VT, Huong HT, Taylor WR, Farrar J, Wertheim H, Nguyen VK. 2012. Severe pandemic H1N1 2009 infection is associated with transient NK and T deficiency and aberrant CD8 responses. PLoS One 7:e31535.
196. Wang Z, Zhu L, Nguyen THO, Wan Y, Sant S, Quinones-Parra SM, Crawford JC, Eltahla AA, Rizzetto S, Bull RA, Qiu C, Koutsakos M, Clemens EB, Loh L, Chen T, Liu L, Cao P, Ren Y, Kedzierski L, Kotsimbos T, McCaw JM, La Gruta NL, Turner SJ, Cheng AC, Luciani F, Zhang X, Doherty PC, Thomas PG, Xu J, Kedzierska K. 2018. Clonally diverse CD38(+)HLA-DR(+)CD8(+) T cells persist during fatal H7N9 disease. Nat Commun 9:824.
197. Thevarajan I, Nguyen THO, Koutsakos M, Druce J, Caly L, van de Sandt CE, Jia X, Nicholson S, Catton M, Cowie B, Tong SYC, Lewin SR, Kedzierska K. 2020. Breadth of concomitant immune responses prior to patient recovery: a case report of non-severe COVID-19. Nat Med 26:453-455.
198. Ruibal P, Oestereich L, Ludtke A, Becker-Ziaja B, Wozniak DM, Kerber R, Korva M, Cabeza-Cabrerizo M, Bore JA, Koundouno FR, Duraffour S, Weller R, Thorenz A, Cimini E, Viola D, Agrati C, Repits J, Afrough B, Cowley LA, Ngabo D, Hinzmann J, Mertens M, Vitoriano I, Logue CH, Boettcher JP, Pallasch E, Sachse A, Bah A, Nitzsche K, Kuisma E, Michel J, Holm T, Zekeng EG, Garcia-Dorival I, Wolfel R, Stoecker K, Fleischmann E, Strecker T, Di Caro A, Avsic-Zupanc T, Kurth A, Meschi S, Mely S, Newman E, Bocquin A, Kis Z, Kelterbaum A, Molkenthin P, Carletti F, Portmann J, et al. 2016. Unique human immune signature of Ebola virus disease in Guinea. Nature 533:100-4.
199. Jia X, Chua BY, Loh L, Koutsakos M, Kedzierski L, Olshansky M, Heath WR, Chang SY, Xu J, Wang Z, Kedzierska K. 2021. High expression of CD38 and MHC class II on CD8(+) T cells during severe influenza disease reflects bystander activation and trogocytosis. Clin Transl Immunology 10:e1336.
200. Glaria E, Valledor AF. 2020. Roles of CD38 in the Immune Response to Infection. Cells 9.
201. Mocroft A, Bofill M, Lipman M, Medina E, Borthwick N, Timms A, Batista L, Winter M, Sabin CA, Johnson M, Lee CA, Phillips A, Janossy G. 1997. CD8+,CD38+ lymphocyte percent: a useful immunological marker for monitoring HIV-1-infected patients. J Acquir Immune Defic Syndr Hum Retrovirol 14:158-62.
202. Ndhlovu ZM, Kamya P, Mewalal N, Kloverpris HN, Nkosi T, Pretorius K, Laher F, Ogunshola F, Chopera D, Shekhar K, Ghebremichael M, Ismail N, Moodley A, Malik A, Leslie A, Goulder PJ, Buus S, Chakraborty A, Dong K, Ndung'u T, Walker BD. 2015. Magnitude and Kinetics of CD8+ T Cell Activation during Hyperacute HIV Infection Impact Viral Set Point. Immunity 43:591-604.
203. Vigano A, Saresella M, Villa ML, Ferrante P, Clerici M. 2000. CD38+CD8+ T cells as a marker of poor response to therapy in HIV-infected individuals. Chem Immunol 75:207-17.
204. Liu Z, Hultin LE, Cumberland WG, Hultin P, Schmid I, Matud JL, Detels R, Giorgi JV. 1996. Elevated relative fluorescence intensity of CD38 antigen expression on CD8+ T cells is a marker of poor prognosis in HIV infection: results of 6 years of follow-up. Cytometry 26:1-7.
205. Burgisser P, Hammann C, Kaufmann D, Battegay M, Rutschmann OT. 1999. Expression of CD28 and CD38 by CD8+ T lymphocytes in HIV-1 infection correlates with markers of disease severity and changes towards normalization under treatment. The Swiss HIV Cohort Study. Clin Exp Immunol 115:458-63.

206. McElroy AK, Akondy RS, Davis CW, Ellebedy AH, Mehta AK, Kraft CS, Lyon GM, Ribner BS, Varkey J, Sidney J, Sette A, Campbell S, Stroher U, Damon I, Nichol ST, Spiropoulou CF, Ahmed R. 2015. Human Ebola virus infection results in substantial immune activation. Proc Natl Acad Sci U S A 112:4719-24.
207. Lin P, Owens R, Tricot G, Wilson CS. 2004. Flow cytometric immunophenotypic analysis of 306 cases of multiple myeloma. Am J Clin Pathol 121:482-8.
208. Damle RN, Wasil T, Fais F, Ghiotto F, Valetto A, Allen SL, Buchbinder A, Budman D, Dittmar K, Kolitz J, Lichtman SM, Schulman P, Vinciguerra VP, Rai KR, Ferrarini M, Chiorazzi N. 1999. Ig V gene mutation status and CD38 expression as novel prognostic indicators in chronic lymphocytic leukemia. Blood 94:1840-7.
209. van de Donk NW, Janmaat ML, Mutis T, Lammerts van Bueren JJ, Ahmadi T, Sasser AK, Lokhorst HM, Parren PW. 2016. Monoclonal antibodies targeting CD38 in hematological malignancies and beyond. Immunol Rev 270:95-112.
210. Gao L, Liu Y, Du X, Ma S, Ge M, Tang H, Han C, Zhao X, Liu Y, Shao Y, Wu Z, Zhang L, Meng F, Xiao-Feng Qin F. 2021. The intrinsic role and mechanism of tumor expressed-CD38 on lung adenocarcinoma progression. Cell Death Dis 12:680.
211. Chen L, Diao L, Yang Y, Yi X, Rodriguez BL, Li Y, Villalobos PA, Cascone T, Liu X, Tan L, Lorenzi PL, Huang A, Zhao Q, Peng D, Fradette JJ, Peng DH, Ungewiss C, Roybal J, Tong P, Oba J, Skoulidis F, Peng W, Carter BW, Gay CM, Fan Y, Class CA, Zhu J, Rodriguez-Canales J, Kawakami M, Byers LA, Woodman SE, Papadimitrakopoulou VA, Dmitrovsky E, Wang J, Ullrich SE, Wistuba, II, Heymach JV, Qin FX, Gibbons DL. 2018. CD38-Mediated Immunosuppression as a Mechanism of Tumor Cell Escape from PD-1/PD-L1 Blockade. Cancer Discov 8:1156-1175.
212. Chatterjee S, Daenthanasanmak A, Chakraborty P, Wyatt MW, Dhar P, Selvam SP, Fu J, Zhang J, Nguyen H, Kang I, Toth K, Al-Homrani M, Husain M, Beeson G, Ball L, Helke K, Husain S, Garrett-Mayer E, Hardiman G, Mehrotra M, Nishimura MI, Beeson CC, Bupp MG, Wu J, Ogretmen B, Paulos CM, Rathmell J, Yu XZ, Mehrotra S. 2018. CD38-NAD(+)Axis Regulates Immunotherapeutic Anti-Tumor T Cell Response. Cell Metab 27:85-100 e8.
213. Allard B, Beavis PA, Darcy PK, Stagg J. 2016. Immunosuppressive activities of adenosine in cancer. Curr Opin Pharmacol 29:7-16.
214. Feng X, Zhang L, Acharya C, An G, Wen K, Qiu L, Munshi NC, Tai YT, Anderson KC. 2017. Targeting CD38 Suppresses Induction and Function of T Regulatory Cells to Mitigate Immunosuppression in Multiple Myeloma. Clin Cancer Res 23:4290-4300.
215. Karakasheva TA, Waldron TJ, Eruslanov E, Kim SB, Lee JS, O'Brien S, Hicks PD, Basu D, Singhal S, Malavasi F, Rustgi AK. 2015. CD38-Expressing Myeloid-Derived Suppressor Cells Promote Tumor Growth in a Murine Model of Esophageal Cancer. Cancer Res 75:4074-85.
216. Munoz P, Mittelbrunn M, de la Fuente H, Perez-Martinez M, Garcia-Perez A, Ariza-Veguillas A, Malavasi F, Zubiaur M, Sanchez-Madrid F, Sancho J. 2008. Antigen-induced clustering of surface CD38 and recruitment of intracellular CD38 to the immunologic synapse. Blood 111:3653-64.
217. Philip M, Fairchild L, Sun L, Horste EL, Camara S, Shakiba M, Scott AC, Viale A, Lauer P, Merghoub T, Hellmann MD, Wolchok JD, Leslie CS, Schietinger A. 2017. Chromatin states define tumour-specific T cell dysfunction and reprogramming. Nature 545:452-456.
218. Hudson WH, Gensheimer J, Hashimoto M, Wieland A, Valanparambil RM, Li P, Lin JX, Konieczny BT, Im SJ, Freeman GJ, Leonard WJ, Kissick HT, Ahmed R. 2019. Proliferating Transitory T Cells with an Effector-like Transcriptional Signature Emerge from PD-1(+) Stem-like CD8(+) T Cells during Chronic Infection. Immunity 51:1043-1058 e4.
219. Verma V, Shrimali RK, Ahmad S, Dai W, Wang H, Lu S, Nandre R, Gaur P, Lopez J, Sade-Feldman M, Yizhak K, Bjorgaard SL, Flaherty KT, Wargo JA, Boland GM, Sullivan RJ, Getz G, Hammond SA, Tan M, Qi J, Wong P, Merghoub T, Wolchok J, Hacohen N, Janik JE, Mkrtichyan M, Gupta S, Khleif SN. 2019. PD-1 blockade in subprimed CD8 cells induces dysfunctional PD-1(+)CD38(hi) cells and anti-PD-1 resistance. Nat Immunol 20:1231-1243.

220. Chen PM, Katsuyama E, Satyam A, Li H, Rubio J, Jung S, Andrzejewski S, Becherer JD, Tsokos MG, Abdi R, Tsokos GC. 2022. CD38 reduces mitochondrial fitness and cytotoxic T cell response against viral infection in lupus patients by suppressing mitophagy. Sci Adv 8:eabo4271.
221. Joosse ME, Menckeberg CL, de Ruiter LF, Raatgeep HRC, van Berkel LA, Simons-Oosterhuis Y, Tindemans I, Muskens AFM, Hendriks RW, Hoogenboezem RM, Cupedo T, de Ridder L, Escher JC, Veenbergen S, Samsom JN. 2019. Frequencies of circulating regulatory TIGIT(+)CD38(+) effector T cells correlate with the course of inflammatory bowel disease. Mucosal Immunol 12:154-163.
222. Ma K, Sun L, Shen M, Zhang X, Xiao Z, Wang J, Liu X, Jiang K, Xiao-Feng Qin F, Guo F, Zhang B, Zhang L. 2022. Functional assessment of the cell-autonomous role of NADase CD38 in regulating CD8(+) T cell exhaustion. iScience 25:104347.
223. DeRogatis JM, Viramontes KM, Neubert EN, Henriquez ML, Guerrero-Juarez CF, Tinoco R. 2022. Targeting the PSGL-1 Immune Checkpoint Promotes Immunity to PD-1-Resistant Melanoma. Cancer Immunol Res 10:612-625.
224. Khalil DN, Smith EL, Brentjens RJ, Wolchok JD. 2016. The future of cancer treatment: immunomodulation, CARs and combination immunotherapy. Nat Rev Clin Oncol 13:394.
225. Topalian SL, Hodi FS, Brahmer JR, Gettinger SN, Smith DC, McDermott DF, Powderly JD, Carvajal RD, Sosman JA, Atkins MB, Leming PD, Spigel DR, Antonia SJ, Horn L, Drake CG, Pardoll DM, Chen L, Sharfman WH, Anders RA, Taube JM, McMiller TL, Xu H, Korman AJ, Jure-Kunkel M, Agrawal S, McDonald D, Kollia GD, Gupta A, Wigginton JM, Sznol M. 2012. Safety, activity, and immune correlates of anti-PD-1 antibody in cancer. N Engl J Med 366:2443-54.
226. Brahmer JR, Tykodi SS, Chow LQ, Hwu WJ, Topalian SL, Hwu P, Drake CG, Camacho LH, Kauh J, Odunsi K, Pitot HC, Hamid O, Bhatia S, Martins R, Eaton K, Chen S, Salay TM, Alaparthy S, Grosso JF, Korman AJ, Parker SM, Agrawal S, Goldberg SM, Pardoll DM, Gupta A, Wigginton JM. 2012. Safety and activity of anti-PD-L1 antibody in patients with advanced cancer. N Engl J Med 366:2455-65.
227. Hodi FS, O'Day SJ, McDermott DF, Weber RW, Sosman JA, Haanen JB, Gonzalez R, Robert C, Schadendorf D, Hassel JC, Akerley W, van den Eertwegh AJ, Lutzky J, Lorigan P, Vaubel JM, Linette GP, Hogg D, Ottensmeier CH, Lebbe C, Peschel C, Quirt I, Clark JI, Wolchok JD, Weber JS, Tian J, Yellin MJ, Nichol GM, Hoos A, Urba WJ. 2010. Improved survival with ipilimumab in patients with metastatic melanoma. N Engl J Med 363:711-23.
228. Hamid O, Robert C, Daud A, Hodi FS, Hwu WJ, Kefford R, Wolchok JD, Hersey P, Joseph RW, Weber JS, Dronca R, Gangadhar TC, Patnaik A, Zarour H, Joshua AM, Gergich K, Elassaiss-Schaap J, Algazi A, Mateus C, Boasberg P, Tumeh PC, Chmielowski B, Ebbinghaus SW, Li XN, Kang SP, Ribas A. 2013. Safety and tumor responses with lambrolizumab (anti-PD-1) in melanoma. N Engl J Med 369:134-44.
229. Ramos-Casals M, Brahmer JR, Callahan MK, Flores-Chavez A, Keegan N, Khamashta MA, Lambotte O, Mariette X, Prat A, Suarez-Almazor ME. 2020. Immune-related adverse events of checkpoint inhibitors. Nat Rev Dis Primers 6:38.
230. Topalian SL, Sznol M, McDermott DF, Kluger HM, Carvajal RD, Sharfman WH, Brahmer JR, Lawrence DP, Atkins MB, Powderly JD, Leming PD, Lipson EJ, Puzanov I, Smith DC, Taube JM, Wigginton JM, Kollia GD, Gupta A, Pardoll DM, Sosman JA, Hodi FS. 2014. Survival, durable tumor remission, and long-term safety in patients with advanced melanoma receiving nivolumab. J Clin Oncol 32:1020-30.
231. Wolchok JD, Kluger H, Callahan MK, Postow MA, Rizvi NA, Lesokhin AM, Segal NH, Ariyan CE, Gordon RA, Reed K, Burke MM, Caldwell A, Kronenberg SA, Agunwamba BU, Zhang X, Lowy I, Inzunza HD, Feely W, Horak CE, Hong Q, Korman AJ, Wigginton JM, Gupta A, Sznol M. 2013. Nivolumab plus ipilimumab in advanced melanoma. N Engl J Med 369:122-33.
232. Galli F, Aguilera JV, Palermo B, Markovic SN, Nistico P, Signore A. 2020. Relevance of immune cell and tumor microenvironment imaging in the new era of immunotherapy. J Exp Clin Cancer Res 39:89.
233. Hashimoto M, Kamphorst AO, Im SJ, Kissick HT, Pillai RN, Ramalingam SS, Araki K, Ahmed R. 2018. CD8 T Cell Exhaustion in Chronic Infection and Cancer: Opportunities for Interventions. Annu Rev Med 69:301-318.

234. Tinoco R, Carrette F, Barraza ML, Otero DC, Magana J, Bosenberg MW, Swain SL, Bradley LM. 2016. PSGL-1 Is an Immune Checkpoint Regulator that Promotes T Cell Exhaustion. Immunity 44:1190-203.
235. Levesque JP, Zannettino AC, Pudney M, Niutta S, Haylock DN, Snapp KR, Kansas GS, Berndt MC, Simmons PJ. 1999. PSGL-1-mediated adhesion of human hematopoietic progenitors to P-selectin results in suppression of hematopoiesis. Immunity 11:369-78.
236. Sultana DA, Zhang SL, Todd SP, Bhandoola A. 2012. Expression of functional P-selectin glycoprotein ligand 1 on hematopoietic progenitors is developmentally regulated. J Immunol 188:4385-93.
237. Perez-Frias A, Gonzalez-Tajuelo R, Nunez-Andrade N, Tejedor R, Garcia-Blanco MJ, Vicente-Rabaneda E, Castaneda S, Gamallo C, Silvan J, Esteban-Villafruela A, Cubero-Rueda L, Garcia-Garcia C, Munoz-Calleja C, Garcia-Diez A, Urzainqui A. 2014. Development of an autoimmune syndrome affecting the skin and internal organs in P-selectin glycoprotein ligand 1 leukocyte receptor-deficient mice. Arthritis Rheumatol 66:3178-89.
238. Angiari S, Rossi B, Piccio L, Zinselmeyer BH, Budui S, Zenaro E, Della Bianca V, Bach SD, Scarpini E, Bolomini-Vittori M, Piacentino G, Dusi S, Laudanna C, Cross AH, Miller MJ, Constantin G. 2013. Regulatory T cells suppress the late phase of the immune response in lymph nodes through P-selectin glycoprotein ligand-1. J Immunol 191:5489-500.
239. He X, Schoeb TR, Panoskaltsis-Mortari A, Zinn KR, Kesterson RA, Zhang J, Samuel S, Hicks MJ, Hickey MJ, Bullard DC. 2006. Deficiency of P-selectin or P-selectin glycoprotein ligand-1 leads to accelerated development of glomerulonephritis and increased expression of CC chemokine ligand 2 in lupus-prone mice. J Immunol 177:8748-56.
240. Yoshizaki A, Yanaba K, Iwata Y, Komura K, Ogawa A, Akiyama Y, Muroi E, Hara T, Ogawa F, Takenaka M, Shimizu K, Hasegawa M, Fujimoto M, Tedder TF, Sato S. 2010. Cell adhesion molecules regulate fibrotic process via Th1/Th2/Th17 cell balance in a bleomycin-induced scleroderma model. J Immunol 185:2502-15.
241. Urzainqui A, Martinez del Hoyo G, Lamana A, de la Fuente H, Barreiro O, Olazabal IM, Martin P, Wild MK, Vestweber D, Gonzalez-Amaro R, Sanchez-Madrid F. 2007. Functional role of P-selectin glycoprotein ligand 1/P-selectin interaction in the generation of tolerogenic dendritic cells. J Immunol 179:7457-65.
242. Spertini C, Baisse B, Spertini O. 2012. Ezrin-radixin-moesin-binding sequence of PSGL-1 glycoprotein regulates leukocyte rolling on selectins and activation of extracellular signal-regulated kinases. J Biol Chem 287:10693-702.
243. Urzainqui A, Serrador JM, Viedma F, Yanez-Mo M, Rodriguez A, Corbi AL, Alonso-Lebrero JL, Luque A, Deckert M, Vazquez J, Sanchez-Madrid F. 2002. ITAM-based interaction of ERM proteins with Syk mediates signaling by the leukocyte adhesion receptor PSGL-1. Immunity 17:401-12.
244. Tinoco R, Neubert EN, Stairiker CJ, Henriquez ML, Bradley LM. 2021. PSGL-1 Is a T Cell Intrinsic Inhibitor That Regulates Effector and Memory Differentiation and Responses During Viral Infection. Front Immunol 12:677824.
245. Veerman KM, Carlow DA, Shanina I, Priatel JJ, Horwitz MS, Ziltener HJ. 2012. PSGL-1 regulates the migration and proliferation of CD8(+) T cells under homeostatic conditions. J Immunol 188:1638-46.
246. Matsumoto M, Miyasaka M, Hirata T. 2009. P-selectin glycoprotein ligand-1 negatively regulates T-cell immune responses. J Immunol 183:7204-11.
247. Wolock SL, Lopez R, Klein AM. 2019. Scrublet: Computational Identification of Cell Doublets in Single-Cell Transcriptomic Data. Cell Syst 8:281-291 e9.
248. Butler A, Hoffman P, Smibert P, Papalexi E, Satija R. 2018. Integrating single-cell transcriptomic data across different conditions, technologies, and species. Nat Biotechnol 36:411-420.
249. Stuart T, Butler A, Hoffman P, Hafemeister C, Papalexi E, Mauck WM, 3rd, Hao Y, Stoeckius M, Smibert P, Satija R. 2019. Comprehensive Integration of Single-Cell Data. Cell 177:1888-1902 e21.
250. Janelle V, Langlois MP, Tarrab E, Lapierre P, Poliquin L, Lamarre A. 2014. Transient complement inhibition promotes a tumor-specific immune response through the implication of natural killer cells. Cancer Immunol Res 2:200-6.

251. Andreatta M, Corria-Osorio J, Muller S, Cubas R, Coukos G, Carmona SJ. 2021. Interpretation of T cell states from single-cell transcriptomics data using reference atlases. Nat Commun 12:2965.
252. Blackburn SD, Shin H, Freeman GJ, Wherry EJ. 2008. Selective expansion of a subset of exhausted CD8 T cells by alphaPD-L1 blockade. Proc Natl Acad Sci U S A 105:15016-21.
253. Mognol GP, Spreafico R, Wong V, Scott-Browne JP, Togher S, Hoffmann A, Hogan PG, Rao A, Trifari S. 2017. Exhaustion-associated regulatory regions in CD8(+) tumor-infiltrating T cells. Proc Natl Acad Sci U S A 114:E2776-E2785.
254. Paley MA, Kroy DC, Odorizzi PM, Johnnidis JB, Dolfi DV, Barnett BE, Bikoff EK, Robertson EJ, Lauer GM, Reiner SL, Wherry EJ. 2012. Progenitor and terminal subsets of CD8+ T cells cooperate to contain chronic viral infection. Science 338:1220-5.
255. Di Pilato M, Kim EY, Cadilha BL, Prussmann JN, Nasrallah MN, Seruggia D, Usmani SM, Misale S, Zappulli V, Carrizosa E, Mani V, Ligorio M, Warner RD, Medoff BD, Marangoni F, Villani AC, Mempel TR. 2019. Targeting the CBM complex causes Treg cells to prime tumours for immune checkpoint therapy. Nature 570:112-116.
256. Wang J, Perry CJ, Meeth K, Thakral D, Damsky W, Micevic G, Kaech S, Blenman K, Bosenberg M. 2017. UV-induced somatic mutations elicit a functional T cell response in the YUMMER1.7 mouse melanoma model. Pigment Cell Melanoma Res 30:428-435.
257. Barrueto L, Caminero F, Cash L, Makris C, Lamichhane P, Deshmukh RR. 2020. Resistance to Checkpoint Inhibition in Cancer Immunotherapy. Transl Oncol 13:100738.
258. Wei SC, Duffy CR, Allison JP. 2018. Fundamental Mechanisms of Immune Checkpoint Blockade Therapy. Cancer Discov 8:1069-1086.
259. Sandu I, Cerletti D, Claassen M, Oxenius A. 2020. Exhausted CD8(+) T cells exhibit low and strongly inhibited TCR signaling during chronic LCMV infection. Nat Commun 11:4454.
260. Zander R, Schauder D, Xin G, Nguyen C, Wu X, Zajac A, Cui W. 2019. CD4(+) T Cell Help Is Required for the Formation of a Cytolytic CD8(+) T Cell Subset that Protects against Chronic Infection and Cancer. Immunity 51:1028-1042 e4.
261. DeRogatis JM, Viramontes KM, Neubert EN, Tinoco R. 2021. PSGL-1 Immune Checkpoint Inhibition for CD4(+) T Cell Cancer Immunotherapy. Front Immunol 12:636238.
262. Kline J, Brown IE, Zha YY, Blank C, Strickler J, Wouters H, Zhang L, Gajewski TF. 2008. Homeostatic proliferation plus regulatory T-cell depletion promotes potent rejection of B16 melanoma. Clin Cancer Res 14:3156-67.
263. Ahmetlic F, Riedel T, Homberg N, Bauer V, Trautwein N, Geishauser A, Sparwasser T, Stevanovic S, Rocken M, Mocikat R. 2019. Regulatory T Cells in an Endogenous Mouse Lymphoma Recognize Specific Antigen Peptides and Contribute to Immune Escape. Cancer Immunol Res 7:600-608.
264. Gambichler T, Schroter U, Hoxtermann S, Susok L, Stockfleth E, Becker JC. 2020. Decline of programmed death-1-positive circulating T regulatory cells predicts more favourable clinical outcome of patients with melanoma under immune checkpoint blockade. Br J Dermatol 182:1214-1220.
265. Ko K, Yamazaki S, Nakamura K, Nishioka T, Hirota K, Yamaguchi T, Shimizu J, Nomura T, Chiba T, Sakaguchi S. 2005. Treatment of advanced tumors with agonistic anti-GITR mAb and its effects on tumor-infiltrating Foxp3+CD25+CD4+ regulatory T cells. J Exp Med 202:885-91.
266. Liakou CI, Kamat A, Tang DN, Chen H, Sun J, Troncoso P, Logothetis C, Sharma P. 2008. CTLA-4 blockade increases IFNgamma-producing CD4+ICOShi cells to shift the ratio of effector to regulatory T cells in cancer patients. Proc Natl Acad Sci U S A 105:14987-92.
267. Larkin J, Chiarion-Sileni V, Gonzalez R, Grob JJ, Rutkowski P, Lao CD, Cowey CL, Schadendorf D, Wagstaff J, Dummer R, Ferrucci PF, Smylie M, Hogg D, Hill A, Marquez-Rodas I, Haanen J, Guidoboni M, Maio M, Schoffski P, Carlino MS, Lebbe C, McArthur G, Ascierto PA, Daniels GA, Long GV, Bastholt L, Rizzo JI, Balogh A, Moshyk A, Hodi FS, Wolchok JD. 2019. Five-Year Survival with Combined Nivolumab and Ipilimumab in Advanced Melanoma. N Engl J Med 381:1535-1546.
268. Nowicki TS, Hu-Lieskovan S, Ribas A. 2018. Mechanisms of Resistance to PD-1 and PD-L1 Blockade. Cancer J 24:47-53.

269. Kim JY, Kronbichler A, Eisenhut M, Hong SH, van der Vliet HJ, Kang J, Shin JI, Gamerith G. 2019. Tumor Mutational Burden and Efficacy of Immune Checkpoint Inhibitors: A Systematic Review and Meta-Analysis. Cancers (Basel) 11.
270. Kleffel S, Posch C, Barthel SR, Mueller H, Schlapbach C, Guenova E, Elco CP, Lee N, Juneja VR, Zhan Q, Lian CG, Thomi R, Hoetzenecker W, Cozzio A, Dummer R, Mihm MC, Jr., Flaherty KT, Frank MH, Murphy GF, Sharpe AH, Kupper TS, Schatton T. 2015. Melanoma Cell-Intrinsic PD-1 Receptor Functions Promote Tumor Growth. Cell 162:1242-56.
271. Lin H, Wei S, Hurt EM, Green MD, Zhao L, Vatan L, Szeliga W, Herbst R, Harms PW, Fecher LA, Vats P, Chinnaiyan AM, Lao CD, Lawrence TS, Wicha M, Hamanishi J, Mandai M, Kryczek I, Zou W. 2018. Host expression of PD-L1 determines efficacy of PD-L1 pathway blockade-mediated tumor regression. J Clin Invest 128:805-815.
272. Mehta N, Maddineni S, Kelly RL, Lee RB, Hunter SA, Silberstein JL, Parra Sperberg RA, Miller CL, Rabe A, Labanieh L, Cochran JR. 2020. An engineered antibody binds a distinct epitope and is a potent inhibitor of murine and human VISTA. Sci Rep 10:15171.
273. Rosenbaum SR, Knecht M, Mollaee M, Zhong Z, Erkes DA, McCue PA, Chervoneva I, Berger AC, Lo JA, Fisher DE, Gershenwald JE, Davies MA, Purwin TJ, Aplin AE. 2020. FOXD3 Regulates VISTA Expression in Melanoma. Cell Rep 30:510-524 e6.
274. Pendl GG, Robert C, Steinert M, Thanos R, Eytner R, Borges E, Wild MK, Lowe JB, Fuhlbrigge RC, Kupper TS, Vestweber D, Grabbe S. 2002. Immature mouse dendritic cells enter inflamed tissue, a process that requires E- and P-selectin, but not P-selectin glycoprotein ligand 1. Blood 99:946-56.
275. DeRogatis JM, Neubert EN, Viramontes KM, Henriquez ML, Nicholas DA, Tinoco R. 2023. Cell-Intrinsic CD38 Expression Sustains Exhausted CD8(+) T Cells by Regulating Their Survival and Metabolism during Chronic Viral Infection. J Virol doi:10.1128/jvi.00225-23:e0022523.
276. Kar A, Mehrotra S, Chatterjee S. 2020. CD38: T Cell Immuno-Metabolic Modulator. Cells 9.
277. Ohta A, Gorelik E, Prasad SJ, Ronchese F, Lukashev D, Wong MK, Huang X, Caldwell S, Liu K, Smith P, Chen JF, Jackson EK, Apasov S, Abrams S, Sitkovsky M. 2006. A2A adenosine receptor protects tumors from antitumor T cells. Proc Natl Acad Sci U S A 103:13132-7.
278. Beavis PA, Milenkovski N, Henderson MA, John LB, Allard B, Loi S, Kershaw MH, Stagg J, Darcy PK. 2015. Adenosine Receptor 2A Blockade Increases the Efficacy of Anti-PD-1 through Enhanced Antitumor T-cell Responses. Cancer Immunol Res 3:506-17.
279. Moskophidis D, Lechner F, Pircher H, Zinkernagel RM. 1993. Virus persistence in acutely infected immunocompetent mice by exhaustion of antiviral cytotoxic effector T cells. Nature 362:758-61.
280. Speiser DE, Utzschneider DT, Oberle SG, Munz C, Romero P, Zehn D. 2014. T cell differentiation in chronic infection and cancer: functional adaptation or exhaustion? Nat Rev Immunol 14:768-74.
281. Utzschneider DT, Gabriel SS, Chisanga D, Gloury R, Gubser PM, Vasanthakumar A, Shi W, Kallies A. 2020. Early precursor T cells establish and propagate T cell exhaustion in chronic infection. Nat Immunol 21:1256-1266.
282. Nicholas D, Proctor EA, Raval FM, Ip BC, Habib C, Ritou E, Grammatopoulos TN, Steenkamp D, Dooms H, Apovian CM, Lauffenburger DA, Nikolajczyk BS. 2017. Advances in the quantification of mitochondrial function in primary human immune cells through extracellular flux analysis. PLoS One 12:e0170975.
283. Timperi E, Barnaba V. 2021. CD39 Regulation and Functions in T Cells. Int J Mol Sci 22.
284. Sen DR, Kaminski J, Barnitz RA, Kurachi M, Gerdemann U, Yates KB, Tsao HW, Godec J, LaFleur MW, Brown FD, Tonnerre P, Chung RT, Tully DC, Allen TM, Frahm N, Lauer GM, Wherry EJ, Yosef N, Haining WN. 2016. The epigenetic landscape of T cell exhaustion. Science 354:1165-1169.
285. Morandi F, Morandi B, Horenstein AL, Chillemi A, Quarona V, Zaccarello G, Carrega P, Ferlazzo G, Mingari MC, Moretta L, Pistoia V, Malavasi F. 2015. A non-canonical adenosinergic pathway led by CD38 in human melanoma cells induces suppression of T cell proliferation. Oncotarget 6:25602-18.
286. Perrot I, Michaud HA, Giraudon-Paoli M, Augier S, Docquier A, Gros L, Courtois R, Dejou C, Jecko D, Becquart O, Rispaud-Blanc H, Gauthier L, Rossi B, Chanteux S, Gourdin N, Amigues B, Roussel A, Bensussan A, Eliaou JF, Bastid J, Romagne F, Morel Y, Narni-Mancinelli E, Vivier E, Paturel C,

Bonnefoy N. 2019. Blocking Antibodies Targeting the CD39/CD73 Immunosuppressive Pathway Unleash Immune Responses in Combination Cancer Therapies. Cell Rep 27:2411-2425 e9.
287. Deaglio S, Robson SC. 2011. Ectonucleotidases as regulators of purinergic signaling in thrombosis, inflammation, and immunity. Adv Pharmacol 61:301-32.
288. Antonioli L, Pacher P, Vizi ES, Hasko G. 2013. CD39 and CD73 in immunity and inflammation. Trends Mol Med 19:355-67.
289. Bahri R, Bollinger A, Bollinger T, Orinska Z, Bulfone-Paus S. 2012. Ectonucleotidase CD38 demarcates regulatory, memory-like CD8+ T cells with IFN-gamma-mediated suppressor activities. PLoS One 7:e45234.
290. Ostendorf L, Burns M, Durek P, Heinz GA, Heinrich F, Garantziotis P, Enghard P, Richter U, Biesen R, Schneider U, Knebel F, Burmester G, Radbruch A, Mei HE, Mashreghi MF, Hiepe F, Alexander T. 2020. Targeting CD38 with Daratumumab in Refractory Systemic Lupus Erythematosus. N Engl J Med 383:1149-1155.
291. Callan MF, Tan L, Annels N, Ogg GS, Wilson JD, O'Callaghan CA, Steven N, McMichael AJ, Rickinson AB. 1998. Direct visualization of antigen-specific CD8+ T cells during the primary immune response to Epstein-Barr virus In vivo. J Exp Med 187:1395-402.
292. Morandi F, Horenstein AL, Malavasi F. 2021. The Key Role of NAD(+) in Anti-Tumor Immune Response: An Update. Front Immunol 12:658263.
293. Li W, Liang L, Liao Q, Li Y, Zhou Y. 2022. CD38: An important regulator of T cell function. Biomed Pharmacother 153:113395.
294. Liikanen I, Lauhan C, Quon S, Omilusik K, Phan AT, Bartroli LB, Ferry A, Goulding J, Chen J, Scott-Browne JP, Yustein JT, Scharping NE, Witherden DA, Goldrath AW. 2021. Hypoxia-inducible factor activity promotes antitumor effector function and tissue residency by CD8+ T cells. J Clin Invest 131.
295. Kamada T, Togashi Y, Tay C, Ha D, Sasaki A, Nakamura Y, Sato E, Fukuoka S, Tada Y, Tanaka A, Morikawa H, Kawazoe A, Kinoshita T, Shitara K, Sakaguchi S, Nishikawa H. 2019. PD-1(+) regulatory T cells amplified by PD-1 blockade promote hyperprogression of cancer. Proc Natl Acad Sci U S A 116:9999-10008.
296. Kavanagh B, O'Brien S, Lee D, Hou Y, Weinberg V, Rini B, Allison JP, Small EJ, Fong L. 2008. CTLA4 blockade expands FoxP3+ regulatory and activated effector CD4+ T cells in a dose-dependent fashion. Blood 112:1175-83.
297. Marangoni F, Zhakyp A, Corsini M, Geels SN, Carrizosa E, Thelen M, Mani V, Prussmann JN, Warner RD, Ozga AJ, Di Pilato M, Othy S, Mempel TR. 2021. Expansion of tumor-associated Treg cells upon disruption of a CTLA-4-dependent feedback loop. Cell 184:3998-4015 e19.
298. Jie HB, Gildener-Leapman N, Li J, Srivastava RM, Gibson SP, Whiteside TL, Ferris RL. 2013. Intratumoral regulatory T cells upregulate immunosuppressive molecules in head and neck cancer patients. Br J Cancer 109:2629-35.
299. Syed Khaja AS, Toor SM, El Salhat H, Ali BR, Elkord E. 2017. Intratumoral FoxP3(+)Helios(+) Regulatory T Cells Upregulating Immunosuppressive Molecules Are Expanded in Human Colorectal Cancer. Front Immunol 8:619.
300. Takeuchi Y, Nishikawa H. 2016. Roles of regulatory T cells in cancer immunity. Int Immunol 28:401-9.
301. Zebley CC, Youngblood B. 2022. Mechanisms of T cell exhaustion guiding next-generation immunotherapy. Trends Cancer 8:726-734.
302. Kumagai S, Togashi Y, Kamada T, Sugiyama E, Nishinakamura H, Takeuchi Y, Vitaly K, Itahashi K, Maeda Y, Matsui S, Shibahara T, Yamashita Y, Irie T, Tsuge A, Fukuoka S, Kawazoe A, Udagawa H, Kirita K, Aokage K, Ishii G, Kuwata T, Nakama K, Kawazu M, Ueno T, Yamazaki N, Goto K, Tsuboi M, Mano H, Doi T, Shitara K, Nishikawa H. 2020. The PD-1 expression balance between effector and regulatory T cells predicts the clinical efficacy of PD-1 blockade therapies. Nat Immunol 21:1346-1358.
303. van den Broek T, Borghans JAM, van Wijk F. 2018. The full spectrum of human naive T cells. Nat Rev Immunol 18:363-373.
304. Kurtulus S, Madi A, Escobar G, Klapholz M, Nyman J, Christian E, Pawlak M, Dionne D, Xia J, Rozenblatt-Rosen O, Kuchroo VK, Regev A, Anderson AC. 2019. Checkpoint Blockade

Immunotherapy Induces Dynamic Changes in PD-1(-)CD8(+) Tumor-Infiltrating T Cells. Immunity 50:181-194 e6.
305. Hogan KA, Chini CCS, Chini EN. 2019. The Multi-faceted Ecto-enzyme CD38: Roles in Immunomodulation, Cancer, Aging, and Metabolic Diseases. Front Immunol 10:1187.
306. Canale FP, Ramello MC, Nunez N, Bossio SN, Piaggio E, Gruppi A, Rodriguez EVA, Montes CL. 2018. CD39 Expression Defines Cell Exhaustion in Tumor-Infiltrating CD8(+) T Cells-Response. Cancer Res 78:5175.
307. Vignali PDA, DePeaux K, Watson MJ, Ye C, Ford BR, Lontos K, McGaa NK, Scharping NE, Menk AV, Robson SC, Poholek AC, Rivadeneira DB, Delgoffe GM. 2023. Hypoxia drives CD39-dependent suppressor function in exhausted T cells to limit antitumor immunity. Nat Immunol 24:267-279.